Valorization of Loblolly Pine (*Pinus taeda*) Downed Timber: Degradation and Recovery of Natural Polymers to Improve Bioeconomy Strategies

by

Javier Abraham Hernández Díaz

A dissertation submitted to the Graduate Faculty of
Auburn University
in partial fulfillment of the
requirements for the Degree of
Doctor of Philosophy

Auburn, Alabama
May 4, 2024

Keywords: Downed timber degradation rates, stumpage price forecasting, wavelet analysis, natural polymers recovery, lignin

Approved by

Dr. Maria Soledad Peresin, Associate Professor of Forest Biomaterials, College of Forestry, Wildlife, and Environment
Dr. Brian K. Via, Regions Bank Professor, Forest Products, College of Forestry, Wildlife, and Environment
Dr. Adam Maggard, Harry E. Murphy Associate Professor and Extension Specialist, College of Forestry, Wildlife, and Environment
Dr. Yucheng Peng, Assistant Professor, College of Forestry, Wildlife, and Environment
Dr. Stephen Chmely, Assistant Professor of Agricultural and Biological Engineering, Pennsylvania State University

Abstract

In the aftermath of events such as hurricanes, downed timber's economic impact can reach billions. Accurate forecasting of stumpage prices post-events is crucial yet challenging due to data nature. This study innovatively applies wavelet analysis in forestry economic analysis to uncover relationships between timber market indices and hurricane seasons. Combining traditional correlation and wavelet coherence analysis deepens the understanding of timber market dynamics and the effects of hurricanes. The study highlights recent advancements in wavelet methodology, leveraging open-source R packages like WaveletComp and Wavelet-ARIMA. The Wavelet-ARIMA model effectively reduces noise, enhancing prediction accuracy across an extensive dataset encompassing various indices.

Simultaneously, the study investigates hurricane-downed timber degradation in Alabama using near-infrared spectroscopy (NIR) and acoustic technology. Analyzing 30 loblolly pine trees, the research focuses on wood composition analysis, employing nonlinear techniques, smoothing optimization, and first derivative as a mathematical pretreatment, coupled with Box-Behnken (BB) experimental design. Utilizing 15 core samples, the models demonstrate efficiency comparable to complete sets, showcasing the potential for resource-efficient wood composition prediction. Spectral pretreatment investigations underscore the first derivative's efficacy and the balanced distribution of explained variance. Support Vector Machines (SVM) models exhibit superior predictive performances, particularly with a polynomial kernel. This innovative approach, combining reduced sample sizes and simplified spectral treatments, not only presents a promising avenue for wood composition prediction but also offers streamlined methodologies for scalability in forestry and wood industry practices, with implications for research and practical applications.

Moreover, the study unveils distinct temporal patterns in sound-wave propagation and NIR measurements. NIR data’s principal component analysis (PCA) captures temporal phases, while transverse sound-wave measurements indicate consistent stress wave velocity variations. Thermogravimetric analysis (TGA) reveals significant shifts, emphasizing temporal dynamics, and chemical characterization highlights

variations in lignin and carbohydrate fractions. The findings underscore the dynamic degradation process of hurricane-downed timber, emphasizing potential applications in timber quality assessment and biorefinery operations. Contributing to resilient and sustainable timber utilization post-natural disasters, the study enriches understanding of composition changes over time and the weathering process.

Furthermore, the study delves into the weathering effects on downed timber over 12 months, mainly focusing on lignin and carbohydrate composition changes. The model study with harvested loblolly pine trees reveals gradual increases in Klason lignin content over time, indicating potential improvements in recovery operations. Changes in Fourier transform infrared (FTIR) spectra and Thermogravimetric analysis (TGA) demonstrate alterations in chemical composition, structure, and thermal properties of co-solvent enhanced lignin fractionation (CELF) lignin samples. Differential scanning calorimetry (DSC) analysis provided specific glass transition temperature (Tg) values, while Gel-permeation chromatography (GPC) indicated differences in molecular weight distribution consistent with expected natural degradation. Nuclear magnetic resonance (NMR) of the cell wall composition and CELF lignin obtained corroborate the observations. This comprehensive investigation contributes to understanding the intricate weathering effects on timber, offering valuable insights for sustainable utilization and recovery operations post-natural disasters.

The consistency in lignin quality suggests the robustness and reliability of the CELF process in effectively isolating lignin from different stages of timber degradation. The process appears to be resilient to variations in the structural integrity and chemical composition of the starting material, ensuring that the resulting lignin maintains similar characteristics regardless of the initial state of the downed timber.

Acknowledgements

The author would like to express immense gratitude to Dr. Maria Soledad Peresin for the opportunity to complete my Ph.D. under her exceptional supervision. These years have been an invaluable journey, thanks to your constant support, insightful guidance, and unwavering encouragement at every step. Your mentorship has extended far beyond academics, shaping my personal development in profound ways.

Special thanks to my Ph.D. committee members. Thank you, Dr. Brian Via, Dr. Adam Maggard, Dr. Yucheng Peng, Dr. Stephen Chmely, for your support and guidance during these years. I sincerely thank you for your invaluable help and knowledge throughout this academic journey. You have played a crucial role in my growth by providing insightful feedback and guidance. I am deeply grateful for the opportunity to learn and develop under your expertise. Thank you to my university reader, Dr. Hossein Jahromi.

The author extends sincere gratitude to Dr. Munkaila Musah for the extensive collaborative fieldwork that served as the foundation for this work. The author would like to thank Dr. Raquel Martín-Sampedro from the INIA-Forest Research Center for her invaluable advice and guidance during the chemical characterization and analysis of the core samples.

The author would like to thank the team from the Sustainable Bio-based Materials Lab for their hard work. Thank you for your passion towards our common research. My heartfelt appreciation goes out to everyone at the Forest Products Laboratory. Thank you for the wonderful moments and lasting memories. Working alongside you has been a genuine pleasure, and I've gained valuable insights from each of you. Gratitude extends to the dedicated staff, esteemed faculty, colleagues, and friends of the College of Forestry, Wildlife Science, and Environment.

Lastly, the author expresses heartfelt appreciation to his Mexican friends and the Auburn friends who have evolved into family over the years. Thank you for your enduring friendship and unwavering support. This journey would not have been as meaningful without each one of you.

To my dear grandmother Irma, words will never describe the chest pain of seeing you only in pictures or video calls at your sunset and not being able to travel and see you. The distance aches in my chest, a constant reminder of all the hugs I missed and the laughter we can't share again until I exit this world. To my uncle Oscar, your strength, humor, and generosity will continue to guide us through life's challenges, just as you always did. We'll miss you dearly, but your memory will forever be cherished.

To my wonderful parents, though distance keeps us apart, know that you're constantly in my thoughts. I dream of the day I can travel again and be there to shower you with love in person. Let's hold onto that hope and create even more beautiful memories together soon. Love you always. To my amazing brother and his wife, I am so inspired by the beautiful family you've built together. The way you support each other and prioritize quality time with each other truly warms my heart. I miss you both dearly and cannot wait to meet my niece. To my precious niece, welcome to the world! I can't wait to meet you and shower you with all my love. No matter what path you choose in life, know that I'll always be your biggest cheerleader, supporting you with open arms and unconditional love.

To my dear godson, maybe my journey of pursuing education can inspire you on your own path. Remember, challenges are inevitable, but they are also opportunities for growth. I believe in you and your strength to overcome any hurdle life throws your way. Even though I may not be there every step of the way, know that I'm always cheering you on and sending you all my love. I can't wait to see you again soon and hear all about your adventures.

To my beloved extended family, both those who have departed and those who remain—too numerous to count, like the stars in the sky. Throughout every step of my journey, I have carried each of you close to my heart. I am profoundly grateful for the unwavering love and support you continue to shower upon me. The knowledge that I am backed by such a strong and united family fills me with the courage to pursue my dreams. The invaluable lessons and enduring values instilled by all of you serve as the bedrock upon which I am constructing my future.

A mi querida abuela Irma, las palabras nunca describirán el dolor en el pecho al verte solo en fotos o videollamadas, viendo tu ocaso y sin poder viajar para verte. La distancia duele en mi pecho, un recordatorio constante de todos los abrazos que me he perdido y las risas que ya no podemos compartir. A mi tío Oscar, tu fuerza, humor y generosidad seguirán guiándonos a través de los desafíos de la vida, tal como siempre lo hiciste. Te extrañaremos mucho, pero tu memoria será recordada para siempre.

A mis maravillosos padres, aunque la distancia nos separe, sepan que están constantemente en mis pensamientos. Sueño con el día en que pueda viajar nuevamente y estar allí para colmarlos de amor en persona. Aferrémonos a esa esperanza y creemos aún más hermosos recuerdos juntos pronto. A mi hermano y su esposa, estoy inspirado por la hermosa familia que han construido juntos. La forma en que se apoyan mutuamente y priorizan el tiempo de calidad. Los extraño mucho y no puedo esperar para conocer a mi sobrina. A mi preciosa sobrina, ¡bienvenida al mundo! No puedo esperar para conocerte y colmarte con todo mi amor. No importa qué camino elijas en la vida, sabes que siempre seré tu mayor animador, apoyándote con los brazos abiertos y amor incondicional.

A mi ahijado, tal vez mi viaje en busca de la educación pueda inspirarte en tu propio camino. Recuerda, los desafíos son inevitables, pero también son oportunidades de crecimiento. Creo en ti y en tu fuerza para superar cualquier obstáculo que la vida te presente. Aunque no pueda estar allí en cada paso del camino, sabe que siempre estoy animándote. No puedo esperar para verte de nuevo pronto y escuchar todas tus aventuras.

A mi amada familia extendida, tanto a aquellos que han partido como a los que permanecen, demasiado numerosos para contar, como las estrellas en el cielo. A lo largo de cada paso de mi trayectoria, los he llevado a todos cerca de mi corazón. Agradezco profundamente el amor inquebrantable y el apoyo que continúan derramando sobre mí. El conocimiento de que cuento con una familia tan fuerte y unida me llena de valor para perseguir mis sueños. Las invaluables lecciones y valores perdurables inculcados por todos ustedes sirven como la base sobre la cual estoy construyendo mi futuro.

Table of Contents

List of Tables

List of Figures

List of Equations

1. Introduction

1.1. Impact of Hurricanes on timber economics on the US southeast

The impact of hurricanes on timber revenue can be significant, with billions of dollars at stake (Henderson et al., 2022). Past hurricane events, such as Hurricane Hugo in 1989 and Hurricanes Katrina and Rita in 2005, have resulted in substantial timber losses (Beven et al., 2008; Prestemon & Holmes, 1997). After hurricanes make landfall, forest landowners face numerous challenges that impact local economies, including quality degradation, price declines, salvage difficulties, and decay-related issues (Peralta et al., 1993; Taylor & Foster, 2005). The timber market experiences price depression during salvage sales, followed by a gradual recovery (Sun, 2016). To preserve timber value, landowners are advised to prioritize high-value products and initiate prompt recovery efforts (Van Hensbergen & Cedergren, 2021).

Despite salvage efforts, a significant untapped value remains in the damaged timber (Brandeis et al., 2022). Biorefinery operations and extracting natural polymers from biomass offer potential economic opportunities for utilizing degraded timber (Yamakawa et al., 2018). Biorefineries convert biomass into energy, chemicals, and polymers, contributing to a circular economy (Cherubini, 2010). The degraded DT can facilitate biological and chemical reactions in the polymer recovery process, supporting the development of high-end applications for natural polymers in various industries (Dutta & Saha, 2019; Martelli-Tosi et al., 2018; Vermaas et al., 2015).

The impact of natural disasters on economic variables has long been a subject of interest among researchers. In that regard, Hurricane Hugo (1989) has been subject to great study interest in U.S. Forest history. One of the first studies by Prestemon and Holmes found that Hurricane Hugo caused a 35% drop in pine sawtimber prices, which recovered within seven quarters. Pine pulpwood prices crashed by 60% initially and remained 35% lower than pre-Hugo levels for a more extended period (Prestemon & Holmes, 1997). The researchers employed a method to identify Hugo's price effect by comparing South Carolina’s

price series with the price series of the southern regions based on market cointegration. However, other authors have pointed out that caution should be exercised regarding the potential contamination of the results due to the employed methodology (Yin & Newman, 1999). Runsheng Yin and David H. Newman (1999), in their study employing intervention analysis and utilizing data from Timber Mart-South (TMS), sought to investigate the hypotheses regarding the effects of Hurricane Hugo on stumpage prices in the region (Yin & Newman, 1999). The researchers focused on the coastal plain region of South Carolina, using quarterly data from TMS spanning from the first quarter of 1977 to the fourth quarter of 1996. This dataset encompassed both hardwood and softwood stumpage prices for sawtimber and pulpwood. In their research, intervention analysis is a statistical technique that assumes that the time series, in the absence of the intervention, follows a pure autoregressive integrated moving average (ARIMA) process. The findings were that there was no significant immediate impact on hardwood pulpwood prices in South Carolina's market due to Hurricane Hugo. However, a gradual die-down price effect was observed in the hardwood sawtimber market, indicating a slow decrease in prices over time. No persistent price increase was observed in the hardwood sawtimber market. Unfortunately, specific findings regarding the pine pulpwood market were not mentioned.

Moreover, in another publication, Prestemon and Holmes (2000) found that Hurricane Hugo had both short-run (there was a 30% price decline due to salvage of damaged timber) and long-run (timber prices were estimated to be 10% to 30% higher than if the hurricane had not occurred) effects on the prices of timber stocks in the South Carolina Coastal Plain (Prestemon & Holmes, 2000). Their methodology included intervention analysis, impulse-response functions, and cointegration testing. In a subsequent study, Prestemon and Holmes (2004) utilized three valid replications for sawtimber and four for pulpwood to estimate the hurricane price effect equations. These replications compared South Carolina prices with submarkets from other states. The parameter estimates and standard errors were derived from these replications, and the bootstrap method was employed to account for variation and uncertainty (Prestemon & Holmes, 2004).

Furthermore, Prestemon and Holmes (2004) examined the challenges of determining the appropriate assumption of price behavior in the timber industry. They used Monte Carlo simulations to demonstrate how aggregating observations and temporal averaging can influence unit root tests on timber prices. The authors find that recognizing temporal aggregation errors can lead to unit root tests favoring stationarity, particularly for pulpwood stumpage. The study highlights the significance of considering data problems and temporal aggregation complexities when analyzing timber prices. The authors sourced data from the United States Department of Commerce for the Producer Price Index (PPI) and Consumer Price Index (CPI). Nevertheless, they do not specify if they used the general US or a particular index. Stock market returns were obtained from the average value of investments, including reinvested dividends, based on the Standard and Poor's 500 index for deflating timber prices (Prestemon et al., 2004).

Finally, Prestemon and Holmes (2010) utilized a welfare approach to measure the implications of Hugo and more recent Hurricanes. Initially, consumer welfare increased due to lower prices and increased quantity consumed. Undamaged producers experienced a brief negative impact from salvage activities, while damaged producers were able to capture some value for a few quarters. However, in the long term, consumers were harmed, undamaged producers benefited, and damaged producers faced losses. Their conclusions point to prices in the sawtimber market returning to pre-storm levels around 2012, approximately 90 quarters (23 years) after the hurricane (Prestemon & Holmes, 2010). In recent times, Ivan and Frances in 2004 and Katrina and Rita in 2005 had significant impacts on the timber market and landowners in their landfall areas (Beven et al., 2008; Franklin et al., 2006). The combined damage from Katrina and Rita was at least double that caused by Hurricane Hugo in 1989 (Blake et al., 2011). Hurricane Michael in 2018 affected an estimated 2.8 million acres of forest land (Florida Forest Service, 2018).

The timber market in the southeastern United States holds significant importance within the forest products industry. This region is renowned for its vast pine and hardwood forests, making it one of the country's largest timber-producing areas (Prestemon & Abt, 2002). Various stakeholders contribute to the industry, including timberland owners, sawmills, pulp and paper mills, and various wood products

manufacturers (M. Zhang et al., 2011). Public interest in timber assets to hedge against inflation has grown (Chudy & Cubbage, 2020). Timberland can hedge inflation based on three advantages: biological growth, timber price change, and land appreciation (Lappalainen, 2023). Ownership of timberland has shifted from vertically integrated forest products companies to institutional investors like pension funds, mutual funds, university endowments, foundations, private owners, and publicly traded timber real estate investment trusts (Zhang et al., 2011). In recent decades, organizations such as Timber Investment Management Organizations (TIMOs) and Real Estate Investment Trusts (REITs) control nearly 5% of the total forestland in the US and about 7% of the timberland (Fernholz et al., 2007). Some of these organizations are listed as stocks themselves (for example, Weyerhaeuser or Rayonier) or as part of an exchange-traded fund (ETF) (D. Zhang et al., 2012). These trusts provide a transparent and accessible platform for investors to access the timber market while offering valuable data and insights into market trends, performance, and financial indicators (Mendell et al., 2007). Through data mining techniques, investors and researchers can analyze historical patterns and identify market trends (Angadi & Kulkarni, 2015).

Accurate forecasts of stumpage prices after adverse weather events are crucial for investment decisions and salvage operations (Stanturf et al., 2007). The Timber Mart-South (TMS) quarterly reports provide a primary database of stumpage prices, but more detailed and up-to-date market insights are needed (Martin et al., 2007). However, in today's rapidly evolving information technology landscape, more than quarterly or even monthly data might be needed for organizations seeking detailed market insights (Modugno, 2013).

In addition to the economic challenges hurricanes pose on timber revenue, analyzing the impact and understanding the patterns of hurricane events is crucial for effective planning and mitigation strategies (Clarke et al., 2023). Wavelet analysis offers a powerful tool for examining and reconstructing time series data, including studying hurricane events (Cazelles et al., 2008). Wavelet analysis provides a comprehensive approach to analyzing time series data’s temporal and frequency characteristics (Rhif et al., 2019). It allows for the decomposition of a signal into different frequency components, enabling the

identification of localized variations and patterns at different scales (Martínez & Gilabert, 2009). This analysis technique has been widely used in various fields, including signal processing, image analysis, and geophysics (Kumar & Foufoula-Georgiou, 1997; W. Liu & Chen, 2019; Rhif et al., 2019). More recently this procedure has been used in analyzing the synchronized movement between US lumber futures and southern pine sawtimber prices during COVID-19 events (Gan et al., 2022).

This research aims to address the challenges of forecasting stumpage prices accurately by analyzing local market price variations resulting from recent high-cost hurricane seasons. The primary data source for this analysis will be the Timber Mart-South (TMS) database. Additionally, the study will explore the availability and frequent updates of open-access market data. By examining the price correlation between TMS and open-access market indices, this research seeks to provide organizations and individuals with additional data sources and techniques to enhance their ability to forecast stumpage prices reliably and more dynamically. Ultimately, the study supports the idea of bridging the market gap through the biorefinery business, maximizing the utilization of biomass that would otherwise remain unexploited and that is widely available at discounted prices.

1.2. Southeastern US Timber Market

The southeastern US timber market is a significant component of the forest products industry in the United States. The region is one of the largest timber-producing areas in the country, with significant amounts of pine and hardwood forests. The industry in the southeastern US is made up of a wide range of stakeholders, including timberland owners, sawmills, pulp and paper mills, and other wood products manufacturers (M. Zhang et al., 2011). A variety of factors, including supply and demand, weather conditions, transportation costs, government regulations, and international trade policies influence the market for timber in the southeastern, US. In recent years, the market has been affected by several trends, including increased demand for wood pellets for bioenergy production, changes in forest ownership patterns, and shifts in global trade patterns.

In recent years, investors has been increasingly interested in timber assets to hedge against inflation. Timberland ownership has changed considerably from vertically integrated forest products companies to institutional investors like pension funds, mutual funds, university endowments, foundations, private owners, and more publicly traded timber real estate investment trusts (Binkley & Zhang, 2021; M. Zhang et al., 2011). Timberland can hedge inflation based on three advantages: biological growth, timber price change, and land appreciation. The first can be analyzed in two factors: the growth in volume and the growth into larger and more valuable product classes (M. Zhang et al., 2011).

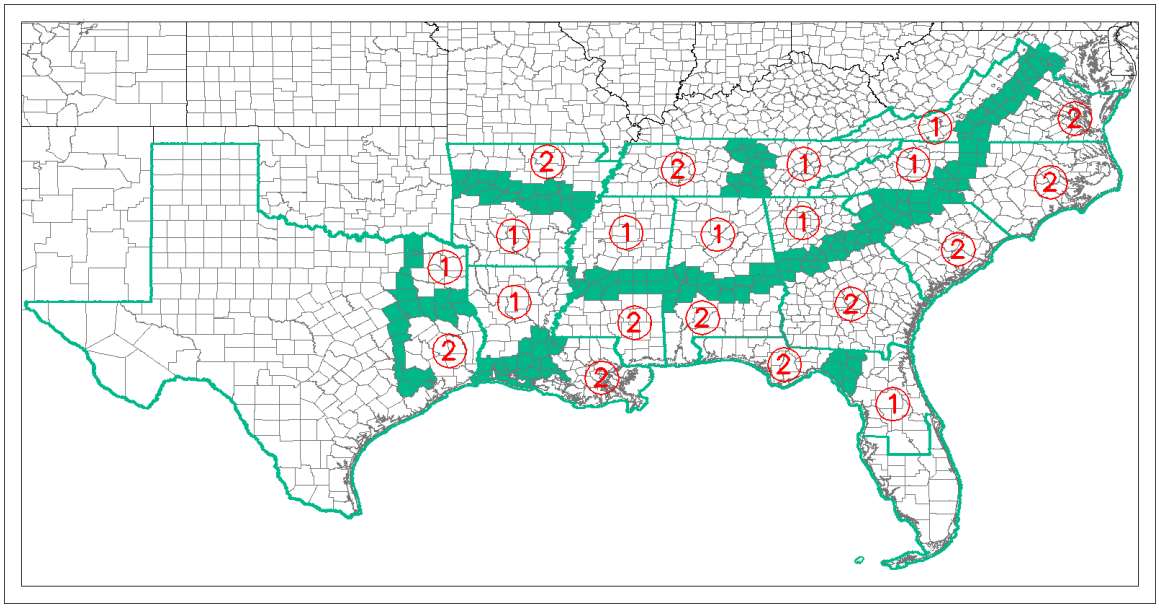

Figure 1.1. Southeastern US Timber Market. Regions marked as reported in quarterly TMS report (TimberMart-South | Resources, 2023).

Overall, the southeastern US timber market plays a critical role in the forest products industry, providing a key source of raw materials for many products, including lumber, paper, and bioenergy. The market is subject to a range of economic, environmental, and social pressures and is likely to continue to evolve in response to changing market conditions and emerging trends. The Southeastern US Timber Market consists of states from the Gulf of Mexico, the South Atlantic, and two interior states: Texas,

Louisiana, Arkansas, Tennessee, Mississippi, Alabama, Georgia, Florida, South Carolina, North Carolina, and Virginia (**Figure 1.1)**.

1.3. Saffir-Simpson Hurricane Wind Scale

The Saffir-Simpson Hurricane Wind Scale (SSHWS) is a 1 to 5 rating based on a hurricane's maximum sustained wind speed, where the maximum sustained wind speed is measured as the peak 1-minute wind at the standard meteorological observation height of 10 m [33 ft] over unobstructed exposure (Saffir, 1973). Earlier definitions of the scale in the 70s - 80s also incorporated the central pressure and storm surge as components. This was due to the reduced availability of aircraft reconnaissance measurements before 1990 (Sheets, 1990). Nowadays, the scale does not address the potential for other hurricane-related impacts, such as storm surges, rainfall-induced floods, and tornadoes. The scale was originally developed by wind engineer Herb Saffir and meteorologist Bob Simpson (National Hurricane Center, 2021). Additionally, it is common for tornadoes to occur in areas affected by severe weather systems. Tornadoes can form in the outer bands or ahead of the central storm systems, and their paths can vary, affecting different regions within the impacted states.

Table 1.1. Saffir Simpson Hurricane Wind Scale

Hurricane Category	Maximum Sustained Winds km/h [mph]	Types of Damages Expected
1	119 – 153 [74 - 95]	Large branches of trees will snap, and shallowly rooted trees may be toppled.
2	154 – 177 [96 – 110]	Many shallowly rooted trees will be snapped or uprooted and block numerous roads.
3*	178 – 208 [111 – 129]	Many trees will be snapped or uprooted and power poles downed.
4*	209 – 251 [130 -156]	Most trees will be snapped or uprooted and power poles downed.
5*	> 252 [> 157]	Catastrophic damage will occur.

*Hurricanes rated Category 3 and higher are known as major hurricanes (National Hurricane Center, 2021).

1.4. Atlantic Hurricane Seasons

The Atlantic hurricane season is the period in the North Atlantic Ocean during which tropical cyclones, known as hurricanes or tropical storms, are most likely to occur. The official Atlantic hurricane

season runs from June 1st to November 30th each year, although hurricanes can occasionally form outside of this timeframe. This period was chosen because it encompasses the time when ocean and atmospheric conditions are most conducive to developing these storms. During the Atlantic hurricane season, warm ocean waters provide the energy needed for tropical cyclones to strengthen, and other atmospheric factors, such as low wind shear and high humidity, contribute to their formation and intensification. As the season progresses, conditions can become less favorable, leading to a decline in storm activity toward the end of November.

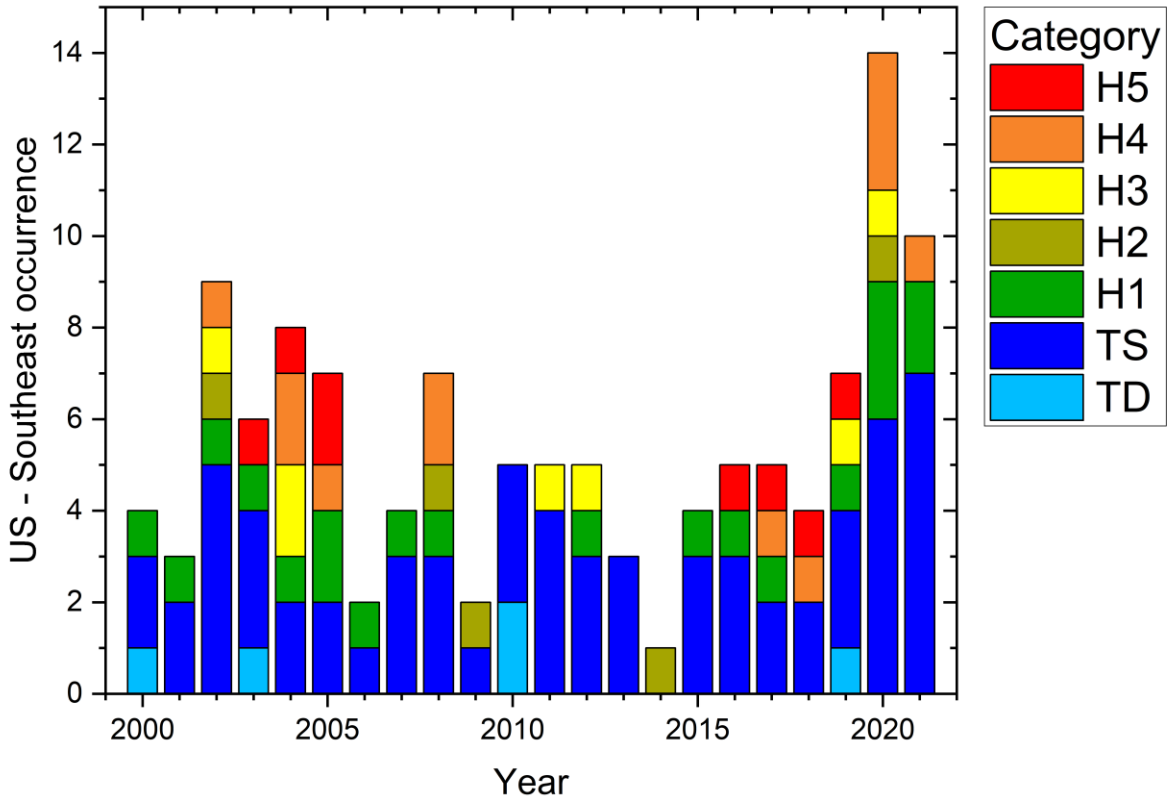

Figure 1.2. Atlantic Storms affecting the US southeast. Data compiled from (NOAA, 2022)

Figure 1.2 provides an insightful representation of the maximum category achieved by hurricanes that have affected the southeast timber market in the Atlantic basin in the first 20 years of the new millennium. It is important to note that this maximum category often does not match the landfall category of the storm.

1.4.1. 2018 Hurricane season

The hurricane season, especially the occurrence of Hurricane Michael, offered the justification and resources appropriation for this research. **Figure 1.3** shows the tracked storm paths for the 2018 Atlantic hurricane season. Hurricane Florence became a hurricane on September 4 and underwent rapid intensification, reaching Category 4 status by the following day. It achieved a significant milestone by becoming the farthest northeast Category 4 hurricane in the Atlantic during the satellite era. However, increased wind shear caused rapid weakening, and Florence weakened to a tropical storm on September 7. Florence regained hurricane status on September 9 and underwent a second period of rapid intensification, reaching Category 4 intensity again on September 10. After further strengthening, it reached its peak intensity on September 11 with maximum sustained winds of 150 mph (240 km/h) and a minimum pressure of 937 mbar (27.7 inHg). Weakening ensued due to upwelling and eyewall replacement cycles, and Florence fell below major hurricane status on September 13 as it approached the Carolinas. It made landfall near Wrightsville Beach, North Carolina, as a Category 1 hurricane with winds of 90 mph (150 km/h) on September 14. Moving towards the southwest along the coast, Florence weakened to a tropical storm over eastern South Carolina on September 15 and further weakened to a tropical depression over the western part of the state on the following day before turning northward. It transitioned into an extratropical system over West Virginia and continued northeastward, dissipating over Massachusetts on September 18 (Avila, 2019a).

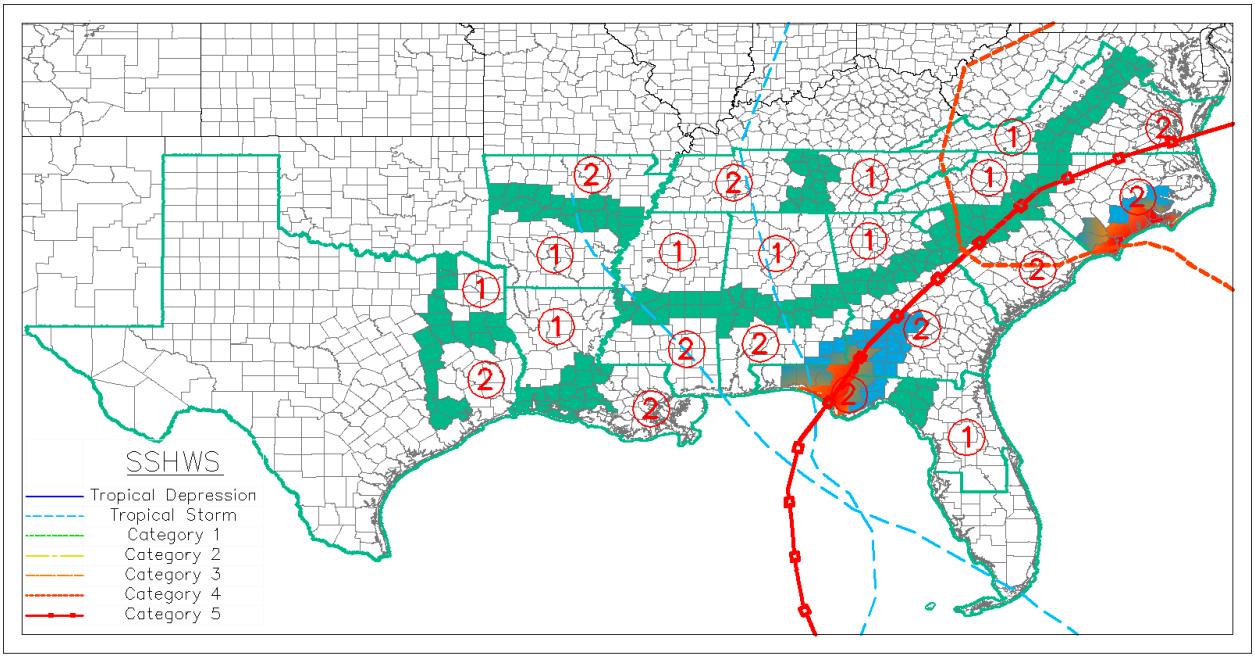

Figure 1.3. Storms tracks of the 2018 Atlantic Hurricane Season. Areas in red indicate the highest damage produced to timber (A Bird's Eye View: Aerial Surveyors Map Timber Damage from Hurricane Florence | In the Field, 2018; Florida Forest Service, 2018).

Florence brought catastrophic flooding to North Carolina and South Carolina. In North Carolina, the storm set a record as the rainiest tropical cyclone in the state's history, with a maximum precipitation total of 35.93 inches (913 mm) near Elizabethtown. The overall damage in North Carolina amounted to approximately $22 billion (*A Bird's Eye View: Aerial Surveyors Map Timber Damage from Hurricane Florence | In the Field*, 2018). In South Carolina, Florence also became the wettest tropical cyclone on record, with a maximum precipitation total of 23.63 inches (600 mm) in Loris. Though the flooding was not as severe as in North Carolina, the storm caused a multi-billion dollar disaster, resulting in around $2 billion in damages (US Department of Commerce, 2018). Virginia experienced minor flooding and the formation of 11 tornadoes caused by Florence. Overall, Florence claimed the lives of 54 people and caused just over $24 billion in damages (Avila, 2019a).

Hurricane Michael underwent rapid intensification and became a hurricane around midday on October 8. Continuing to strengthen, the storm reached the Gulf of Mexico a few hours later and became a

major hurricane late on October 9. At 17:30 UTC on October 10, Michael made landfall near Panama City, Florida, as a Category 5 hurricane with maximum sustained winds of 160 mph (260 km/h) and a minimum central pressure of 919 mbar (27.1 inHg). Michael became the most intense storm of the season and the third-strongest hurricane to make landfall in the United States in terms of central pressure. After landfall, Michael quickly weakened over land, transitioning to a tropical storm over Georgia on October 11. By October 12, it became an extratropical cyclone over Virginia.

The Florida Panhandle, including Mexico Beach, Panama City, and Panama City Beach, suffered catastrophic damage from Hurricane Michael. More than 45,000 structures were damaged, and over 1,500 were destroyed in Bay County alone. Significant wind damage extended inland, with approximately 1,000 structures experiencing substantial damage or destruction in Jackson County. In Georgia, Seminole County saw 99% of homes affected to some degree, and damage was reported in thousands of other homes as far north as Dougherty County. Southeastern Alabama also experienced extensive wind damage. The remnants of Michael caused flooding in western North Carolina and Virginia, with a maximum precipitation total of 13.01 inches (330 mm) near Black Mountain, North Carolina. Across Florida, Georgia, North Carolina, and Virginia, at least 59 people lost their lives, with the majority of the fatalities occurring in Florida. The property damage in the United States from Hurricane Michael was estimated to be at least $25 billion (Florida Forest Service, 2018).

Atlantic Hurricane seasonal boundaries:

- 2017 → First system formed: Apr 19. Last system dissipated: November 9.
- 2018 → First system formed: May 25. Last system dissipated: October 31.
- 2019 → First system formed: May 20. Last system dissipated: November 24.

1.5. Price Data from Timber Marth South

Timber Mart-South (TMS) is a price reporting service that provides market information and pricing data for timber and wood products in the southeastern United States. It is based on a voluntary reporting

system in which timber buyers, sellers, and brokers report prices for various timber and wood products, including sawtimber, pulpwood, and wood chips. It collects and compiles data on timber prices from various sources, including private timberland owners, wood products manufacturers, logging contractors, and state and federal agencies. The University of Georgia (UGA) Warmell School of Forestry & Natural Resources is contracted with the Frank W. Norris Foundation to compile and publish TMS quarterly reports, available via paid subscription (Avila, 2019a).

TMS provides quarterly reports with stumpage and delivered statewide prices of major timber products for 11 states in the US South. Each state is separated into two sub-regions and average prices are reported for the entire state and both sub-regions within a state as in **Figure 1.1**. These regions were restructured in the first quarter of 1992. From 1977 to 1987, TMS published monthly data. After 1988, the data started to be published quarterly, and the previous monthly data was averaged to fit the quarterly reports. The reports are also used by government agencies, academics, and researchers to analyze market trends and inform policy decisions related to forestry and natural resource management (*TimberMart-South | Resources*, 2023). The prices are categorized and reported in three main groups: pulpwood, chip-n-saw, and sawtimber. The categories are defined by the diameter at breast height (DBH), 6" & up, 8"-11", 12" & up, respectively. The stumpage and delivered prices are published in $/ton, and States/areas using other measurements are adjusted for comparative purposes.

As per TMS disclaimer: "Data published is gathered from sources considered reliable. However, we are not responsible for errors or omissions. Information is gathered and published as it exists, and each price is independently determined; that is, not based on mathematical relationships with other items. No attempt to set or influence prices is intended. These are not absolute lows or highs, but an average of lows and average of highs. Specific prices, because of variations in fieldwork and time element, sometimes result in prices which are somewhat lower or higher than those published. Be aware that prices vary greatly depending on many factors and a reported price does not represent the only price at which an item has been sold". Finally, TMS does not normally include salvage sales or special products in the State or Complete

reports. These prices appear in the Logging Rates & Other Products report (TimberMart-South | Resources, 2023).

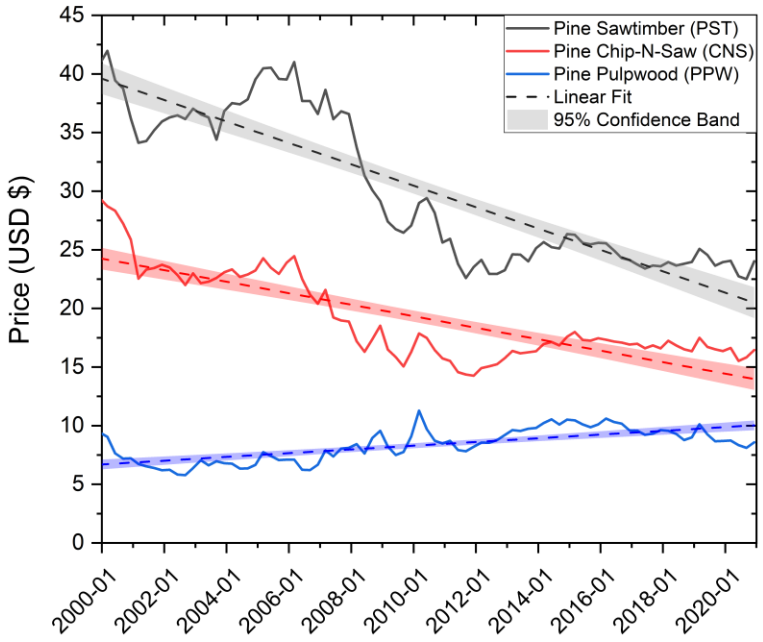

Figure 1.4. Linear fit and 95% confidence interval. Nominal prices.

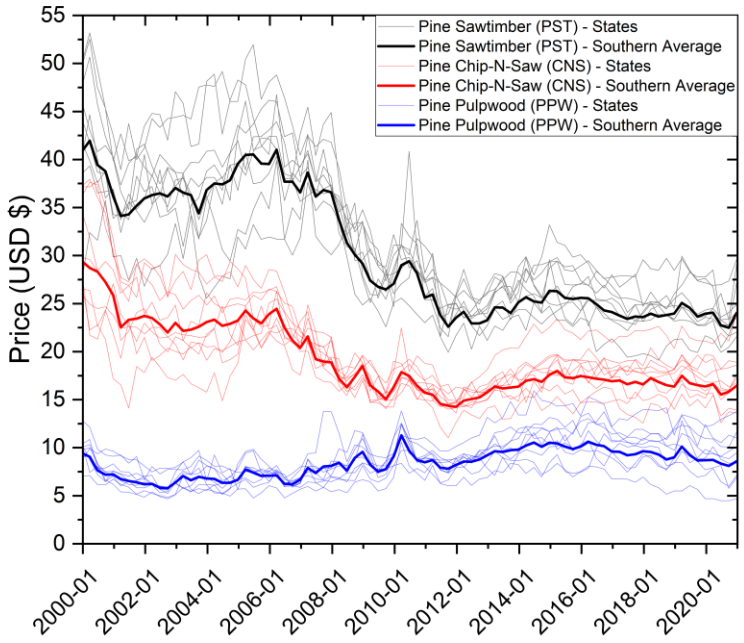

Figure 1.5. Southern average and individual state stumpage price indices. Nominal prices. This figure shows individual states price series for each of the pine products in the TMS quarterly reports and product average for the southeastern market.

For analysis involving long time periods, it is frequently necessary to convert current or nominal dollars into constant or real dollars. This is done by multiplying each dollar amount by a ratio of price indexes (Perrins & Nilsen, 2010).

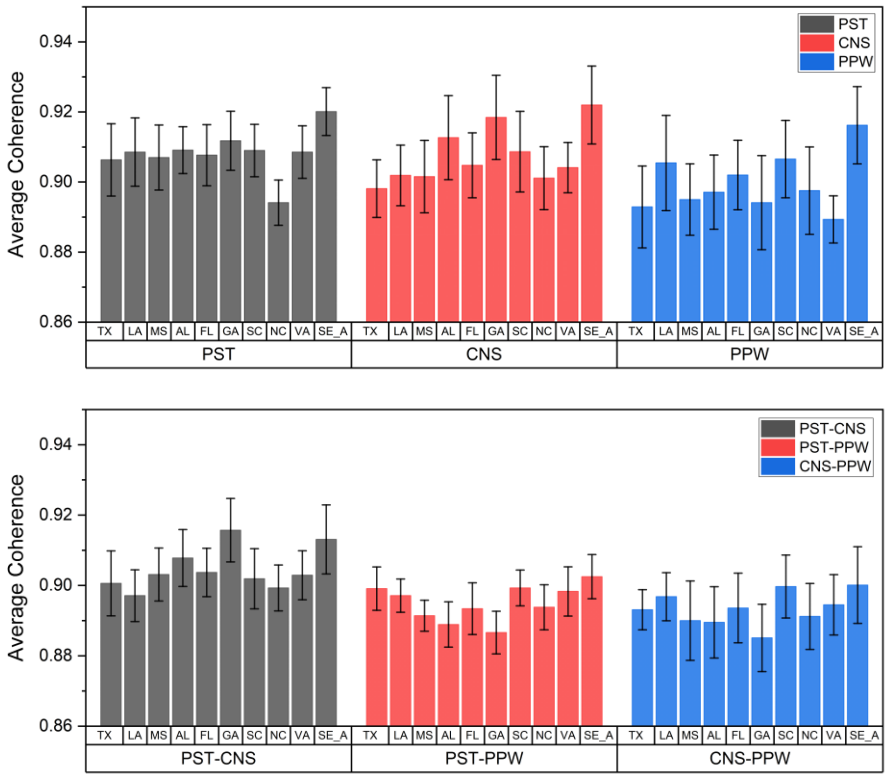

Figure 1.6. Average Coherence between states and product.

1.6. Open Market High Frequency sources

ETF, REIT, Stock, and Futures are financial instruments traded in financial markets. ETF (Exchange-Traded Fund): An ETF is an investment fund that trades on an exchange, like a stock. It's a basket of securities that tracks an underlying index, commodity, or other asset. ETFs provide diversification across many different securities, making them a popular choice for individual investors who want exposure to a particular sector or asset class. Real Estate Investment Trust (REIT) is an investment vehicle that owns and operates income-generating real estate properties. Investors can buy shares in a REIT, which gives them access to a portion of the income and profits generated by the real estate holdings. Stock: A stock, also known as a share or equity, represents ownership in a company. When a stock is purchased, a small piece of the company is bought, and the purchaser becomes a shareholder. Stocks are bought and sold on stock exchanges, and their price can fluctuate based on the company's financial performance, market conditions,

and other factors. Futures: A futures contract is a standardized agreement to buy or sell an underlying asset at a specified price and date in the future. Futures can be traded on commodities like gold, oil, or wheat, and financial instruments like stock indexes and currencies. Traders use futures to speculate on price movements, hedge against potential losses, or as a way to lock in a price for a future transaction.

Table 1.2. Financial instruments.

Type	Series ID	Series Title	Data Since	Periodicity[1]
ETF	WOOD	iShares Global Timber & Forestry ETF	June-25-2008	Quarterly, Monthly, Weekly, Daily
REIT	PCH	PotlatchDeltic Corporation	Jan-01-1969	Quarterly, Monthly, Weekly, Daily
REIT	RYN	Rayonier Inc.	Feb-17-1994	Quarterly, Monthly, Weekly, Daily
Stock	WY	Weyerhaeuser Company	Jan-02-1968	Quarterly, Monthly, Weekly, Daily
Stock	ADN[2]	Acadian Timber Corp	Jan-31-2006	Quarterly, Monthly, Weekly, Daily
Futures	LBS1!	Random length lumber futures	Nov-16-1972	Quarterly, Monthly, Weekly, Daily

[1]Some instruments are available for up to 1-hour frequencies.
[2]In CAD ($).

The iShares Global Timber & Forestry ETF (WOOD) is an exchange-traded fund that invests in companies involved in producing and distributing timber and forestry products. The companies in the index and the ETF are involved in a wide range of activities related to timber and forestry, including logging, wood processing, paper and packaging production, and distribution of forestry products. Some of the largest holdings in the iShares Global Timber & Forestry ETF include companies such as West Fraser Timber Co. Ltd, Rayonier Inc., and Canfor Corporation. The ETF provides investors with exposure to the global timber and forestry industry, which is influenced by various factors such as supply and demand for wood products, economic conditions, and environmental regulations. The ETF is a diversified investment that can hedge against inflation, as timber prices tend to rise with inflation. However, like any investment, there are risks associated with the ETF, such as market volatility and changes in the regulatory environment.

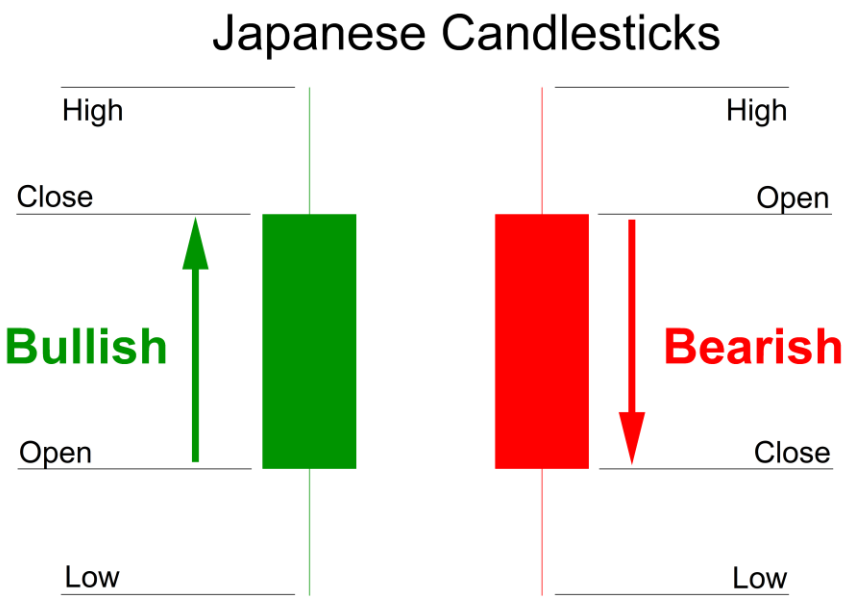

Figure 1.7. Japanese Candlesticks interpretation (Nison, 2001).

PotlatchDeltic Corporation (PCH) is a publicly traded company on the NASDAQ stock exchange that produces and sells lumber, plywood, and other wood products in the United States. It also operates timberlands, which are used to grow and harvest trees for its wood products. As a common stock, PCH represents ownership in the company and gives investors the right to vote on important company decisions, such as the election of board members and significant acquisitions or mergers. Common stockholders also have the potential to receive dividends if the company chooses to distribute profits to its shareholders. The value of PCH's common stock can fluctuate based on various factors, including the company's financial performance, market conditions, and investor sentiment. Investors can buy and sell PCH's common stock on the NASDAQ exchange through a brokerage account. As with any investment, risks are associated with investing in PCH's common stock, including the possibility of losing money if the value of the stock declines.

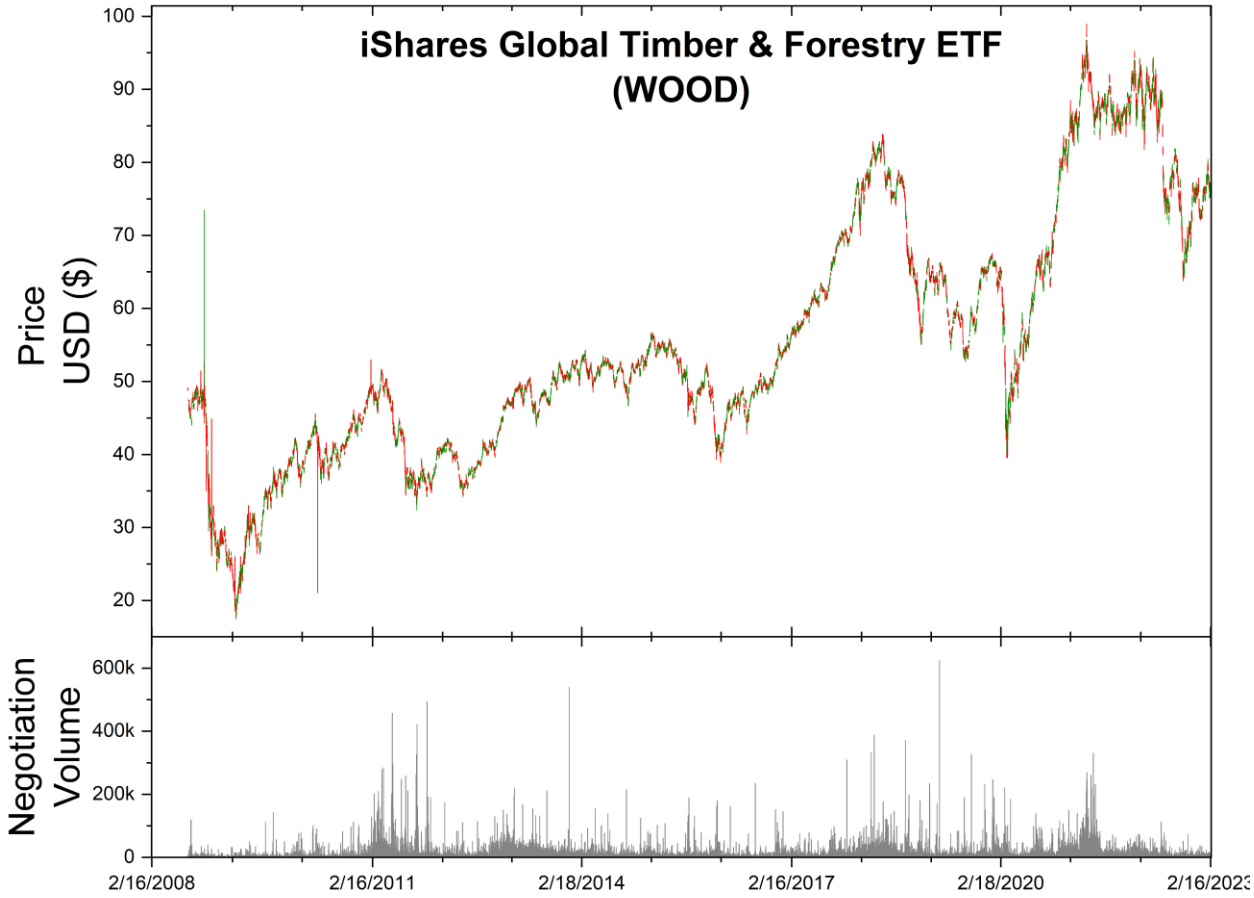

Figure 1.8. WOOD ETF Daily market data (*NASDAQ Stock Market*).

Rayonier Inc. (RYN) is a Real Estate Investment Trust (REIT) that operates in the timberland and forest products industry. As a REIT, Rayonier Inc. owns and manages land and natural resources, primarily in the United States and New Zealand, focusing on sustainable forestry practices. Rayonier's timberland assets are used to produce and sell various forest products, including logs, wood fiber, and biomass. The company also engages in activities related to producing renewable energy from its forest resources. As a REIT, Rayonier is required by law to distribute at least 90% of its taxable income to its shareholders in the form of dividends. This means that investors who own shares in Rayonier have the potential to receive regular dividend payments, which can provide a steady source of income. Investing in Rayonier as a REIT offers the potential for capital appreciation and dividend income while also providing exposure to the timberland and forest products industry. However, as with any investment, risks are associated with

investing in Rayonier's REIT, including changes in market conditions, fluctuations in commodity prices, and regulatory changes that could impact the company's operations.

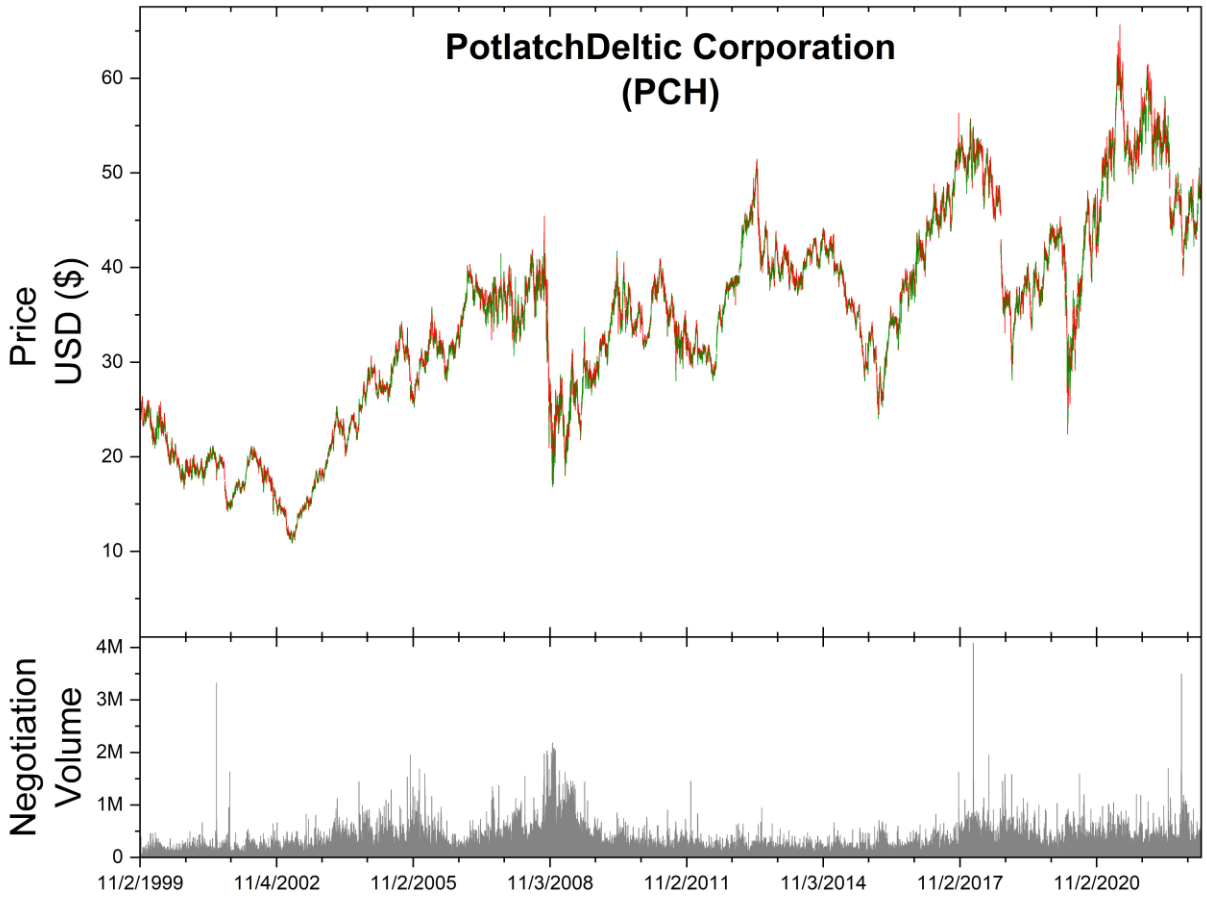

Figure 1.9. PCH-REIT Daily market data (*NASDAQ Stock Market*).

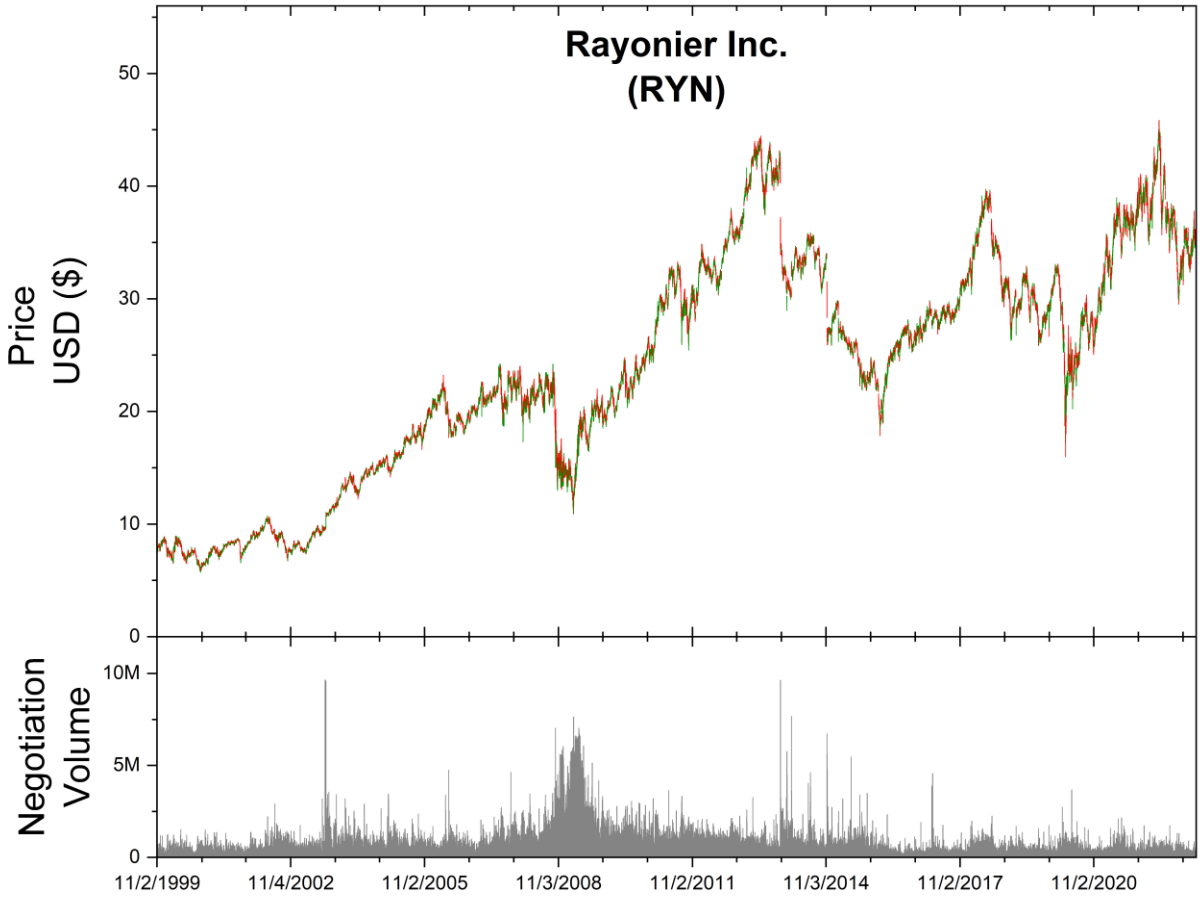

Figure 1.10. RYN-REIT Daily market data (*NASDAQ Stock Market*).

Weyerhaeuser Company (WY) is a timberland owner and operator engaged in producing, distributing, and selling forest products. The company operates in North America other regions worldwide. Weyerhaeuser owns and manages timberlands used to grow and harvest trees for various forest products, including lumber, plywood, and other building materials. In addition, the company also operates facilities for the manufacture of cellulose fibers, which are used in a range of products such as textiles and personal care items. As a publicly traded company, Weyerhaeuser's common stock is listed on the New York Stock Exchange and can be bought and sold through a brokerage account.

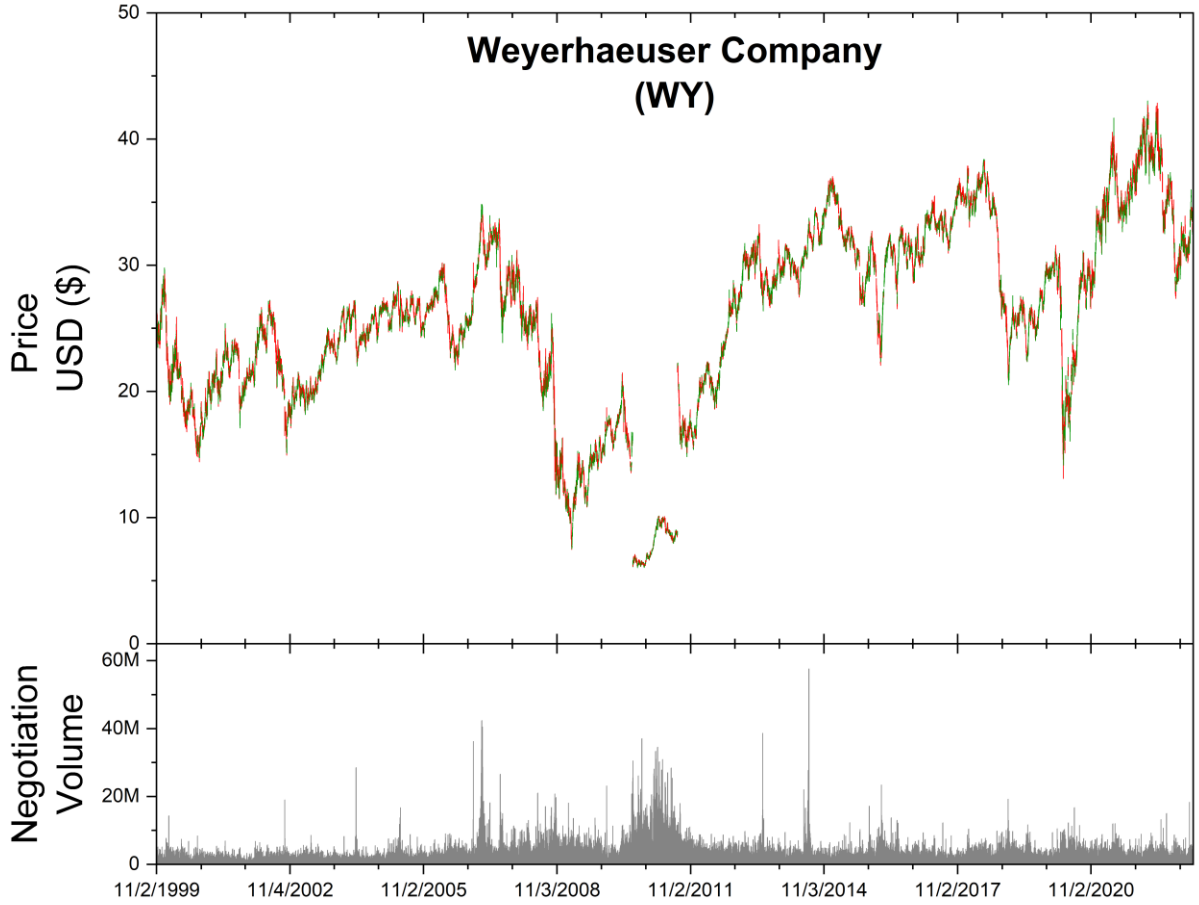

Figure 1.11. WY-Stock Daily market data.

Figure 1.12. ADN-Stock Daily market data.

Random Length Lumber futures are a type of commodity futures contract that are traded on the Chicago Mercantile Exchange (CME). The futures contract represents an agreement to buy or sell a standardized quantity of lumber at a predetermined price and delivery date in the future. Random Length Lumber futures are used as a tool for hedging and speculation by market participants, including lumber producers, wholesalers, retailers, and speculators. Producers and wholesalers can use futures contracts to lock in a price for their lumber products in advance, reducing the risk of price fluctuations. On the other hand, retailers can use futures contracts to manage their inventory and ensure a steady supply of lumber products at a predictable cost. Various factors, including supply and demand factors, market conditions, and macroeconomic trends, influence the price of Random Length Lumber futures. Trading in lumber

futures requires a high level of expertise and involves risks, such as the potential for loss due to fluctuations in the market price.

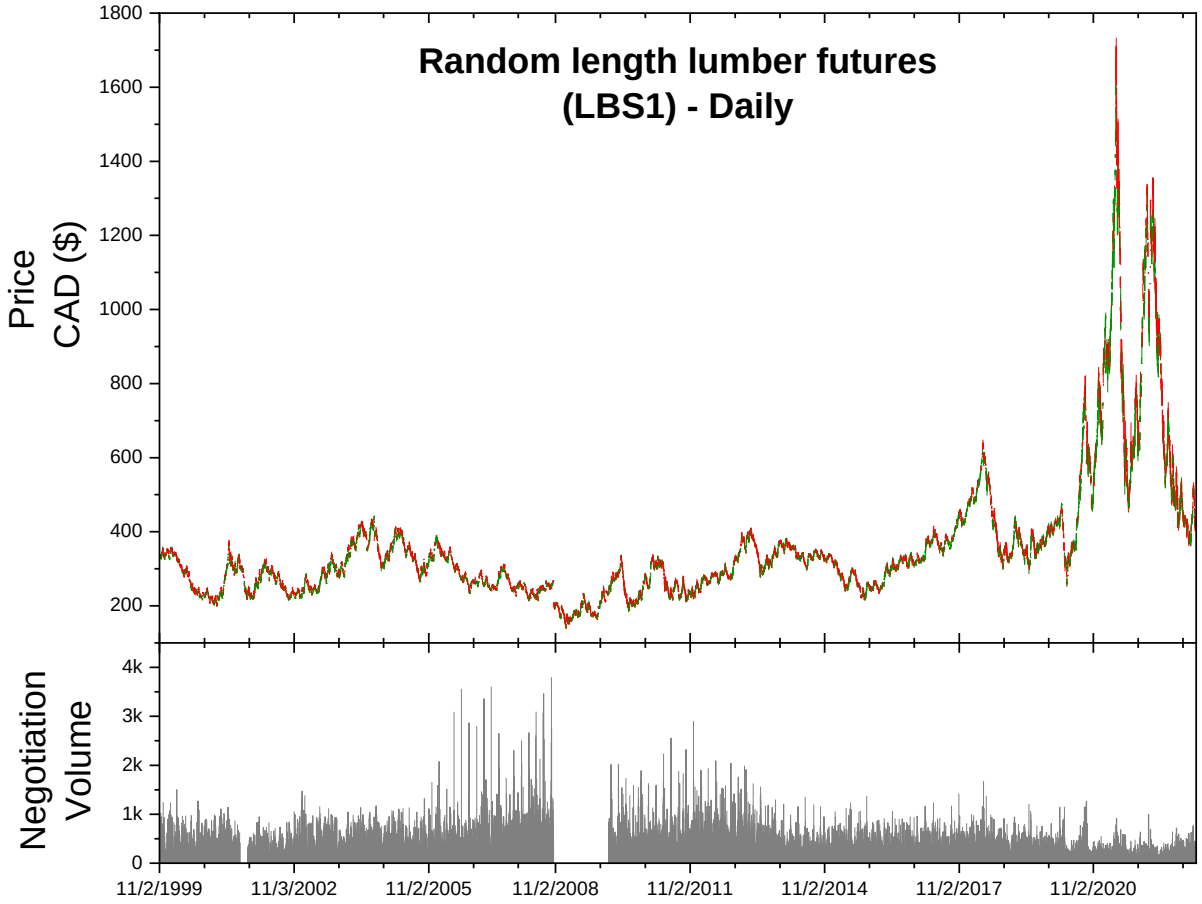

Figure 1.13. LBS1-Futures Daily market data.

1.7. Downed timber predictive modeling

As one of the dominant silvicultural species in the US Southeast, loblolly pine (Pinus taeda L.) has received attention from a growing group of researchers on many fronts, including the development of rapid and non-destructive methods for measuring wood properties (Jones et al., 2006). Near-infrared (NIR) spectroscopy, jointly with multivariate statistical techniques, has long been employed to characterize wood and various forms of biomass (Marten et al., 1985). Over time, this approach has matured, allowing for

more precise and insightful analyses. NIR offers advantages over other characterization techniques, like non-destructive acquisition and portability in the field (Kelley, Rials, Groom, et al., 2004). Early applications of NIR in forestry included cellulose and lignin content on foliage using a range of statistical techniques like partial least squares (PLS) (Aber et al., 1994; Newman et al., 1994). Complete analysis of the chemical composition of wood, e.g., cellulose, lignin, hemicellulose, glucose, xylose, and acetyl, can also be conducted with NIR (L. R. Schimleck et al., 2021). Most reports have focused on the full spectrum using the full NIR spectral range (1000 nm to 2500 nm) because it contains the most distinct spectral information on the first overtone and combination bands (Kelley, Rials, Groom, et al., 2004).

In NIR analysis for wood, prevalent approaches involve spectral preprocessing, such as utilizing first or second derivatives, employing multiplicative scattering correction, signal smoothing, and noise reduction (Hao et al., 2021). One significant advantage of using the first derivative is its ability to remove any baseline variation that could increase the noise in the data (B. K. Via & Jiang, 2013). Advanced statistical techniques such as PLS regression have emerged as powerful tools for creating predictive models of NIR for wood. PLS excels in modeling relationships between datasets, deftly handling multicollinearity and accommodating collinear responses, making it indispensable for unraveling the complexities of wood composition.

The less frequently used Principal Component Regression (PCR) technique, which integrates Principal Component Analysis (PCA) and regression modeling, has been used for managing multicollinearity and optimizing predictive performance, particularly in the context of high-dimensional datasets prevalent in wood analysis (B. Via et al., 2012). Usually, the PLS technique has been preferred by researchers, although some reports have proposed hybrid use of both (Fang et al., 2011). Conversely, PCR has exhibited more precise loading peak estimates to interpret results (B. K. Via et al., 2014). However, a Box-Behnken design proved competitive advantages for nonlinear calibration models with reduced sample size (B. Via et al., 2012). The Box-Behnken design is a powerful tool in response surface methodology, a statistical technique for optimizing processes by understanding how multiple factors influence a desired

outcome (Zhu & Liu, 2013). With three levels per factor, a focus on quadratic relationships, and an absence of embedded factorial designs, it minimizes experimental runs while providing robust insights. Visualized as a cube, it strategically places experiments, balancing efficiency and comprehensive exploration (Dean et al., 2017).

The usage of machine learning (ML) in forestry as an addition to traditional statistical analysis has become a viable option for data post-processing due to its ability to generalize models, increase the accuracy of parameter estimations, and provide better feature prediction (Z. Liu et al., 2018; Nasiri et al., 2022; Pham et al., 2020). The quality of many forest and forest products has been predicted using a combination of ML and near-infrared methodologies such as wood physical properties like MOE or MOR (L. Schimleck et al., 2023) nitrogen contents in trees (Prado Osco et al., 2019), biomass and estimation (Tao et al., 2020), presence of wood defects (Sandak et al., 2020), and pellet quality (Mancini et al., 2020). However, there are limited studies on the prediction of wood composition and wet chemistry (Yang et al., 2020).

The objectives of this study were to integrate nonlinear techniques synergistically with mathematical pretreatment, specifically the use of the first derivative, and incorporate a Box-Behnken design to reduce the required sample size for wet chemistry substantially. The focus was developing equivalently accurate and efficient predictive models for characterizing wood components in downed loblolly pine timber. By combining advanced statistical methodologies, such as Support Vector Machines (SVM) and Principal Component Regression (PCR), with the strategic design principles of the Box-Behnken approach, we aimed to optimize the modeling process. This innovative integration aimed not only to enhance the precision of predictions but also to minimize the resource-intensive nature of traditional approaches, paving the way for more cost-effective and sustainable practices in the field of wood composition analysis.

1.8. Downed timber deterioration rates

Natural disasters, such as hurricanes, profoundly impact various aspects of the environment and economy, often leaving a trail of destruction in their wake. Among the many domains affected, the timber industry is a prime example of an economic sector that bears the brunt of nature's fury. The intersection of meteorological events and timber revenue is underscored by staggering financial implications, with billions of dollars hanging in the balance (Henderson et al., 2022). Historical hurricanes, like Hurricane Hugo in 1989 and the catastrophic tandem of Hurricanes Katrina and Rita in 2005, have spotlighted the intense losses inflicted upon the timber sector (Beven et al., 2008; Prestemon & Holmes, 1997).

Beyond the financial setbacks, the implications of this downed timber (DT) cascade across a spectrum of environmental concerns. Microbial and insect proliferation threatens forest ecosystems, while the DT potential as fuel for wildfires amplifies the risk of catastrophic blazes (Johnson et al., 2023; Radu, 2006). Wildlife habitat degradation, operational delays in harvesting, and increased costs compound the challenges. The consequential loss of carbon sequestration capacity in standing trees bears wider-reaching impacts on atmospheric carbon dioxide levels (Russell et al., 2015).

Moreover, the journey of Hurricane DT does not end with its initial salvage. Instead, much of this resource is relegated to low-value applications, such as pulp mill furnishings, which predominantly serve the sawlog and wood pellet industries (Kärhä et al., 2018). However, the rapid influx of storm-impacted timber into the market can quickly overwhelm traditional channels, precipitating a downward spiral in market prices. Mitigating such losses necessitates an innovative approach that assesses timber quality post-storm and identifies new avenues for the utilization of salvaged timber.

In that regard, biorefineries, alongside extracting natural polymers from biomass, open doors to economic opportunities rooted in the utilization of degraded timber (Yamakawa et al., 2018). In the context of biorefineries, the conversion of biomass into energy, chemicals, and polymers emerges as a key player in cultivating a circular economy (Cherubini, 2010). In addition to the burden of timely harvesting DT after

a catastrophic event, the degradation could be pivotal in facilitating biological and chemical reactions integral to the polymer recovery process. This, in turn, paves the way for developing high-end applications for natural polymers across diverse industries (Martelli-Tosi et al., 2018; Vermaas et al., 2015).

Within the forest industry, techniques centered around the non-destructive evaluation (NDE) of trees and logs via sound-wave propagation have solidified their position as dependable predictors of timber quality (Fundová, 2012; C. Wang & Ross, 2007). These acoustic methodologies stand as pivotal tools for segregating logs and enhancing value recovery (Dickson et al., 2003). By offering insight into crucial intrinsic wood properties such as stiffness and bending strength prior to processing, these acoustic technologies contribute to informed decision-making (L. R. Schimleck et al., 2018). Emerging as a promising avenue, NIR, coupled with advanced multivariate data analysis, proves its mettle as a swift and non-destructive analytical tool (L. R. Schimleck et al., 2002). This amalgamation holds a track record in accurately predicting internal wood quality traits, encompassing even the context of storm DT. The industry gains substantially from these expedient and accurate analytical approaches in order to establish accurate predictive models for various facets, ranging from wood mechanical properties to the effective repurposing of DT (Musah et al., 2022).

Pursuing this objectiveestablishes the foundation for a more resilient and sustainable future. This report delves into the frequently neglected aspects of the time frame during which timber can be effectively utilized. The focus is on correlating in-field measurements (NIR) with chemical composition to evaluate the optimal utilization window. Through the correlation of in-field measurements, namely near-infrared spectroscopy, and sound wave propagation, coupled with chemical characterization, the aim is to identify the optimal utilization window for hurricane DT within biorefinery operations.

1.9. Lignin recovery from downed timber

The aftermath of hurricanes can exact a substantial toll on timber revenue, potentially amounting to billions of dollars in losses (Henderson et al., 2022). Historic hurricane events, such

as the devastating Hurricane Hugo in 1989, followed by Hurricanes Katrina and Rita in 2005 and Michael in 2018, have left in their wake significant timber losses and economic challenges for forest landowners (Avila, 2019a; Beven et al., 2008; Henderson et al., 2022; Prestemon & Holmes, 1997). However, while there exists a substantial body of literature detailing the impacts of isolated storm events and strategies for mitigating potential damage to forest stands, ambiguity surrounding the critical timeframe during which logs remain salvageable before succumbing to fungal discoloration, decay, and infestation by insects remains (McCarthy et al., 2010).

One of the most documented examples of downed timber recovery efforts is Hurricane Hugo, which made landfall on September 22, 1989. It unleashed its destructive fury with winds roaring at 135 mph, battering the South Carolina coast before rampaging through central South Carolina into North Carolina. The most profound economic blow was dealt to the timber resource in Hugo's path, causing estimated losses of $1.18 billion, equivalent to four years' worth of sawtimber harvest (Hook et al., 1991; Syme, 1992). In the aftermath, South Carolina established the Forest Disaster Salvage Council on October 5, 1989. A salvage goal of 625 million cubic feet, representing 25% of the total estimated volume of timber destroyed, was set. Over the ensuing months, the forest industry launched an extensive timber salvage operation that harvested approximately 383 million cubic feet, primarily comprising softwood (Peralta et al., 1993). However, it is important to note that despite these impressive salvage efforts, most of the estimated volume of timber destroyed (over 2,000 million cubic feet) by Hurricane Hugo was not recovered for sawmills. This unharvested timber represents a substantial loss in terms of economic value and potential resource utilization.

Understanding the factors that affect the salvageability and degradation of downed timber over time is crucial to maximize resource recovery and minimize waste in the aftermath of such

natural disasters. This study seeks to contribute to this understanding by investigating the weathering effects on downed timber and the potential for recovery, focusing on changes in lignin over a 12-month period. The findings of this research hold promise not only for the forest industry but also for emerging biorefineries, which aim to recover natural polymers like lignin for sustainable utilization in various applications.

2. Research objectives

2.1. Overall aim of the study

To comprehensively investigate and address the existing knowledge gaps pertaining to the valorization of Southeastern Loblolly Pine (*Pinus taeda*) Downed Timber within the bioeconomy framework, with a focus on enhancing post-hurricane timber utilization strategies.

2.2. Objective 1: Analyze Timber Market Dynamics Post-Hurricanes

- Explore the application of wavelet analysis in forestry economic analysis.
- Investigate relationships between timber market indices and hurricane seasons using wavelet coherence analysis.
- Implement the Wavelet-ARIMA model for time series forecasting in the context of hurricane-induced timber market fluctuations.

2.3. Objective 2: Advance Wood Composition Analysis Techniques

- Integrate nonlinear techniques, mathematical pretreatments (smoothing and first derivative), and Box-Behnken design to achieve a substantial reduction in the required sample size for wet chemistry.
- Evaluate the performance of Support Vector Machines (SVM) models, in predicting cellulose, hemicellulose, and lignin content.

2.4. Objective 3: Investigate Hurricane-Downed Timber Degradation

- Conduct a model study in Alabama using loblolly pine trees, focusing on temporal patterns revealed by sound-wave propagation and NIR measurements.

- Employ Principal Component Analysis (PCA) to capture temporal phases in NIR data.
- Utilize Near-Infrared Spectroscopy (NIR), thermogravimetric (TGA) and acoustic technology to study the degradation of hurricane-downed timber.
- Characterize changes in lignin and carbohydrate fractions over time.

2.5. Objective 4: Enhancing Timber Utilization Post-Natural Disasters

- Investigate non-destructive evaluation (NDE) techniques, particularly sound-wave propagation and NIR, for predicting timber quality.
- Assess the potential of NIR coupled with advanced multivariate data analysis in predicting wood properties and facilitating effective repurposing of downed timber.
- Correlate in-field measurements (NIR and sound wave propagation) with chemical composition to identify the optimal utilization window for hurricane-downed timber within the context of biorefinery operations.

2.6. Objective 5: Understanding Weathering Effects on Downed Timber

- Investigate factors affecting salvageability and degradation of downed timber over a 12-month period.
- Focus on changes in lignin content as a key indicator of weathering effects.
- Contribute to the understanding of resource recovery and waste minimization strategies in the aftermath of natural disasters, particularly hurricanes.

3. Methodology

3.1. Wavelet analysis

Wavelet analysis is a time-frequency domain analysis method that allows for measuring the co-movement and phase difference between two time series (Vacha & Barunik, 2012). It utilizes a continuous wavelet transform to represent a time series and calculate cross-wavelet spectra and wavelet coherence (J. W. Goodell & Goutte, 2021). The wavelet coherence provides a measure of co-movement between two time series, revealing any phase differences between them (Gan et al., 2022). This approach offers several advantages, including the ability to capture both transient and stationary features of a signal with high precision and a multiscale representation of signals, allowing for the examination of different frequency components at various levels of detail (Ganesan et al., 2004). The ability to zoom in and out of the signal is particularly useful for detecting patterns and analyzing signal characteristics across different scales. Additionally, by decomposing a signal into wavelet coefficients, it is possible to remove noise or unnecessary details while retaining important features, resulting in efficient data compression and noise reduction (Rösch & Schmidbauer, 2016).

For the processing and wavelet analysis, two R packages were utilized: WaveletComp 1.1 and Wavelet-ARIMA (R. K. Paul et al., 2017; Rösch & Schmidbauer, 2016). The frequency structure of time series is analyzed by WaveletComp through the utilization of the Morlet wavelet (Merry, 2005). The continuous, complex-valued wavelet transform is a valuable tool for analyzing time series data as it preserves information and allows for careful selection of time and frequency resolution parameters (Percival & Walden, 2000). The complex-valued wavelet transform provides a crucial prerequisite for investigating coherency between two time series (Aguiar-Conraria & Soares, 2014). By analyzing coherency, it becomes possible to uncover the degree of synchronization or association between the two series (Soares, 2011). The transform's ability to capture both amplitude and phase information facilitates the assessment of coherence

between the time series, revealing patterns of similarity, periodicity, or relationships that might not be apparent in other types of analysis (Dima et al., 2015). This information is particularly relevant when studying the effects of hurricanes on stumpage prices, as it allows for a comprehensive examination of the relationship between these variables, considering both their magnitudes and their phase relationships.

Meanwhile, the 'Wavelet-ARIMA' package combines the benefits of wavelet analysis and ARIMA modeling (R. K. Paul et al., 2017). It enables users to perform wavelet decomposition and forecasting on time series data, facilitating the examination of localized frequency components and their variations over time (Kriechbaumer et al., 2014). The package incorporates AutoRegressive Integrated Moving Average (ARIMA) modeling, which is a widely used technique for modeling and forecasting time series data. ARIMA models are composed of three primary components, namely the AutoRegressive (AR) component, the Integrated (I) component, and the Moving Average (MA) component (Luceño & Peña, 2008). By combining these components, an ARIMA model can effectively capture a wide range of time series patterns, including trends, seasonality, and cyclic behavior (L. Wang et al., 2013). The AR component captures the linear relationship between the current observation and a certain number of lagged observations, modeling the dependence of the current value on its past values. The integration component involves differencing the time series to make it stationary, removing trends or seasonality present in the data. The moving average component models the dependency between the current observation and a series of lagged forecast errors, capturing the influence of past errors on the current value (Salazar et al., 2019).

3.2. Price data sources

The data for this study was obtained from the forestry extension office and the library of Auburn University, specifically the TMS quarterly reports. TMS compiles and publishes timber prices for 22 US Southern market areas, reporting on pine sawtimber (PST), chip-n-saw (CNS), and pulpwood (PPW) (Misztal, 2018). It is important to note that there have been two major revisions in TMS reports: a shift from monthly to quarterly frequency since 1988 and a change in the reporting areas in coastal states from three to two in 1992 (Prestemon & Pye, 2000). Previous research has examined temporal and spatial

aggregation issues and the efficacy of different statistical tests on TMS timber prices (Prestemon & Pye, 2000). The data obtained from TMS covers the time range from the fourth quarter of 1976 to the fourth quarter of 2020 for statewide averages. Additionally, quarterly data for subregions one and two of the states were transcribed for the years 2017, 2018, and 2019.

Consumer Price Indices (CPIs) provided by the US Department of Labor, Bureau of Labor Statistics (2022), were used to evaluate the effect of inflation correction on the TMS price series. **Figure 4.1** provides an overview on the different CPI indices available and its characteristics like geographical coverage, publication frequency and base period. **Figure 4.3** supplies the Producer Price Indices (PPIs) considered, which measure the average change over time in the prices received by domestic producers for their goods and services (U.S. Bureau of Labor Statistics, 2022). Apart from one, the rest of the PPIs lack a geographical coverage component, which could be crucial to understand the price shifts experienced in the southeast after a hurricane landfall. The comparison between CPIs and PPIs concurrently allows for a more comprehensive understanding of the overall price dynamics within an economy. It provides a broader perspective on the inflationary pressures experienced by both consumers and producers. It can help identify potential supply chain disruptions or shifts in pricing power between consumers and producers (Shah et al., 2021).

Six open market indices specializing in lumber futures or forestry-related data were used for high-frequency data: iShares Global Timber & Forestry ETF (WOOD), PotlatchDeltic Corporation (PCH), Rayonier Inc. (RYN), Weyerhaeuser Company (WY), Acadian Timber Corp (AND), and Random length lumber futures (LBS) (CME Group Inc., 2009; *NASDAQ Stock Market*; TradingView, 2021). Pearson's correlation coefficients and coherence were evaluated to select the most suitable public data source for wood prices.

3.3. Statistical analysis

Statistical analysis was conducted to examine the relationship between the TMS data and the selected market indices. Pearson's correlation coefficients were calculated to assess the degree of correlation between the TMS data and the market indices. (Puth et al., 2015). Pearson's correlation coefficient measures the linear association between two variables, providing insights into the strength and direction of the relationship. A positive correlation coefficient indicates a positive linear relationship, while a negative coefficient indicates a negative linear relationship (Udovičić et al., 2007).

The calculation of Pearson's correlation coefficients allowed for a comprehensive analysis of the association between the TMS data and the market indices. This statistical measure provided insights into the direction and strength of the relationships, enabling a better understanding of the market dynamics and potential impacts of external factors such as hurricanes. However, to gain a deeper understanding of the co-movement and phase difference between the TMS data and the market indices, wavelet coherence analysis was also employed. Wavelet coherence analysis is a powerful tool that measures the level of synchronization or association between two time series across different frequencies and time intervals.

3.4. Forecasting

To forecast the wood prices, the last quarter’s price before the event point from TMS was taken as the base. This approach provides a reference point for comparing and predicting future price movements. In the selection process of the six open market indices, the correlation and coherence tables generated were examined. The correlation table was used to assess the linear association between the TMS data and each market index. The coherence table, derived from wavelet analysis, provided insights into the co-movement and phase difference between the TMS data and each market index. From these tables, the highest value was identified as the most suitable open market index for wood price analysis. This selection criterion prioritizes indices that exhibit a stronger correlation and coherence with the TMS data, indicating a closer relationship and potential predictive power. By selecting the open market index with the highest value, it is

expected to capture the most relevant information and provide more accurate forecasts of wood prices. This approach enhances the reliability and validity of the analysis by focusing on the index that demonstrates the strongest statistical relationship with the TMS data.

In R, the "wavelets" package provides various wavelet families for analysis (Aldrich, 2013). Here are some commonly used wavelet families available in the package: Daubechies ("haar", "db1", "db2", ..., "db10"), Symlets ("sym2", "sym3", ..., "sym10"), (Coiflets: "coif1", "coif2", ..., "coif5"), Biorthogonal ("bior1.1", "bior1.3", "bior2.2", ..., "bior6.8"), Reverse Biorthogonal ("rbio1.1", "rbio1.3", "rbio2.2", ..., "rbio6.8"), Haar-like ("haar0", "haar1", "haar2", ..., "haar15"). These are just a few examples of the wavelet families available in the "wavelets" package. Each family has different properties and characteristics, making them suitable for different types of data and analysis.

The parameters for the Wavelet-ARIMA package include the wavelet filter, for this work we used the “la8” wavelet filter, with 5 levels wavelets decomposition, forecast horizon = 360, AR = 3 and MA = 0. The "la8" wavelet is a member of the Daubechies wavelet family. It is also known as the Daubechies 8-tap wavelet, with characteristics: orthogonal, 8 coefficients, compact support, symmetry, and frequency response (R. Paul & Garai, 2021). It is characterized by having eight coefficients, making it a compactly supported wavelet. Compact support means that the wavelet function is nonzero only within a finite interval and vanishes outside that interval (Vonesch et al., 2007). The high-pass and low-pass filters associated with the "la8" wavelet allow for analysis of both high-frequency and low-frequency components of a signal. The wavelet exhibits both time and frequency localization properties. It provides a good balance between time and frequency resolution, allowing it to capture both rapid changes in the time domain and localized frequency information (Tzabazis et al., 2018).

3.5. Downed timber model study

Thirty (30) fresh loblolly pine trees were cut down to model storm-down timber at the Solon Dixon Forestry Education Center, nestled in Covington County, Alabama. Core samples were collected on each

field visit resulting in 176 cores collected for the study. To preserve the characteristics of the cores, the samples were stored in resealable plastic bags inside an ice chest until returned to be dried in a convection oven at 105°C for at least 48 h. After drying, the samples were stored in sealed glass vials at 4°C for characterization. The selected sites were located within the premises of the Solon Dixon Forestry Education Center, in Covington County, Alabama. The first site accommodated 15 trees, the second 10, and the third 5: aged 15, 30, and 40 years respectively. Thes sites are 99, 86, and 87 m above sea level, respectively. Within the loblolly pine (*Pinus taeda L.*) plantation at the study site, the trees were planted with an 8 × 6 ft spacing pattern. All rows were oriented in an east–west direction, with a public road separating the third site from the first and second sites.

3.6. Sound-wave propagation

Figure 3.1 shows the measurements encompassing 6 replicates at 5 marked positions spanning the timber length, commencing 30 cm from the base of the DT. These measurements extended at intervals of 1.4 m, encompassing the length of the timber to achieve the 5 positions. This comprehensive measurement regimen led to over 8000 measurements undertaken for all 30 DT. These measurements were conducted bi-weekly over seven months, transitioning to a monthly schedule, thereafter, culminating in a full year of data collection.

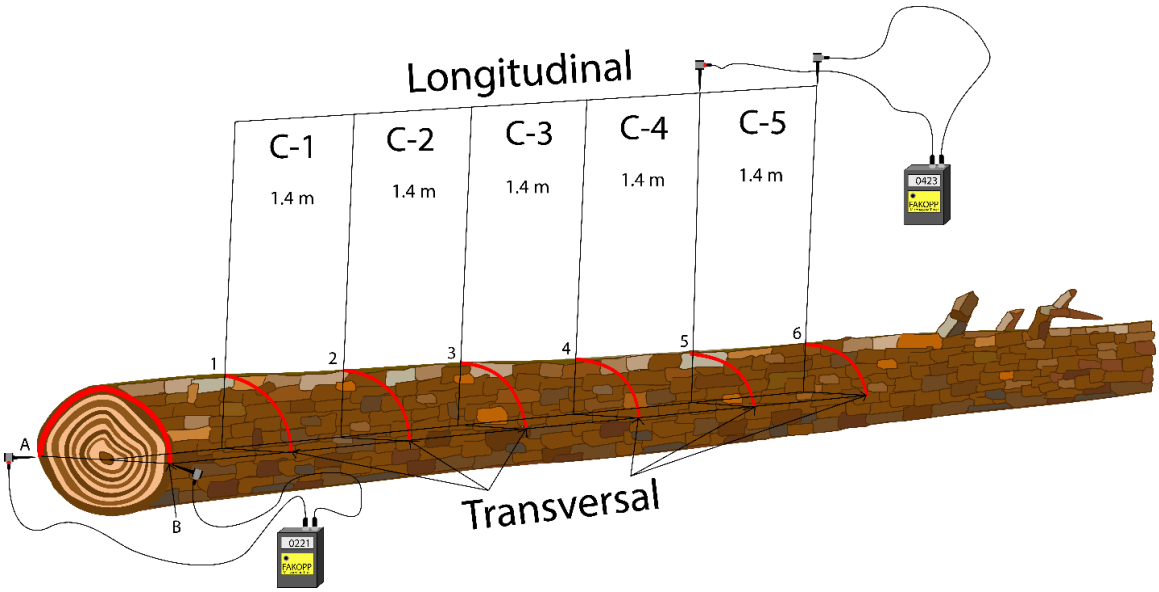

Figure 3.1. Downed timber acoustic measurement locations.

The study harnessed the widely employed time of flight (TOF) technique to gauge stress wave velocity with the Fakopp 1D Microsecond Timer (Fakopp Enterprise, Agfalva, Hungary). The probes were positioned at a 45-degree angle within the sapwood of each DT. These probes, pointed toward one another from opposing ends, facilitated the transmission and reception of stress waves. Two distinct positions were measured: transverse and longitudinal as shown in Error! Reference source not found.. For the transverse technique, probes were positioned symmetrically on opposing sides of the DT, with the probe's distance (D) contingent upon the diameter and circumference, determined by the equation ($D = \pi d/2$).

3.7. Core sampling

Core samples were collected from the first DT of each site at 1.22, 4.27, 7.32, 10.36, and 13.41 meters (4, 14, 24, 34 and 44 ft., respectively) of height from the cut end on each field visit. Additionally, for each remaining DT on the sites, the core was collected at 1.22 m (4 ft.) in each field outing. This resulted in 176 cores collected for the study. To preserve the characteristics of

the cores, the samples were stored in resealable bags inside an ice chest until returned to be dried in a convection oven at 105°C the following day after collection. After drying, the samples were stored in sealed glass vials at 4°C for analysis using NIR, TGA, and chemical characterization.

3.8. Stump sampling

We developed a model study to replicate the impact of a typical tropical storm. For this purpose, we deliberately felled 30 freshly harvested loblolly pine trees using a chainsaw. Stump samples were collected from each site at three distinct time points: at the beginning of the experiment (0 months), and subsequently at 6 and 12 months. At each collection time, a section from the bottom end of the first tree on each site was carefully removed using a chainsaw. The collected individual stump weights ranged from 3.8 to 8.3 kilograms, resulting in a total of 63.8 kilograms collected. These samples were then transported to a freezer storage room maintained at -20°C immediately upon returning from the field to ensure their preservation for subsequent analysis.

3.9. Near Infrared Spectroscopy

Near Infrared Spectroscopy (NIR) technique quantifies the absorption, transmission, or reflection of near-infrared light by a sample, based on its chemical composition (Türker-Kaya & Huck, 2017). A Perkin Elmer Spectrum 400 Fourier-transform infrared (FT-IR)/FT-NIR spectroscope (Waltham, MA, USA) was used to collect the NIR spectra of the dried core samples. The spectra were collected from the radial face of dried core samples, with the smoothest surface chosen for spectroscopic data gathering. Absorbance measurements were taken across a spectral range of 4,000 cm^{-1} (2,500 nm) to 10,000 cm^{-1} (1,000 nm) utilizing a resolution of 2 cm^{-1}, and each

measurement involved 128 scans. These NIR measurements were meticulously conducted within a controlled environment featuring a relative humidity of 40 percent and a temperature of 20°C. The spectrum of a Spectralon standard was taken as the background reference sample every 20 min to correct for potential drifts with time (Acquah, Essien, et al., 2018). To apply a Savitzky-Golay (SG) smoothing to the first derivative, the “sgolayfilt” function from the “signal” package has been used with parameters p = 2 (polynomial order) and n = 17 (frame length) for the function in the initial modeling (Developers, 2013). Subsequently, the SG parameters were explored for optimization of the models in the ranges 1-10 and 3-99 for p and n, respectively.

3.10. Experimental design, machine learning approaches, and model development

To clean the complex spectral data obtained from NIR analysis into meaningful information, first derivatives were calculated and then treated by PCA. PCA was computed using the “pcr” function from the “pls” package in R software (Sanchez, 2013). To streamline the chemical characterization process, a Box-Behnken (BB) experimental design was adopted. This technique employs a central point, often the midpoint of each factor's range, which serves as a reference point. From this central point, the design expands into a series of levels for each factor, forming a multidimensional grid. This resulted in 15 cores selected for chemical characterization in duplicate for a total of 30 response variables. The set was divided randomly into a calibration set (with a probability weight of 2/3) and a test set (1/3). In R software the “ksvm” function from the “kernlab” library was used for Support Vector Machines (SVM) with type "eps-svr" for epsilon support vector regression (Karatzoglou et al., 2004). The kernel parameter was tested with the radial, Bessel, Anova RBF, and polynomial kernels.

In R, the ksvm function is part of the kernlab package, which is used for kernel-based machine learning methods (Karatzoglou et al., 2004). The radial kernel, often referred to as the

Radial Basis Function (RBF) kernel or Gaussian kernel, is a popular choice for kernelized support vector machines (SVM) (Scholkopf & Smola, 2018; Schölkopf & Smola, 2002). Tuning the sigma parameter is crucial for the performance of the radial kernel (Tharwat, 2019). In the Bessel kernel, the Bessel function introduces oscillatory behavior, and the ν parameter controls the number of oscillations. The scaling factor α influences the spread of the oscillations. The ANOVA RBF (Radial Basis Function) kernel is a variant of the standard RBF kernel that incorporates the idea of ANOVA (Analysis of Variance) decomposition (Müller et al., 2018). The ANOVA decomposition allows the kernel to capture interactions between individual features in addition to their individual contributions. It is particularly useful when dealing with high-dimensional data where interactions between subsets of features may play a crucial role. The ANOVA RBF kernel automatically considers interactions between features, and additional parameters like in the standard RBF kernel need not be explicitly specified (Luts et al., 2010).

Radial Kernel

$$\mathrm{K}(\mathrm{x},\mathrm{y}) = \exp\left(-\frac{\|\mathrm{x}-\mathrm{y}\|^2}{2\sigma^2}\right) \qquad \text{Equation 1}$$

Where *x* and *y* are data points, ‖*x*-*y*‖ denotes the Euclidean norm (distance), and σ is a parameter that controls the width of the Gaussian function.

Bessel Kernel

$$\boldsymbol{K(x,y) = J_v(\alpha * \|x-y\|)} \qquad \text{Equation 2}$$

Where *x* and *y* are data points, ‖*x*-*y*‖ denotes the Euclidean norm (distance) between points, J_v is the Bessel function of the first kind and order *v*, and α is a positive scaling factor.

ANOVA Kernel

$$\boldsymbol{K(x,y) = exp\left(-\sum_{i=1}^{d}\frac{\|x_i-y_i\|^2}{2\sigma_i^2}\right)} \qquad \text{Equation 3}$$

Where x and y are data points with d features, x_i and y_i represent the values of the i-th feature of x and y, respectively, σ_i is a parameter controlling the width of the Gaussian function for the i-th feature.

Polynomial Kernel

$$K(x, y) = (\boldsymbol{x} \cdot \boldsymbol{y} + \boldsymbol{c})^{\boldsymbol{d}} \quad \text{Equation 4}$$

Where x and y are data points, $\cdot$ represent the dot product of the input vectors, c is a constant term, and d is the degree of the polynomial.

The polynomial kernel is another popular kernel used in support vector machines (SVMs) and other machine learning models. It allows the SVM to capture non-linear relationships in the data. Adjusting the parameters, particularly the degree, allows you to control the flexibility of the polynomial kernel. The predictive performance of the models was evaluated by the coefficient of determination (R2), root mean square error of calibration (RMSEC), and root mean square error of prediction (RMSEP) (B. K. Via et al., 2014).

3.11. Chemical characterization

Selected samples using BB design were ground with a Wiley mill using a 20-mesh screen and stored in sealed glass vials at 4°C for chemical characterization. Carbohydrate and lignin compositions were determined by the following quantitative methods. Extractives content was determined following NREL/TP-510-42619 (Sluiter, Ruiz, et al., 2008). Briefly, using a Soxhlet apparatus, water and subsequently ethanol were used to extract the sample. Solvent was evaporated from the extract using a rotary evaporator. The extract was then dried, and the final mass was measured for extractives content determination. Carbohydrates and lignin were determined

following NREL/TP-510-42618 (Sluiter, Hames, et al., 2008). Briefly, the samples were hydrolyzed in two steps: the first one at 30ºC with 72% (w/w) sulfuric acid for 1 hour, and the second one at 121°C with 4% (w/w) sulfuric acid for 1 hour inside an autoclave. The total lignin was computed as the sum of acid-soluble lignin (ASL) and acid insoluble lignin (AIL). ASL was determined with a Genesys UV-Visible spectrophotometer (Thermo Fisher Scientific, Waltham, MA, USA) immediately after hydrolysis. Absorbance of a test sample was measured at the recommended wavelength of 240 nm, ensuring that the absorbance ranged between 0.7–1.0. The filtrate was separated in two fractions; the first one was neutralized with $CaCO_3$, the second was not neutralized. An Agilent 1260 Infinity (Santa Clara, California) high-performance liquid chromatograph (HPLC) with a Refractive Index Detector and an Agilent Hi-Plex Pb/H columns were used for monomeric sugars determination (i.e., glucose, xylose, galactose, arabinose, and mannose) equipped with the appropriate guard column at a column temperature of 70°C and run time of 35 min. All determinations were performed in duplicate.

3.12. Thermogravimetric Analysis (TGA)

TA Instruments Q5000 IR (New Caste, DE, USA) was employed to delve into the thermal degradation behavior of the wood samples. This technique is founded on the principle of measuring the weight changes of a material as it undergoes controlled temperature elevation. The experimental conditions, including heating rate (20 °C/min), sample mass (15-20 mg), gas atmosphere (air) was precisely controlled to ensure accurate and reproducible results from 0-700 °C. Triplicates of the samples were run and averaged.

3.13. Co-Solvent Enhanced Lignocellulosic Fractionation (CELF)

A specially equipped 1-liter Paar reaction vessel, which offered precise control over reaction parameters was used for lignocellulosic fractionation. The solvent system consisted of Tetrahydrofuran (THF) and water in a 3:1 ratio, complemented by a 0.1M sulfuric acid catalyst load. The lignocellulosic sample was prepared and introduced into the reaction vessel leaving a 20% of headspace that was purged with nitrogen. To promote effective interaction between the sample and the solvent system, a soaking period of 14 hours was observed. The reaction was conducted at a controlled temperature of 160°C for a duration of 25 minutes. The reactor's jacket was preheated (to 300°C) before the reaction to reduce the heating ramp (15-20 min). During the reaction the reactor rotor was set at 200 rpm. After completion, the reactor vessel was rapidly cooled by submerging it in a water and ice bath. Post-reaction, the sample underwent filtration to separate the cellulosic residue from the liquid fraction containing the extracted lignin. Afterwards the sample was neutralized with ammonium hydroxide extra pure, 5% in water. Lignin was washed in a series of steps using a centrifuge: two times with pure DI water, two times with diethyl ether, and two more times with DI water. Finally, the samples were dried in a vacuum oven at 45°C (Beckham, 2018).

3.14. Fourier transform infrared spectroscopy (FTIR)

A PerkinElmer Spectrum 400 Fourier-transform infrared (FT-IR)/FT-NIR spectroscope with attenuated total reflectance (ATR) was employed (Waltham, MA, USA). The spectra of CELF lignin samples were taken in triplicate with 128 scans.

3.15. Differential scanning calorimetry (DSC)

TA Q2000 Instruments (New Caste, DE, USA) was employed to evaluate the thermal stability and differences of the various CELF lignin obtained. A Heat-cool-heat mode was used with a heating/cooling rate of 20°C/min. nitrogen.

3.16. Molecular weight

An Agilent 1260 Infinity (Santa Clara, California) high-performance liquid chromatograph (HPLC) / gel permeation chromatograph (GPC) with an Ultraviolet (UV) detector was used to determine the molecular weight of lignin obtained. The samples were injected automatically, chromatographed using two columns, and monitored at 35 °C by UV at 260 nm with RI detection. Parameters: one Agilent PolarGel-M column 7.5×300 mm (5 µm particle size) with its corresponding guard column (7.5×50 mm), followed by one Agilent PLgel 100Å column 7.5×300 mm (3 µm particle size). THF was used as eluent at 1 mL/min flow rate, columns temperature was 50 °C, injection volume 20 µL, and run time 25 min. Polystyrene standards (Agilent PL2010-0301) were used for calibration (Tolbert et al., 2014).

3.17. Nuclear Magnetic Resonance Spectroscopy (NMR)

The lignin and cell wall samples were examined in DMSO-d6:pyridine-d5 (4:1, v/v) as previously described in (Kim et al., 2008; Kim & Ralph, 2010). NMR spectra were acquired on a Bruker Biospin (Billerica, MA) Avance NEO 700 MHz spectrometer equipped with a 5-mm QCI 1H/31P/13C/15N cryoprobe with inverse geometry (proton coils closest to the sample) or on an Avance III 500 MHz spectrometer equipped with a 5-mm TCI 1H/13C/15N cryoprobe.

3.18. CELF Lignin Particles Production

CELF Lignin samples were dissolved at 2, 4 and 6% wt. in a solvent system of ratio 3:1 of tetrahydrofuran/water-salt (THF:0.1M $NaNO_3$) and left for 12h in a laboratory rotator at room temperature. Afterwards, they were mixed dropwise with 5 times volume of deionized water with magnetic stirring at 450 rpm.

3.19. Dynamic Light Scattering (DLS)

All measurements were done in a Litesizer 500 Anton-Paar (Gratz, Austria). CELF Lignin individual particle size distribution and zeta potential were measured at 500 ppm in water solution without pH adjustment, at 20 C (room temperature) with an equilibration time of 3 minutes and 5 series repetitions. The series quality settings were set at automatic with maximum number of runs of 60 and measurement time of 10 s. The best resulting setting was a backscatter angle (175°), which was used for the following runs over pH range.

The Zeta potential for Lignin particles at 1000 ppm in DI water solution were tested on a pH range from 2 to 12 with 0.5 steps. For all samples, 5 series repetitions were done and averaged. Each series quality control was set up as automatic in the software with a maximum number of runs of 1000. Target temperature was 20°C, with equilibration time 30 s. The titration solutions were 0.01M KOH, 0.01M HCl, and 0.001M KCl as dispersant (Lievonen, 2015; Lievonen et al., 2016).

3.20. Scanning Electron Microscopy (SEM)

100 µL of the 500ppm solutions used in DLS were drop casted on the tape of aluminum studs and allowed to dry in petri dish. The sample were coated by sputtering with gold for 90 s in an EMS × 550 Sputter Coating Device from Science Services (Munich, Germany). Images with

magnifications of × 10,000 were recorded in a Zeiss Evo 50VP SEM (Oberkochen, Germany). ImageJ software was used to measure 200 particles diameter for particle size distribution determination (Schneider et al., 2012).

4. Wavelet Analysis and Forecasting using Open-Access Lumber Market Indices for Assessing the Impact of Hurricanes on Southern US Stumpage Prices

This chapter has been published in "Hernandez, J. A., Musa, M., Tyler, M., Richey, R.G., Maggard, A., Via, B., & Peresin, M. S. (2023). Valorization of Downed Timber: Correlations Between Open-Access Lumber Market Indexes to Southern US Stumpage Prices During Recent High-Damaging Hurricane Seasons. Forest Products Journal. (Accepted December2023)"

4.1. Abstract

In the aftermath of events such as hurricanes, the economic impact of downed timber can reach billions of dollars. Accurate forecasting of stumpage prices after such events is crucial for maximizing recovery value while minimizing salvage costs. However, this poses challenges because of the inherent nature of the data. This study addresses these challenges by exploring the application of wavelet analysis, a novel approach in the field of forestry economic analysis. Wavelet analysis offers a unique framework for studying periodic phenomena in time series data, particularly when frequency changes over time are present. By leveraging wavelet analysis, this study uncovers relationships between timber market indices and hurricane seasons. The combination of traditional correlation analysis and wavelet coherence analysis enhances the statistical analysis in this study, offering a comprehensive examination of the relationship between the Timber Market Survey data and market indices. This innovative analytical approach enables a deeper understanding of the dynamics of the timber market and the potential effects of hurricanes on timber prices. Furthermore, this research highlights the recent advancements in wavelet methodology and the availability of open-source packages in the programming language R, such as WaveletComp and Wavelet-ARIMA, that facilitate wavelet analysis and time series forecasting. The Wavelet-ARIMA model used in this study demonstrates its effectiveness in reducing noise and improving prediction accuracy. The study incorporates an extensive data set consisting of 10 Consumer Price Indices, 7 Producer Price Indices, 30 state-wide Timber Market Survey indices, 54 TMS subregions, and 6 open market series.

4.2. Project partners

The Forest Products Development Center worked in collaboration with the Deptartment of Supply Chain Management of the Harbert College of Business, from Auburn University.

This research was funded by the USDA Forest Service Down Timber Research FS-20-JV-11111122-058 and the State of Alabama appropriated funds for Cross-Laminated Timber Outreach and Research Funds.

4.3. Case of Study

In addition to the selected indices, the analysis focused on examining the behavior of wood prices in the aftermath of Hurricane Michael in 2018. Hurricane Michael made landfall in the Florida Panhandle as a Category 5 storm and caused extensive damage to forests and timber resources in the affected regions (Blake, 2018; Brandeis et al., 2022; Florida Forest Service, 2018; Henderson et al., 2022; NOAA, 2021b, p. Hurricanes in History, 2021a, p. Hurricane Costs).

4.4. Methodology

This chapter's methodology is further explained for Wavelet analysis in section 3.1. The timber price data sources are detailed in section 3.2. The statistical analysis of the data is explained in detail in section 3.3. Finally, the forecasting methodology is clarified in section 3.4.

4.5. Results and discussion

4.5.1. Timber Mart-South Data

Timber Mart-South (TMS) serves as a comprehensive price reporting service, offering valuable market information, and pricing data for timber and wood products in the southeastern United States. Its voluntary reporting system relies on input from various stakeholders, including timber buyers, sellers, and brokers, as well as state and federal agencies, private timberland

owners, and wood product manufacturers. This collaborative approach ensures a wide range of data sources, contributing to the reliability and accuracy of the TMS quarterly reports (*TimberMart-South | Home*, 2022).

The University of Georgia (UGA) Warnell School of Forestry & Natural Resources, under contract with the Frank W. Norris Foundation, compiles and publishes the TMS reports on a quarterly basis. These reports, which are available through paid subscriptions, provide valuable insights into timber market trends and facilitate informed decision-making for government agencies, academics, and researchers involved in forestry and natural resource management (*TimberMart-South | Resources*, 2023).

Figure 1.5 shows the TMS quarterly reports, stumpage prices for major timber products across 11 states in the US South. Starting from 1988, the data transitioned from monthly to quarterly frequency, with previous monthly data averaged together to align with the new reporting format (Prestemon & Pye, 2000). The prices are categorized into three main groups: Pulpwood, Chip-n-saw, and Sawtimber, based on the diameter at breast height (DBH) thresholds of 6 " & up, 8 "-11 ", and 12 " & up, respectively. The reported prices are in $ / ton, and adjustments are made for states or areas using different measurements to facilitate comparative analysis. It is important to note the disclaimer provided by TMS, which highlights that the published data is sourced from reliable sources but may still contain errors or omissions. Each price is independently determined and not influenced by mathematical relationships with other items. “The reported prices are an average of lows and highs and not absolute lows or highs” (*TimberMart-South | Home*, 2022). Variations in fieldwork and the time element may lead to prices that are slightly lower or higher than those published. Furthermore, it is crucial to recognize that timber prices vary significantly based on various factors, and a reported price represents just one of the prices at which an item has

been sold. It is worth mentioning that TMS reports do not typically include salvage sales or special products in the state or complete reports (*TimberMart-South | Resources*, 2023).

4.5.2. Consumer Price Indices

The Consumer Price Index (CPI) is a comprehensive measure of price changes for goods and services in the United States (Bryan & Cecchetti, 1993). It is calculated using a two-stage process that takes into account both geographic and item structures. In the first stage, basic indices are calculated, which represent specific item-area combinations. These basic indices capture the price changes for specific goods and services in particular regions (*Consumer Price Index Summary - 2023 M06 Results*, 2023).

In the second stage of the CPI calculation, the basic indices are aggregated to create broader indices that cover a wider range of items and geographic areas (U.S. Bureau of Labor Statistics, 2023). This aggregation process continues until all items U.S. city average index is reached. This index represents the overall price level for all goods and services across the entire United States(U.S. Bureau of Labor Statistics, 2022).

Table 4.1 provides an overview of the different CPI indices available. For the purpose of this study, the South region was of particular interest. the South region comprises a cluster of states, which includes Alabama, Arkansas, Delaware, District of Columbia, Florida, Georgia, Kentucky, Louisiana, Maryland, Mississippi, North Carolina, Oklahoma, South Carolina, Tennessee, Texas, Virginia, and West Virginia (Consumer Price Index, South Region — February 2023, 2023). Within the South region, further division is made into the South Atlantic, East South Central, and West South-Central regions.

The South Atlantic division encompasses Delaware, District of Columbia, Florida, Georgia, Maryland, North Carolina, South Carolina, Virginia, and West Virginia. The East South-

Central division comprises Alabama, Kentucky, Mississippi, and Tennessee. Lastly, the West South-Central division consists of Arkansas, Louisiana, Oklahoma, and Texas. Further delimitation for calculation includes 3 major metropolitan areas in alternate months. This level of delimitation allows for a more granular analysis of price changes within specific geographic regions and helps capture localized variations in the cost of living.

Table 4.1. Available CPI indices.

Series ID	Series Title	Base Period	Periodicity
CUUR0000SA0	CPI – All items in U.S. city average, all urban consumers, NSA[1]	1982-84=100	Monthly
CUSR0000SA0	CPI – All items in U.S. city average, all urban consumers, SA[2]	1982-84=100	Monthly
SUUR0000SA0	Chained – CPI – All items in U.S. city average, all urban consumers, NSA[1]	December 1999 = 100	Monthly
CUUR0300SA0	CPI - All items in South urban, all urban consumers, NSA	1982-84=100	Monthly
CUUR0350SA0	CPI – All items in South Atlantic, all urban consumers, NSA	December 2017 = 100	Monthly
CUUR0360SA0	CPI – All items in East South Central, all urban consumers, NSA	December 2017 = 100	Monthly
CUUR0370SA0	CPI – All items in West South Central, all urban consumers, NSA	December 2017 = 100	Monthly
CUURS35CSA0	CPI – All items in Atlanta-Sandy Springs-Roswell, GA, NSA.	1982-84=100	Bi-monthly
CUURS35BSA0	CPI – All items in Miami-Fort Lauderdale-West Palm Beach, FL, NSA	1982-84=100	Bi-monthly
CUURS35DSA0	CPI – All items in Tampa-St. Petersburg-Clearwater, FL, NSA	1987=100	Bi-monthly[3]

[1]NSA = not seasonally adjusted
[2]SA = seasonally adjusted
[3]This CPI Index month's publication dates are not the same as the rest.

Rebasing CPI indices by placing a different period as 100 is a technique used to create a new reference point for measuring price changes. The purpose of rebasing in this context is to provide a clearer comparison and understanding of how prices have changed relative to a chosen base period. By setting a specific period, typically an earlier year or a more stable economic period,

as the base with a value of 100, subsequent periods can be easily compared to this benchmark. This makes it easier to gauge the magnitude and direction of price changes over time. For example, for rebasing to December 2019 = 100, missing Index Value (IV) data points had to be recalculated using the formulas below (Perrins & Nilsen, 2010).

$$IV_{Dec-2019} = \sqrt{IV_{Nov-2019} * IV_{Jan-2020}} \quad \text{Equation 5}$$

After December 2020, calculate Index Relative Rate of Change (IRRC) and the new Rebased Index Values (RIV) using the following formulas:

$$IRRC_{month} = \frac{CPI_{month}}{CPI_{previous\ month}} \quad \text{Equation 6}$$

$$RIV_{month} = IRRC_{month} * RIV_{previous\ month} \quad \text{Equation 7}$$

Before December 2019:

$$IRRC_{month} = \frac{CPI_{month}}{CPI_{following\ month}} \quad \text{Equation 8}$$

$$RIV_{month} = IRRC_{month} * RIV_{following\ month} \quad \text{Equation 9}$$

In **Figure 4.1** we presented the results of rebasing the indices to a common period, specifically December 2019. **Figure 4.2** presents representative results from the wavelet analysis of monthly Consumer Price Index (CPI) data. The wavelet power spectrum of the CPI indices, with significant periods (frequency) and corresponding time intervals indicated by the red areas. These red areas represent the periods in which the CPI indices exhibit significant coherence and synchronized behavior.

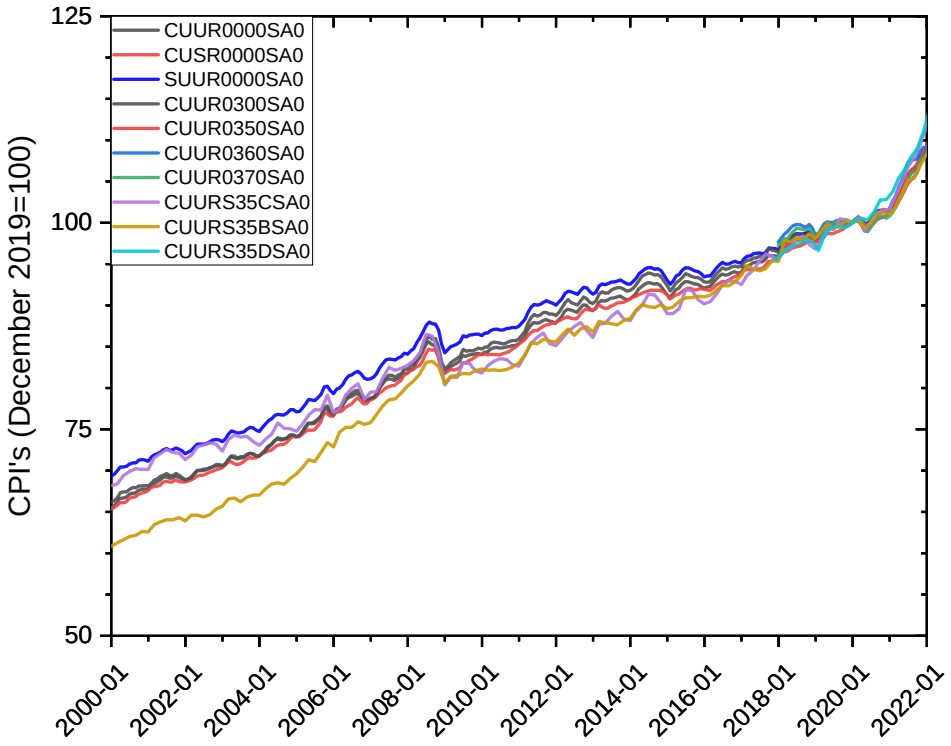

Figure 4.1. CPI indices rebased to December 2019 = 100.

Table 4.2. Correlations tests of wide U.S. CPI's indices monthly observation data.

Pearson	CUUR0000	CUSR0000	SUUR0000	CUUR0300	CUUR0350	CUURS35C	CUURS35D
CUUR0000	1	0.9997	0.9997	0.9991	0.9996	0.9987	0.997
CUSR0000	-	1	0.9993	0.998	0.9991	0.998	0.998
SUUR0000	-	-	1	0.9996	0.9995	0.9989	0.9972
CUUR0300	-	-	-	1	0.9993	0.999	0.9966
CUUR0350	-	-	-	-	1	0.9989	0.9981
CUURS35C	-	-	-	-	-	1	0.9967
CUURS35D	-	-	-	-	-	-	1

Table cells have been formatted conditionally to easily represent the higher and lowest coefficients using color code.

The horizontal arrows in **Figure 4.2** are indicative of the phase relationship between the two series at the respective periods. When arrows point towards the right, it signifies that the two series are in phase. On the other hand, arrows pointing to the left indicate that the two series are in

anti-phase. In this case, we can clearly appreciate the disturbance generated by the world economic crisis around 2008.

Table 4.3. Coherence tests of U.S. CPI's indices monthly percentage change.

		MONTHLY						
		CUUR0000	CUSR0000	SUUR0000	CUUR0300	CUUR0350	CUURS35C	CUURS35D
MONTHLY	CUUR0000	1	0.9322	0.9725	0.9603	0.9612	0.9164	0.9218
	CUSR0000	-	1	0.9242	0.9314	0.9185	0.9018	0.9072
	SUUR0000	-	-	1	0.9535	0.9555	0.9089	0.9152
	CUUR0300	-	-	-	1	0.9701	0.9171	0.9193
	CUUR0350	-	-	-	-	1	0.9288	0.9153
	CUURS35C	-	-	-	-	-	1	0.9236
	CUURS35D	-	-	-	-	-	-	1

Table cells have been formatted conditionally to easily represent the higher and lowest coefficients using color code.

Contrary to statistical intuition, simply making the time series longer does not increase the discriminatory power of the wavelet transform (Rösch & Schmidbauer, 2016). This is because the wavelet transform operates by transforming fixed-length pieces of the time series for a given period. The discriminatory power of the wavelet transform lies in its ability to analyze localized frequency components and variations over time, rather than the length of the time series itself (Rösch & Schmidbauer, 2016).

Table 4.2 and **Table 4.3** present the correlation and coherence coefficients, respectively. As expected, the general indices exhibit higher linear correlation coefficients with decreasing values in the specific delimited regional indices and cities. This indicates that the overall price movements are more closely aligned among the general indices, while the regional and city-specific indices show greater variability. Although the coefficient values will be considered in the literature as highly correlated. On the other hand, coherence analysis is more sensitive to the small changes present between the indices and can capture these subtle differences. Coherence measures

the degree of similarity in the timing and magnitude of fluctuations between two time series. By considering both correlation and coherence coefficients, we gain a comprehensive understanding of the relationships between the indices. Additional figures are supplied in Supplementary information.

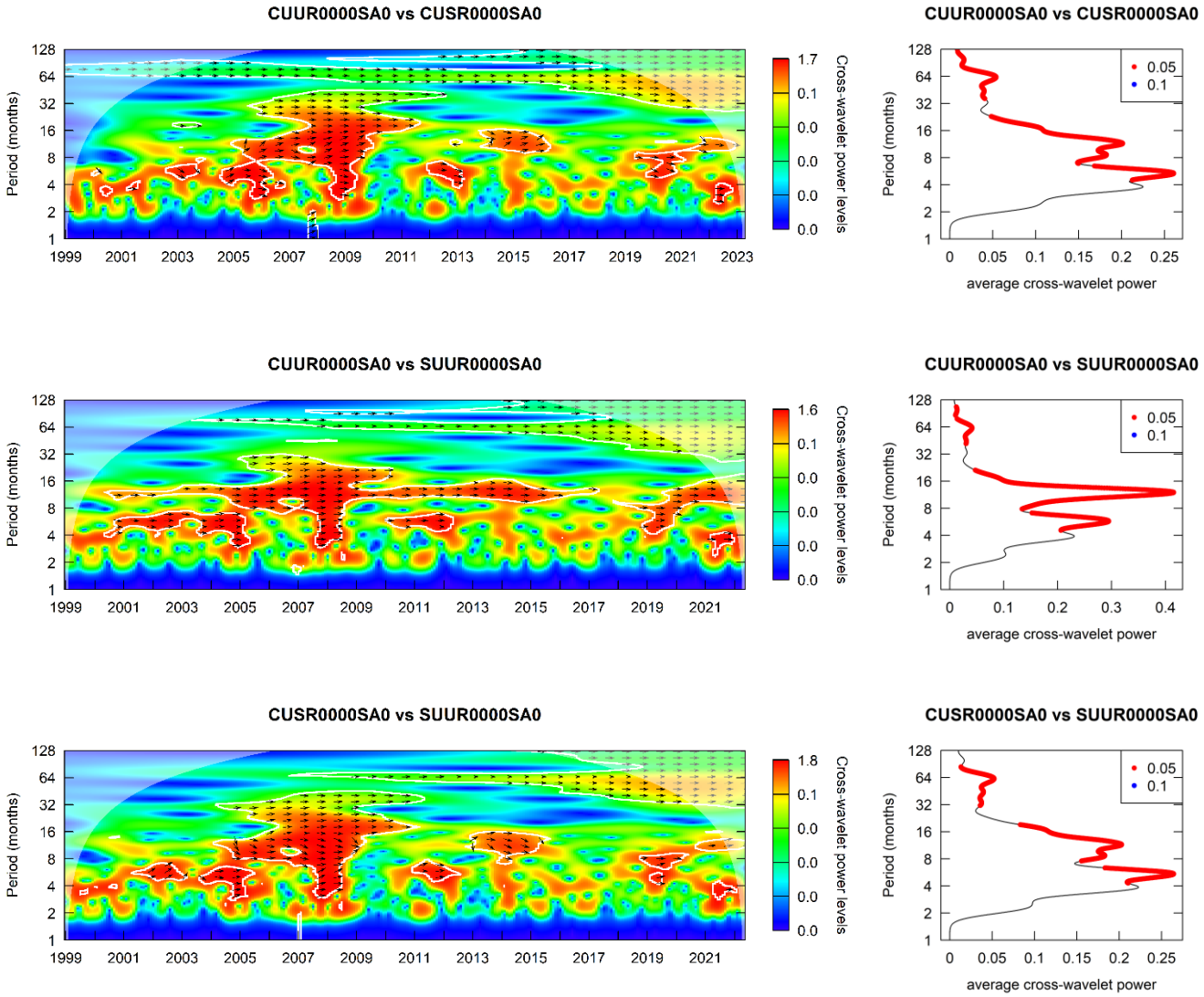

Figure 4.2. CPIs general indices cross-wavelet coherency analysis (monthly % change). Power spectrum (left) and corresponding time-averaged wavelet power (right). Red dots in the averaged wavelet power represent significance level <= 0.05.

4.5.3. Producer Price Indices

The Producer Price Index (PPI) is a metric that quantifies the average fluctuation over time in the prices obtained by domestic producers for their goods and services. It is also compiled by the Bureau of Labor Statistics (BLS) in the United States. The PPI measures price changes from the perspective of the seller, rather than the buyer, as is the case with the Consumer Price Index (CPI). The PPI includes prices at all stages of production, from raw materials to finished goods, and can be broken down by industry and commodity. Like the CPI, the PPI is calculated by selecting a base period and assigning it a value of 100. The prices of goods and services in subsequent periods are then compared to the prices in the base period, and changes in the prices are reflected in the PPI. The PPI is often used by businesses and policymakers to track trends in inflation and to adjust pricing strategies. Because the PPI measures price changes at the wholesale level, it can provide an early indication of inflationary pressures in the economy before those pressures reach consumers.

Table 4.4 provides an overview of the Producer Price Index (PPI) data, shedding light on certain limitations and exclusions that are crucial to address. Firstly, there are specific periods, namely 1991-1997, 2004-2005, and 2011-2013, for which no data is available in certain indices. And in some cases, the PPI data is only accessible from 1982 to 2003, and a data gap exists for the years 1990-1993. Moreover, it is important to note that the hardwood lumber indices were not utilized in this paper. Recognizing these limitations and exclusions is crucial for understanding the scope and constraints of the data, and it is important to consider their implications when interpreting the findings and drawing conclusions from this study. Due to the problems described for WPS0811 it will not be further discussed in this work. Same situation with WPU0812 and WPS0812, since we are not interested in discussing Hardwood lumber stumpage activity for this

paper. Nevertheless, are worth a mention for further studies. In **Figure 4.3** we present the rebased Producer Price Index (PPI) values, using December 2019 as the reference period with a base index of 100.

Table 4.4. PPI's all relevant indices.

Series ID	Series Title	Base Period	Periodicity
WPU08	PPI – Commodity data for Lumber and Wood Products, NSA	1982-84=100	Monthly
WPU081	PPI – Commodity data for Lumber and Wood Products – Lumber, NSA	1982-84=100	Monthly
WPU0811	PPI – Commodity data for Lumber and Wood Products – Softwood Lumber, NSA	1982-84=100	Monthly
WPS0811	PPI – Commodity data for Lumber and Wood Products – Softwood Lumber, SA	1982-84=100	Monthly[1]
WPU0812	PPI – Commodity data for Lumber and Wood Products – Hardwood Lumber, NSA	1982-84=100	Monthly
WPS0812	PPI – Commodity data for Lumber and Wood Products – Hardwood Lumber, SA	1982-84=100	Monthly[2]
PCU1133-1133	PPI - Industry group data for Logging and Sawmills, NSA	Dec 1981=100	Monthly
PCU11331-11331	PPI - Industry group data for Logging, NSA	Dec 1981=100	Monthly
PCU113310113310	PPI - Industry group data for Logging – Tree-length Southern Pine, NSA	Dec 1981=100	Monthly
PCU113310113310P	PPI – Industry group data for Logging - Primary products, NSA	Dec 1981=100	Monthly

[1]No data for 1991-1997, 2004 - 2005, 2011-2013. Not able to rebase.
[2]Only available from 1982 to 2003. No data for 1990-1993. Not able to rebase.
Hardwood lumber indices not used in this paper.

PCU1133 stands for "Logging and Sawmills," and it includes all goods and services related to logging and sawmill operations, such as harvesting, processing, and preparing logs for market. This category includes products such as lumber, veneer, plywood, and other wood-based products. The PPI tracks price changes in PCU1133 over time to provide insights into trends in the cost of producing and selling logging and sawmill products. This information can be useful to businesses

and policymakers who need to make decisions about pricing, investment, and resource allocation in the forestry and wood products industry.

The PPI tracks price changes in PCU1133 over time to provide insights into trends in the cost of producing and selling logging and sawmill products. This information can be useful to businesses and policymakers who need to make decisions about pricing, investment, and resource allocation in the forestry and wood products industry.

PCU11331 stands for "Logging," and it includes all goods and services related to the process of harvesting and transporting logs from forests to sawmills. This category includes items such as felling and bucking equipment, logging trucks, and other tools and machinery used in logging operations.

PCU113310113310 refers to "Tree-length Southern Pine" and includes all goods and services related to the harvesting and transportation of southern pine trees that have not been cut to specific lengths. This category includes items such as cutting equipment, skidders, loaders, and trucks used to transport the tree-length southern pine from the forest to processing facilities. This is the only PPI that has a geographical relation to the southeast.

Table 4.5. Coherence PPI's indices monthly percent change.

		MONTHLY						
		PCU1133-1133	PCU11331-11331	PCU113310 113310	PCU113310 113310P	WPU08	WPU081	WPU0811
MONTHLY	PCU1133-1133	1	1	0.9997	0.9969	0.884	0.88	0.882
	PCU11331-11331	-	1	0.9997	0.9969	0.884	0.88	0.882
	PCU113310 113310	-	-	1	0.9967	0.884	0.881	0.882
	PCU113310 113310P	-	-	-	1	0.886	0.882	0.884
	WPU08	-	-	-	-	1	0.965	0.96
	WPU081	-	-	-	-	-	1	0.984
	WPU0811	-	-	-	-	-	-	1

Table cells have been formatted conditionally to easily represent the higher and lowest coefficients using color code.

Table 4.5 shows the results obtained from the wavelet analysis, they indicate that the WPU indices exhibited stronger and more pronounced fluctuations during the COVID-19 period compared to the PCU indices. These fluctuations may be attributed to the various factors influencing the producer prices, such as supply chain disruptions, changes in production costs, and shifts in market demand. Contrary to the COVID-19 period, the wavelet analysis revealed that the PCU (Consumer Price Index) indices exhibited greater sensitivity to the 2008 global economic crisis.

Supplementary, provides comprehensive figures and additional information that further supports and elaborates on the findings related to the differential sensitivity of the PCU and WPU indices. These supplementary materials enhance our understanding of the wavelet analysis results and provide a more nuanced perspective on the dynamics of price fluctuations in response to global economic downturns. The differential behavior underscores the importance of considering both perspectives when analyzing the effects of major economic events on price dynamics.

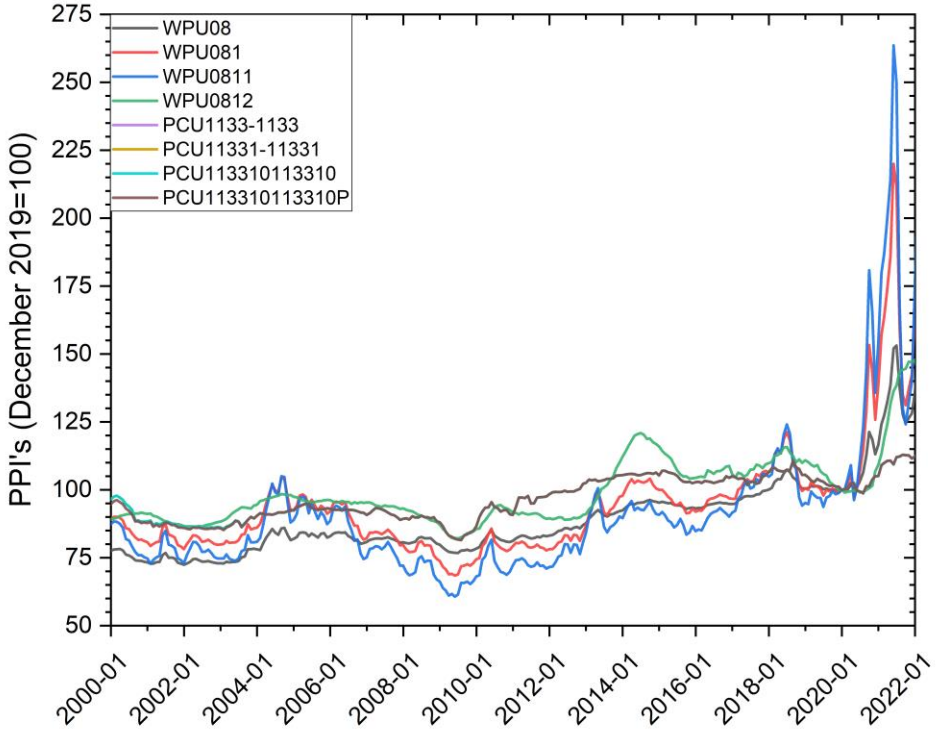

Figure 4.3. PPI's indices rebased to December 2019 = 100.

4.5.4. Open Market Indices

Table 4.6 provides an overview of different investment vehicles, including ETFs (Exchange-Traded Funds), REITs (Real Estate Investment Trusts), stocks, and futures. Each of these investment options offers unique features and benefits for investors seeking exposure to various asset classes and markets.

ETFs are investment funds that trade on exchanges and track the performance of an underlying index, commodity, or asset. They provide diversification by holding a basket of securities, making them attractive to individual investors looking for broad market exposure or specific sector investments.

Table 4.6. Financial instruments.

Type	Series ID	Series Title	Data Since	Periodicity[1]
ETF	WOOD	iShares Global Timber & Forestry ETF	June-25-2008	Quarterly, Monthly, Weekly, Daily
REIT	PCH	PotlatchDeltic Corporation	Jan-01-1969	Quarterly, Monthly, Weekly, Daily
REIT	RYN	Rayonier Inc.	Feb-17-1994	Quarterly, Monthly, Weekly, Daily
Stock	WY	Weyerhaeuser Company	Jan-02-1968	Quarterly, Monthly, Weekly, Daily
Stock	ADN[2]	Acadian Timber Corp	Jan-31-2006	Quarterly, Monthly, Weekly, Daily
Futures	LBS1	Random length lumber futures	Nov-16-1972	Quarterly, Monthly, Weekly, Daily

[1]Some instruments are available for up to 1-hour frequencies.
[2]In CAD ($).

REITs, on the other hand, are investment vehicles that own and operate income-generating real estate properties. Investors can purchase shares in a REIT, which grants them a portion of the income and profits generated by the real estate holdings. REITs are a popular choice for those seeking to invest in the real estate market without directly owning properties.

Stocks, referred to as shares or equities, symbolize ownership in a company. When investors buy stocks, they become shareholders and have a stake in the company's assets and earnings. Stocks are traded on stock exchanges, and their prices can fluctuate based on various factors such as the company's financial performance, market conditions, and investor sentiment.

Futures contracts are predetermined agreements that standardize the buying or selling of an underlying asset at a specific price and date in the future. They can be traded on commodities, financial instruments, or indices. Futures serve multiple purposes, including speculation on price movements, hedging against potential losses, and locking in prices for future transactions.

Lastly, the table presents futures contracts, specifically Random Length Lumber futures (LBS1!), which allow traders to speculate on the price movements of lumber, an essential product in the timber and forestry industry.

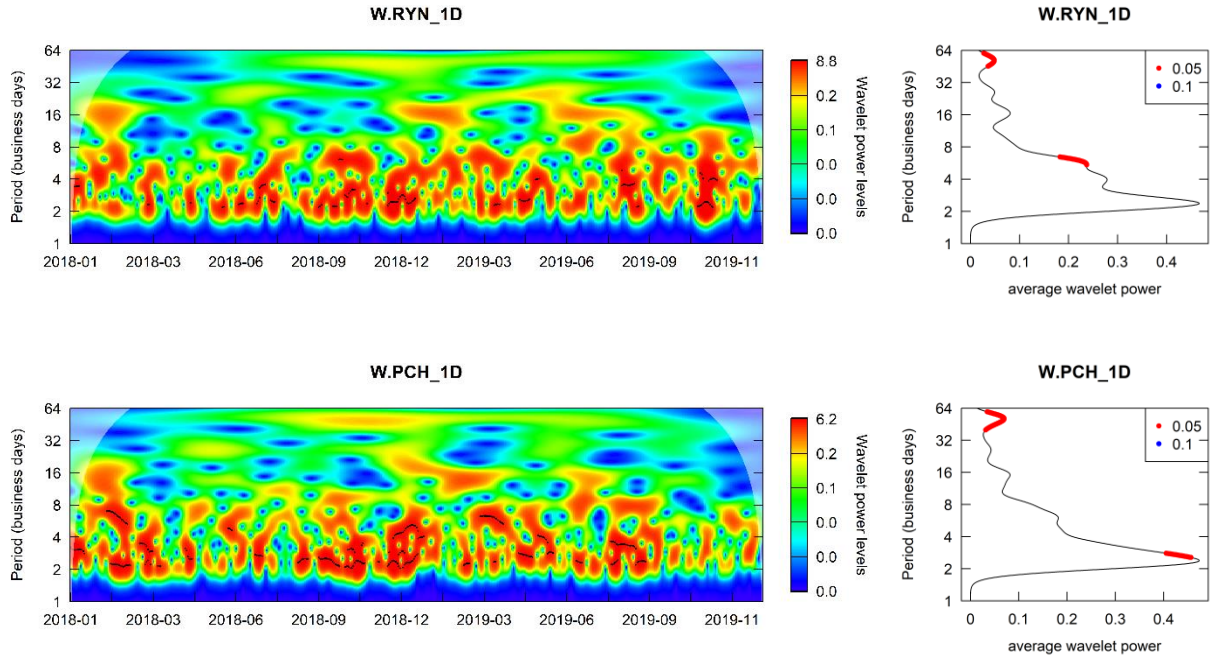

Figure 4.4. Wavelet analysis from open market indices (daily). Power spectrum (left) and corresponding time-averaged wavelet power (right). Red dots in the averaged wavelet power represent significance level <= 0.05.

Figure 4.4 presents the daily percent change wavelet analysis of two openly traded market indices. The analysis reveals significant periods in the range of 2-4 and 32-64 days, particularly during the year 2018. These significant periods are of particular interest as they coincide with the occurrence of Hurricane Michael. **Figure 4.5** presents the price data for various financial instruments relevant to the timber and forestry industry that were utilized for the study and to forecast the price series after hurricane Michael.

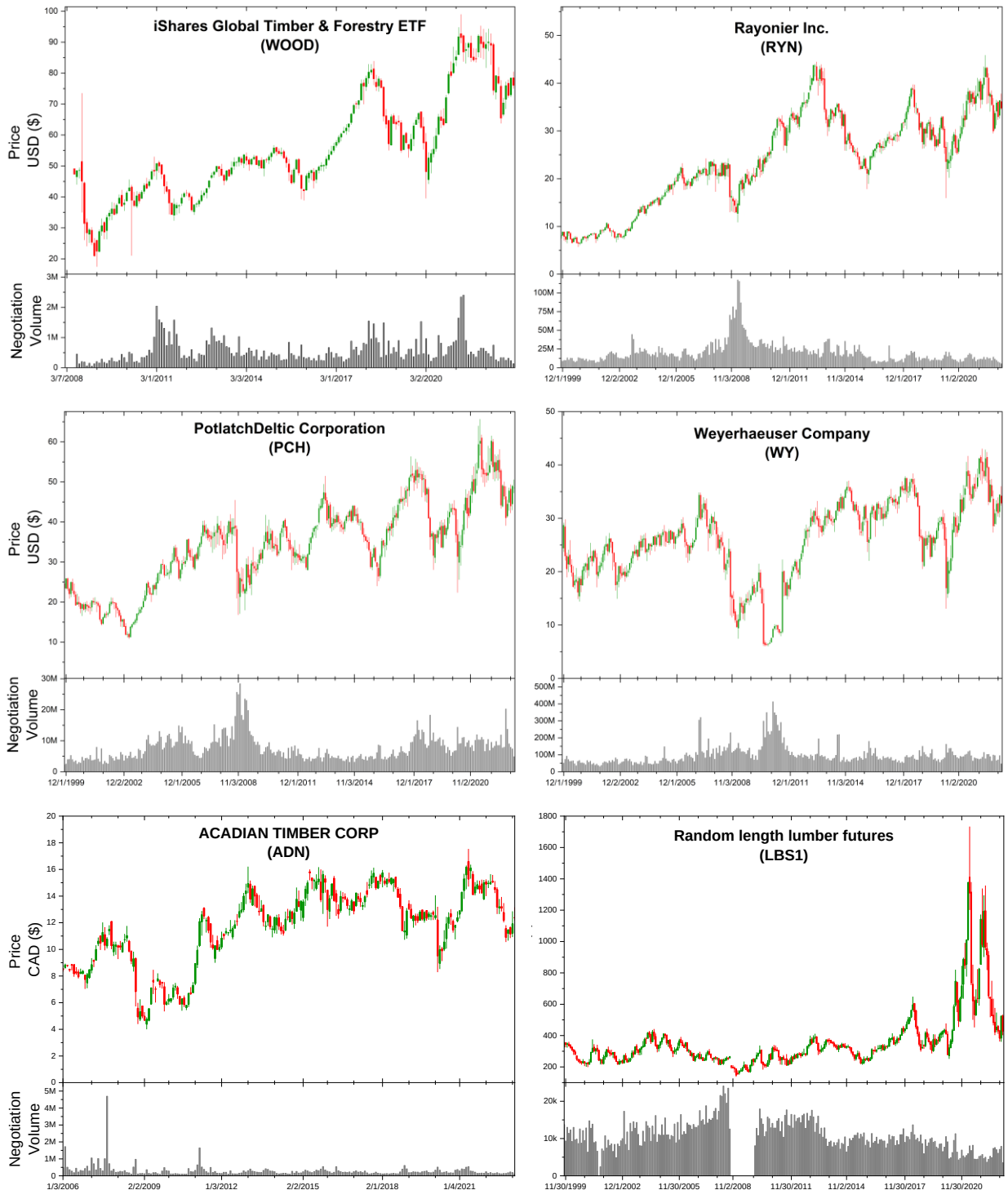

Figure 4.5. Open market indices in Monthly basis.

The representation of price series is in Heikin-Ashi candles and the corresponding negotiation volume below as columns.

4.5.5. Case of study: Hurricane Michael 2018

Hurricane Michael underwent rapid intensification and became a hurricane around midday on October 8. Continuing to strengthen, the storm reached the Gulf of Mexico a few hours later and developed into a major hurricane late on October 9. At 17:30 UTC on October 10, Michael made landfall near Panama City, Florida, as a Category 5 hurricane with maximum sustained winds of 160 mph (260 km/h) and a minimum central pressure of 919 mbar (27.1 inHg). Michael became the most intense storm of the season and the third-strongest hurricane to make landfall in the United States in terms of central pressure. After landfall, Michael quickly weakened over land, transitioning to a tropical storm over Georgia on October 11. By October 12, it became an extratropical cyclone over Virginia (Avila, 2019b).

A comprehensive visual representation of the US Southeast timber market areas, as defined by Timber Mart-South (TMS), overlaid with the tracks of hurricanes that made landfall during the specified year is shown in **Figure 1.3** (NOAA, 2022). In addition, the figure includes the reported areas that were damaged by Hurricane Michael in the Florida Panhandle and Hurricane Florence in North Carolina(*A Bird's Eye View: Aerial Surveyors Map Timber Damage from Hurricane Florence | In the Field*, 2018; Florida Forest Service, 2018). The TMS-defined timber market areas provide a framework for understanding the regional dynamics and market conditions specific to the Southeastern United States.

The Florida Panhandle, including areas such as Mexico Beach, Panama City, and Panama City Beach, suffered catastrophic damage from Hurricane Michael. The property damage in the United States from Hurricane Michael was estimated to be at least $25 billion (Weisbrod, 2022). According to some reports the total downed woody materials left by Michael, reached more than 83 million short tons (Brandeis et al., 2022).

The Atlantic Hurricane seasons are defined by specific boundaries each year. In 2017, the season began with the formation of the first system on April 19 and concluded when the last system dissipated on November 9. Similarly, in 2018, the season started on May 25 with the formation of the first system and ended on October 31 when the last system dissipated. Moving on to 2019, the season began on May 20 with the formation of the first system and continued until November 24 when the last system dissipated. These dates mark the time during which the Atlantic region experiences heightened tropical cyclone activity and serve as a reference for monitoring and assessing the impact of these storms.

4.5.6. Case of study: Results

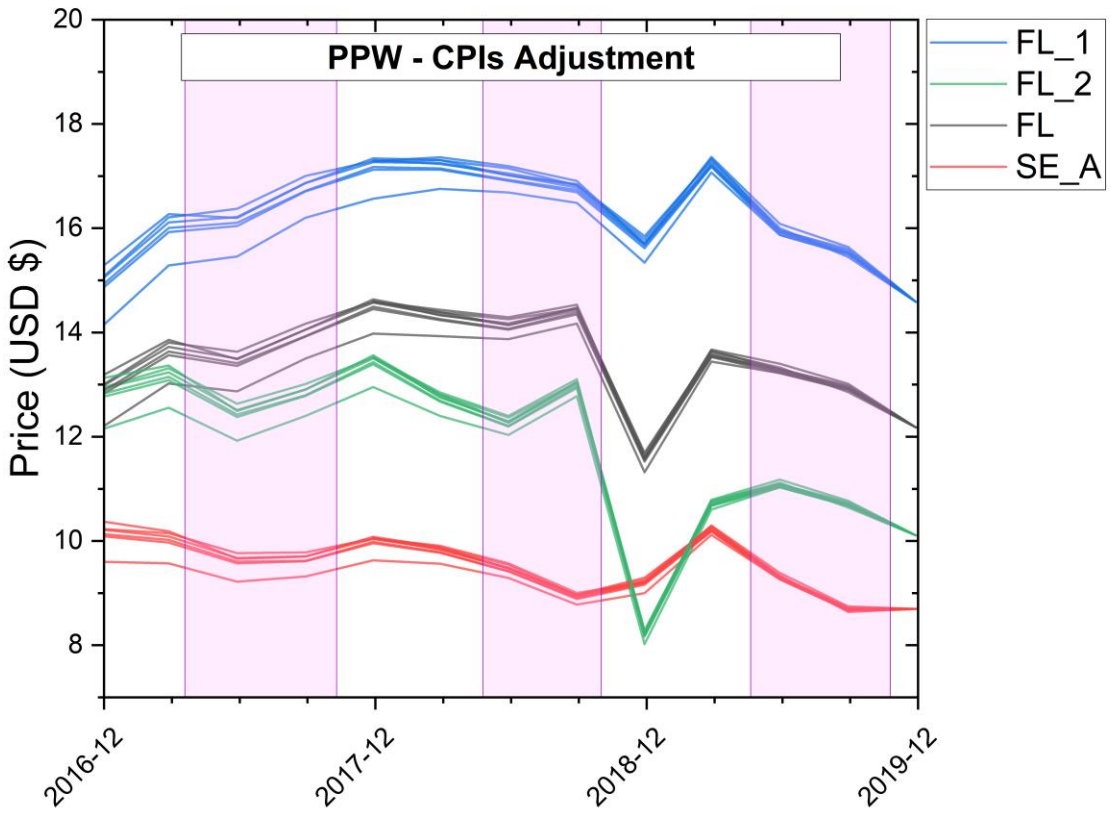

Figure 4.6. Effect of CPI's adjustment in Florida's PPW indices.

Figure 4.6 provides an insightful view of the effect of the Consumer Price Index (CPI) adjustment on the Timber Mart-South (TMS) Florida general average and regional indices for pulpwood, as well as the southeastern average. This analysis specifically focuses on the period during Hurricane Michael. By rebasing the indices to December 2019, the variation in the indices during 2018 is relatively small, with a gradual increase observed as we move further back in time. The CPI adjustment allows for a more accurate representation of the price movements by accounting for inflationary factors and providing a consistent reference point.

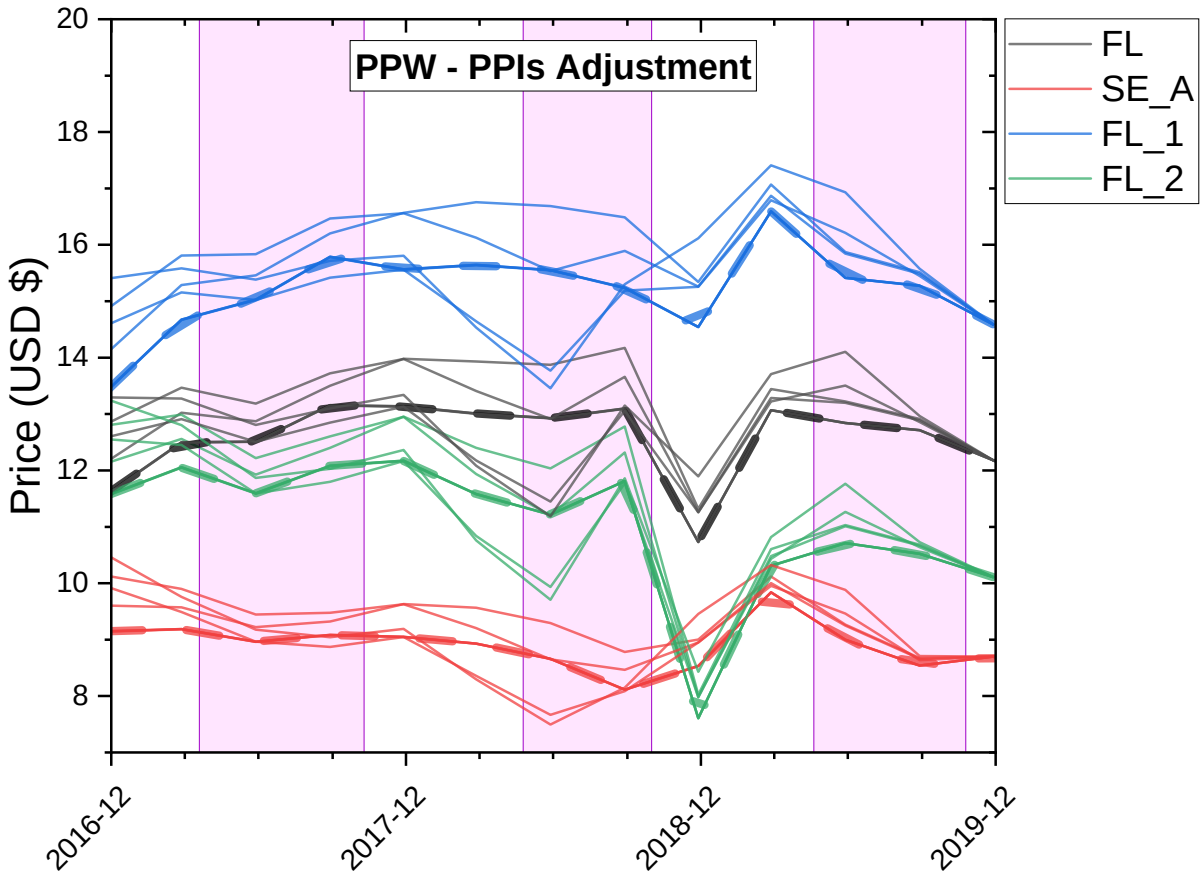

Figure 4.7. Effects of PPIs adjustment on Florida PPW indices.

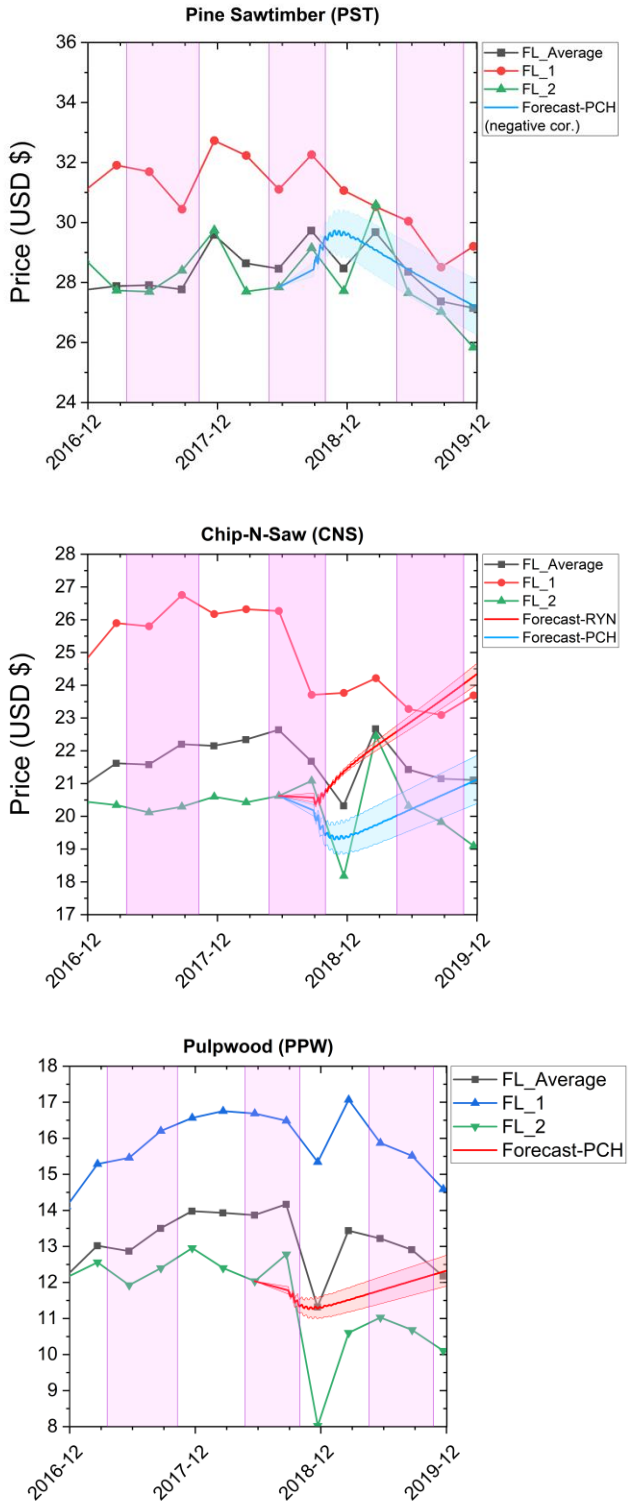

Figure 4.8. Florida PST, CNS and PPW forecasting with RYN and PCH. The forecast center line corresponds to the average of the four series used (open, high, low, close). The probability cone is the standard deviation resulting from the average process.

Figure 4.7 presents the analysis of Producer Price Indices (PPIs). The results of the analysis reveal a higher level of variation compared to Consumer Price Indices (CPIs). This indicates that the PPIs exhibit greater volatility in price movements within the selected period. It is important to note that the higher variation in the PPIs may come at the cost of potentially losing some level of detail in identifying specific price movement patterns. Examples of that are the second and third quarters for 2018 in the figure, in which some adjusted series appear more horizontal than others. This implies that while the PPIs provide a broader perspective on price changes in the market, they may preserve the finer nuances and subtle fluctuations that can be observed by adjusting with the CPIs. The figure uses dashed lines specifically to highlight the adjustment made with the PCU113310113310 index, for logging tree-length southern pine.

In the context of analyzing the effects of hurricanes on stumpage prices in hurricane-affected states, the results of time series analysis using TMS quarterly data have indicated areas of significance at 2-4 periods (quarters). However, this limited resolution may not capture the full dynamics and nuances of the relationship between hurricanes and stumpage prices. The daily percent change wavelet analysis of two openly traded market indices reveals significant periods of 2-4 and 32-64 days, particularly during the year 2018. These significant periods are of particular interest as they align with the occurrence of Hurricane Michael.

Figure 4.8 depicts the price indices for the products pulpwood, chip-n-saw, and pine sawtimber in the TMS Florida region. These indices are accompanied by the forecasted results. The selection of the open market data was performed in conjunction with the correlation coefficients and coherency tables. Once the appropriate dataset was chosen, the forecast was recalculated based on the latest quarterly price available from TMS prior to the occurrence of Hurricane Michael. These forecasts corresponded to the daily data of open, high, low, and close.

Which is one of the advantages of high-frequency open market data. The negative correlation coefficient sign was employed to account for the inverse relationship observed between the forecasted values and the TMS basepoint for pine sawtimber. By multiplying the forecasted values by -1, the direction of the relationship is reversed, allowing for a more accurate alignment with the TMS basepoint. This adjustment ensures that the forecasted values for pine sawtimber align with the historical data and the expected market behavior. It allows for a more reliable assessment of the potential price movements and aids in making informed decisions based on the forecasted values in conjunction with the TMS base point.

The use of openly traded market indices for high-frequency forecasting, as supported by the results presented, offers several advantages in the context of now-casting or high-frequency forecasting. Timeliness: Openly traded market indices provide up-to-date and real-time information about market conditions. This enables analysts to capture and respond to market dynamics quickly, facilitating timely decision-making and forecasting. Granularity: High-frequency data, such as daily or intraday data, provides a more detailed and granular view of market movements. This allows for a more nuanced analysis of short-term fluctuations and patterns, which may not be captured by lower-frequency data. Sensitivity to shocks and events: High-frequency data is more responsive to shocks, events, and news releases that can impact markets. By incorporating these data into forecasting models, analysts can better capture and assess the immediate effects of such events on the market. Improved accuracy: High-frequency forecasting can lead to more accurate predictions by capturing the most recent information and market dynamics. This can be especially beneficial in volatile and rapidly changing markets where traditional lower-frequency data may not adequately reflect the current market conditions. Enhanced risk management: The ability to generate high-frequency forecasts allows for more

effective risk management strategies. Traders, investors, and policymakers can make timely adjustments to their positions or policies based on the most recent market information, reducing potential losses, or maximizing returns. The results obtained from comparing the forecasts with the remaining data from TMS after the impact of the hurricane demonstrated a good fit. These results indicated a recovery in prices within a period of 2-4 quarters. This finding is consistent to a certain degree with the previously reported literature.

However, it is worth noting that the return to the moving average price occurred more rapidly than what has been reported by other authors. The results obtained in this study suggest that there may be structural differences between the market conditions at the time of Hurricane Hugo in 1989 and Hurricane Michael in 2018. These differences include factors such as the acceleration of markets, increased frequency of operation, and improved data availability. These advancements have likely facilitated innovations and more efficient market dynamics, leading to a faster recovery in timber prices after Hurricane Michael compared to previous events.

4.6. Conclusions

In this study, wavelet coherence analysis provided additional insights into the relationship between the TMS data and the market indices. It facilitated the detection of patterns of similarity, periodicity, or relationships that may not have been apparent through traditional correlation analysis alone. The ability to capture both amplitude and phase information allowed for a more nuanced understanding of the coherence between the time series, providing valuable information on the potential impacts of hurricanes on stumpage prices.

The combination of traditional correlation analysis and wavelet coherence analysis enhanced the statistical analysis in this study, offering a comprehensive examination of the relationship between the TMS data and the market indices. Together, these analytical approaches

provided a robust foundation for understanding the dynamics of the timber market and the potential effects of hurricanes on timber prices.

Overall, the combination of correlation and coherence analysis allows us to uncover different aspects of the relationships between the indices. While correlation coefficients capture the broad linear associations, coherence coefficients provide a more nuanced understanding of the subtle differences and commonalities in their fluctuations. This comprehensive analysis enhances our ability to discern the intricate dynamics of the price data and offers valuable insights into the interconnectedness of the indices at various levels of aggregation.

By considering the CPI's geographic and item structures, as well as the specific delimitations for the South region and major metropolitan areas, this study ensures a comprehensive and accurate assessment of price changes and their potential impact on the timber market. The faster recovery observed in this study suggests a more accelerated rebound in prices following the hurricane's impact. This disparity in findings highlights the importance of considering various factors, such as market dynamics, local conditions, and specific characteristics of the hurricane event, when analyzing the impact on timber prices. The market's ability to quickly adapt and respond to the impact of natural disasters may have played a significant role in the observed faster recovery in timber prices.

These findings highlight the importance of considering the specific context and characteristics of each hurricane event when analyzing the impact on timber markets. The dynamic nature of markets, coupled with advancements in technology and data availability, have likely contributed to the observed differences in the recovery patterns of timber prices. Furthermore, it is important to highlight that the programming of the forecasting technique used in this study can be updated on a daily basis following a catastrophic event. This real-time updating capability enables

timely adjustments to the forecast based on the latest available data, allowing for a more accurate assessment of the post-event market conditions.

By continuously integrating new data and adjusting the forecasts, decision-makers can monitor the recovery progress, identify any deviations from the expected trajectory, and make necessary adjustments to their strategies or interventions. This dynamic and adaptive approach to forecasting helps to ensure that the decision-making process remains responsive to the changing market conditions in the aftermath of a natural disaster.

In conclusion, the TMS quarterly reports play a vital role in providing accurate and comprehensive timber price information in the US South. The collaboration among stakeholders, the data collection process, and the categorization of prices based on product types and diameter thresholds ensure a valuable resource for analyzing market trends and informing decision-making in the forestry and natural resource management sectors. While acknowledging the limitations and variations in reported prices, the TMS reports remain a valuable tool for understanding the dynamics of the timber market in the southeastern United States. The computational requirements for analyzing the extensive dataset used in this study are substantial. With the inclusion of 10 Consumer Price Indices (CPIs), 7 Producer Price Indices (PPIs), 30 state-wide Timber Market Survey (TMS) indices, 54 subregions, and 24 open market series, the number of unique correlations pairing combinations alone reaches an overwhelming 7750. These computations require significant computational resources and time to yield meaningful results. The computational challenges encountered highlight the complexity of analyzing the interplay between multiple variables and their correlations within the timber market context. Nevertheless, the extensive computational efforts undertaken in this study contribute to a more comprehensive

understanding of the relationships and dynamics within the dataset, providing valuable insights into the effects of hurricanes on stumpage prices in the Southern US region.

5. Loblolly Pine Downed Timber: Box-Behnken Design and First Derivative Pretreatment Boost Predictive Modeling with Near-Infrared Spectroscopy and Machine Learning (NIRS-ML)

5.1. Abstract

This study aimed to enhance wood composition analysis by integrating nonlinear techniques, employing the first derivative as a mathematical pretreatment, and adopting a Box-Behnken design to significantly reduce the requisite sample size for predictive models in loblolly pine downed timber characterization. Using 15 out of 176 core samples undergoing a year of natural degradation in the field, the models demonstrated efficiency comparable to full set models in the literature. Spectral pretreatment investigations underscored the efficacy of the first derivative and smoothing, achieving a balanced distribution of explained variance. Support Vector Machines (SVM) models, especially with the polynomial kernel, exhibited superior predictive performances. Assessment metrics, including R2 and root mean square errors, revealed cellulose, hemicellulose, and lignin models' performances. The cellulose model excelled, followed by hemicellulose and lignin models, with the polynomial kernel achieving R2 values of 0.61, 0.96, and 0.79, respectively. The study's innovative approach, employing a reduced sample size and simplified spectral treatment, yielded competitive results compared to traditional methods, showing potential for efficient wood composition prediction, even with samples enduring extended degradation times. These findings open avenues for streamlined and resource-efficient wood characterization, with implications for research and practical applications such as biorefineries and circular economy practices.

5.2. Methodology

The methodology for the downed timber model study is addressed in section 3.5. The sampling protocol is explained in section 3.7. Near infrared spectroscopy methodology is further explained in section 3.9. The experimental design and machine learning approach for the model

calibrations is detailed in section 3.10. Finally, the chemical characterization of the downed timber is noted in section 3.11.

5.3. Results and discussion

5.3.1. Near Infrared Spectroscopy (NIR)

The spectra of the 176 wood core samples collected are shown in **Figure 5.1**. The spectra output is typical of loblolly pine, with an evidence of overlap in the wood components signals, as reported in the literature (Kelley, Rials, Groom, et al., 2004). Band assignments for the first overtone of cellulose and hemicellulose hydroxyls between 1400 nm and 1600 nm can be identified. Same as with the 1890 nm and 2020 nm usually assigned to carbohydrate hydroxyls. Additionally, the region from 2020 nm to 2250 nm has been reported as cellulose hydroxyl vibrations (Kelley, Rials, Groom, et al., 2004). Lignin's aromatic and aliphatic C-H bonds reveal their presence in the near-infrared through overlapping first and second overtones (1635-1825 nm and 1075-1250 nm, respectively). Additionally, the first overtone of lignin hydroxyl vibrations (1400-1520 nm) partially overlaps with cellulose hydroxyl vibrations. Usually, the region below 1000 nm extending into the visible 650 nm shows very subtle features and is difficult to assign to wood components, so it was excluded from the region explored on NIR. Nevertheless, in literature, it has been assigned to the second overtones of hydroxyls and third overtones of stretching vibrations of C-H (Tolvaj, 2023).

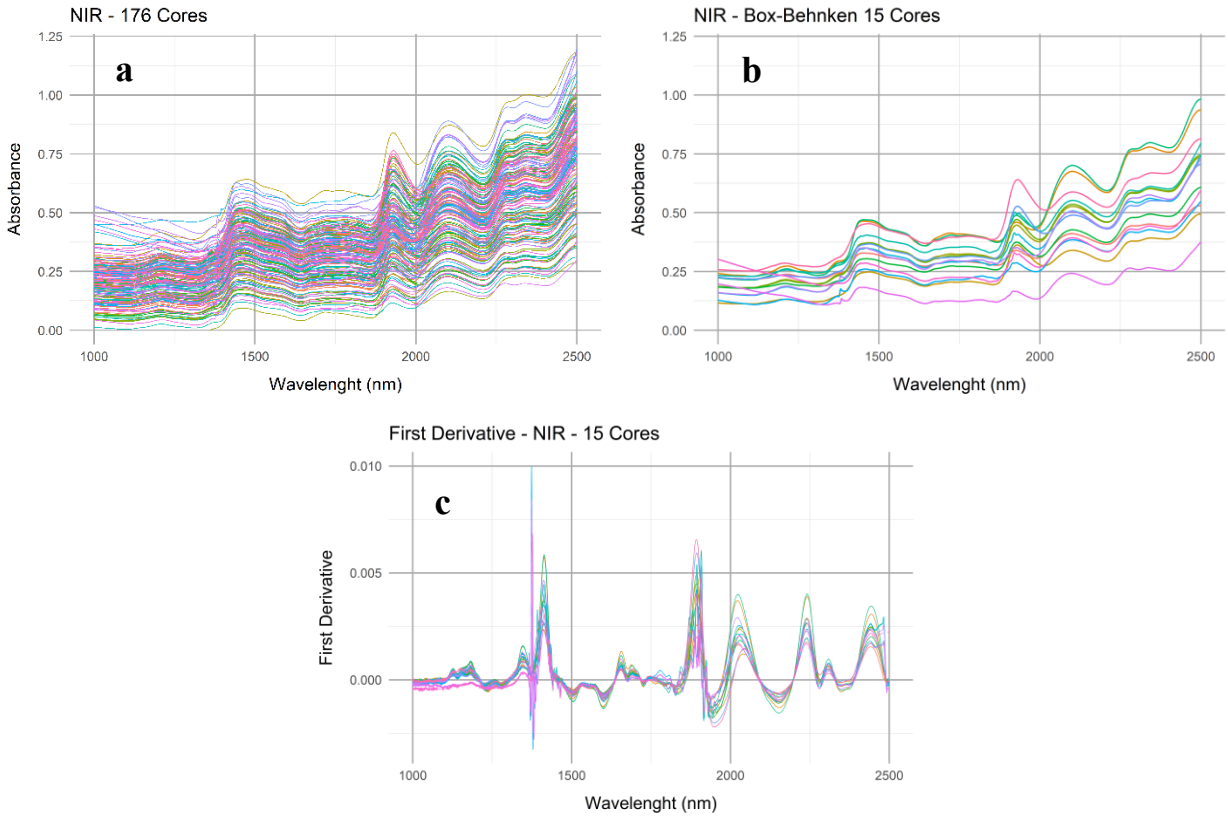

Figure 5.1. The collected NIR data from loblolly pine cores over the spectral range (1000 nm – 2500 nm). a full 176 core samples, b Box-Behnken optimized experiment design of 15 cores, c first derivative of the selected 15 cores. Savitzky-Golay smoothing to the first derivative has been applied for this graphic.

Various publications have underlined the use of spectroscopic techniques to predict the chemical composition of wood, often utilizing very large sets of samples or treating extensively the spectral data (Acquah, Essien, et al., 2018; He & Hu, 2013; Jones et al., 2006; Kelley, Rials, Groom, et al., 2004; B. Via et al., 2012; B. K. Via et al., 2007). This work extends these studies by utilizing the Box-Behnken design, with a simple spectral pretreatment approach and reducing the extensive wet chemical characterization, thus, reducing the use of expensive chemicals, labor, and work time. This design rises to the occasion by delivering a competitive calibration model with a

remarkably reduced sample size compared to the traditional full-sample characterization approaches (Gatius et al., 2004; B. Via et al., 2012).

5.3.2. The effect of pretreatments on Principal Component Analysis

Model development and calibration in literature using NIR often includes multiple pretreatments of the spectrum (Chen et al., 2013). This raises the question of under and over-treatment of the NIR spectra, with several preprocessing methods used by researchers most researchers being mean centering, standard normal variate, multiplicative scatter correction, extended multiplicative scatter correction, inverse scatter correction, and SG smoothing (W. Zhang et al., 2022). Finding the optimal pretreatment that preserves relevant information while avoiding over-complexity should be a key consideration in NIR model development. For example, on several reports, first derivative nonlinear baseline shifts were removed and resulted in a wider spread of explained variance. Distributing the explained variance could be advantageous, as it would facilitate a more refined separation of influences attributable to the fundamental wood polymers (B. Via et al., 2012).

Similarly, the analysis of the percentage of explained spectra variance using the 176 cores NIR spectra is shown below in Fig. 2. Savitzky-Golay smoothing was first applied to the raw NIR data before derivation, with parameters p = 2 (polynomial order) and n = 17 (frame length). Among the settings to control in the pcr function in R, the centering and scaling could also be sources of difference in the predictive power of the models. The differences in the percentage of explained variance by using raw, first derivative, second derivative, centering, and scaling are shown in **Figure 5.2**. Without smoothing, is evident that the first derivative is more balanced in distributing the explained variance among certain limits of factor numbers (namely between 5 and 10). The raw spectra achieved 99% explained variance without significative difference with only 3 factors

in every case. Nevertheless, there are significant differences in the centering and scaling using the pcr function for the first and second derivatives. The first derivative achieves 99% of the explained variance with 7 factors without centering and scaling. Meanwhile, it reaches 95% with 8 factors when using centering in the pcr function and only 63% with centering and scaling. The second derivative in this case would be out of the question for modeling.

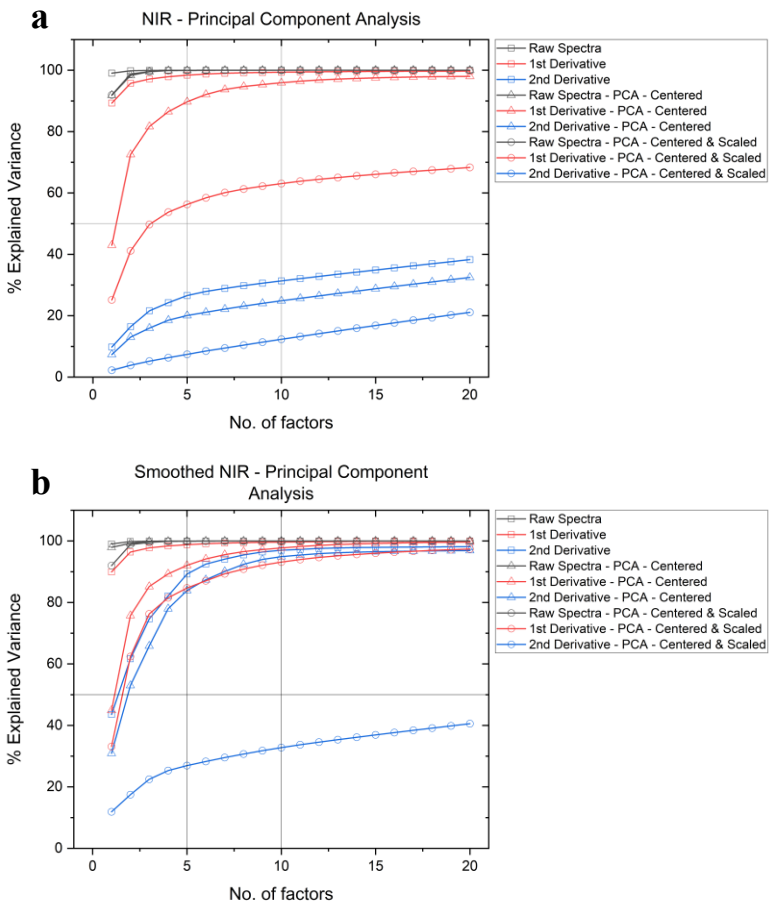

Figure 5.2. Percentage of explained variance for each sequential principal component that was computed, of 176 samples of loblolly pine cores. a when no smoothing is applied to the raw spectra, b when Savitzky-Golay smoothing was first applied to the raw NIR.

On the other hand, when first applying Savitzky-Golay smoothing there is little difference with raw spectra in all cases as in the previous case. The differences are notable only with how the first and second derivatives get closer except in the case of the second derivative centered and scaled. Moreover, the first derivative centered achieves 96% of the explained variance with 7 factors and 93% while centered and scaled with 10 factors. Similarly, the second derivative achieves 95% with 8 factors and 10 factors (non-centered/scaled, and centered, respectively). Finally, PCA was performed with the 15 NIR spectra selected using the BB design. The results were similar, the best balance in the percentage of explained variance was achieved with the Savitzky-Golay smoothed first derivative spectra when centered and scaled. To achieve 95% and 99% of the variance explained 7 and 10 factors were required, respectively.

5.3.3. Model development

The range of chemical compositions determined by chemical wet chemistry is shown in **Table 5.1**. The random selection of calibration and test resulted in sets with almost similar ranges to the original set. To explore the relationship between chemical composition and NIR spectra, a series of regression models were constructed using wet chemistry data and NIR spectra acquired. Preprocessing with the 1st derivative has demonstrated better prediction in other reports and our preprocessing showed similar behavior with our full NIR spectral set (B. K. Via et al., 2014). The ratios 2/3 and 1/3 were used to populate the calibration and test sets respectively. 22 samples were used to construct the models. Then the models were used to predict the chemical composition of the test set that has not previously been included in the data used for model development. Evaluating the model using samples that were not part of the initial model is an illustration of how these models can be employed to forecast the composition of numerous unidentified samples.

Table 5.1. Compositional range of the loblolly pine samples used for the construction of the models of wood chemistry. All values are weight percent.

	Lignin	Cellulose	Hemicellulose
All samples			
Min	31.25	24.15	9.45
Max	38.82	49.24	18.94
Average	34.82	36.03	12.77
Median	34.54	35.06	12.52
CAL set			
Min	32.06	24.15	9.45
Max	38.82	49.24	18.94
Average	34.94	35.25	12.63
Median	34.50	33.22	12.57
TEST set			
Min	31.25	27.34	11.06
Max	37.74	46.62	17.5
Average	34.50	38.18	13.14
Median	35.15	38.19	12.52

Upon examination of **Figure 5.3**, the data points for the CAL are mostly uniformly spread for lignin and cellulose models, with the cellulose model better clustered around the regression line. Meanwhile, for the hemicellulose, model points tend to cluster at the lower end of the wt.% regression line. Moreover, these correspond to two points that fall in the higher hemicellulose wt.% for the core samples, one was randomly chosen as part of the calibration set and the other as part of the test set. This shows that the Box-Behnken design was able to pick centered and extreme values to integrate with the model and the random function is equilibrated. The Lignin model showed the lowest prediction quality.

He and Hu achieved higher performance models after studying the influence of exhaustive preprocessing and iterative wavenumber range selection (He & Hu, 2013). However, for NIR field applications their approach might be prohibitively complicated. The parameter constraints of the SVM selected such as the degree parameters (limited to the third degree here) were selected to reduce the model complexity, overfitting, and computational cost (Bishop, 2006). The Cross parameter (Cross-Validation) parameter was set at 10. Performing cross-validation involves training multiple models, which can be computationally expensive, especially for large datasets and many folds (Cristianini & Shawe-Taylor, 2007). The number of folds in cross-validation influences the bias-variance trade-off, for example, >10 can reduce bias but increase variance, potentially leading to overfitting. Meanwhile, >5 can reduce variance but increase bias, potentially leading to underfitting (K.-P. Wu & Wang, 2009).

The quality of the models can be measured in several ways. In this work, the coefficient of determination (R2), the root means square error of prediction (RMSEP) and the root mean square error of calibration (RMSEC) were used as a way to compare the models, this data is shown in Although some kernels achieved a higher R2 value, the RMSEP and its ratio with RMSEC was not satisfactory. Therefore, the polynomial kernel was selected and tested for optimization with the SG-smoothing parameters. This work achieved models using lower preprocessing of the NIR spectra and significantly reducing the number of samples to undergo wet chemistry. Specifically, this work used 15 samples in duplicate for wet chemistry (corresponding to <10% of samples collected). Additionally, the sample variation in this study was affected mainly by the long-term natural degradation of the field over a year. It could be expected that fresher samples will perform better for modeling using SVM.

Table 5.2. Overall, the best-performing model was the cellulose model, followed by hemicellulose and lignin. Although some kernels achieved a higher R2 value, the RMSEP and its ratio with RMSEC was not satisfactory. Therefore, the polynomial kernel was selected and tested for optimization with the SG-smoothing parameters. This work achieved models using lower preprocessing of the NIR spectra and significantly reducing the number of samples to undergo wet chemistry. Specifically, this work used 15 samples in duplicate for wet chemistry (corresponding to <10% of samples collected). Additionally, the sample variation in this study was affected mainly by the long-term natural degradation of the field over a year. It could be expected that fresher samples will perform better for modeling using SVM.

Table 5.2. Calibration and root mean square errors for NIR models using 1st derivative. Utilizing 22 samples for calibration and 8 for test sets.

	Lignin			Cellulose			Hemicelluloses		
	R^2	RMSEC	RMSEP	R^2	RMSEC	RMSEP	R^2	RMSEC	RMSEP
PLS									
	0.539	1.26	2.26	0.366	5.398	6.277	0.499	1.525	2.016
SVM – Radial kernel									
	0.6	1.174	2.232	0.713	3.634	7.777	0.52	1.493	2.142
SVM – Bessel kernel									
	0.611	1.157	2.243	0.953	1.477	5.979	0.667	1.242	1.994
SVM – ANOVA RBF kernel									
	0.707	1.004	2.231	0.975	1.081	6.711	0.822	0.908	1.976
SVM – Polynomial kernel*									
	0.613	1.354	1.139	0.963	1.295	1.802	0.792	1.004	1.227

Partial Least Squares (PLS), Support Vector Machine (SVM).

*Optimization of SG smoothing parameters for Lignin: p=4, n=49. Cellulose: p=10, n=47. Hemicellulose: p=4, n=69.

5.3.4. Sensitivity of models to smoothing pretreatment

The potential of Savitzky-Golay (SG) smoothing pretreatment to enhance the accuracy of NIR-based prediction models for lignin, cellulose, and hemicellulose was investigated. The r code was modified to systematically explore combinations of polynomial degree (p) ranging from 1 to 10 and window size (n) ranging from 3 to 99 (odd, exceeding p) for the pretreatment. **Figure 5.4** shows the results of this exploration.

For the cellulose model, SG smoothing further improved the predictive performance, reaching $R^2 = 0.986$ with p = 10 and n = 95 (Fig. 4b and Fig. 5a). Interestingly, comparable R^2 values (>0.96) were achievable in less complex regions, such as p = 3 and n = 19 ($R^2 = 0.984$) and p = 2 and n = 93 ($R^2 = 0.985$). This suggests that optimal smoothing parameters can affect the resulting models greatly depending on spectral complexity. Nevertheless, the values for RMSEC and RMSEP were optimal with p=10 and n=47 (Fig. 5b-c). Thus, those smoothing settings were selected as the best performing model for cellulose.

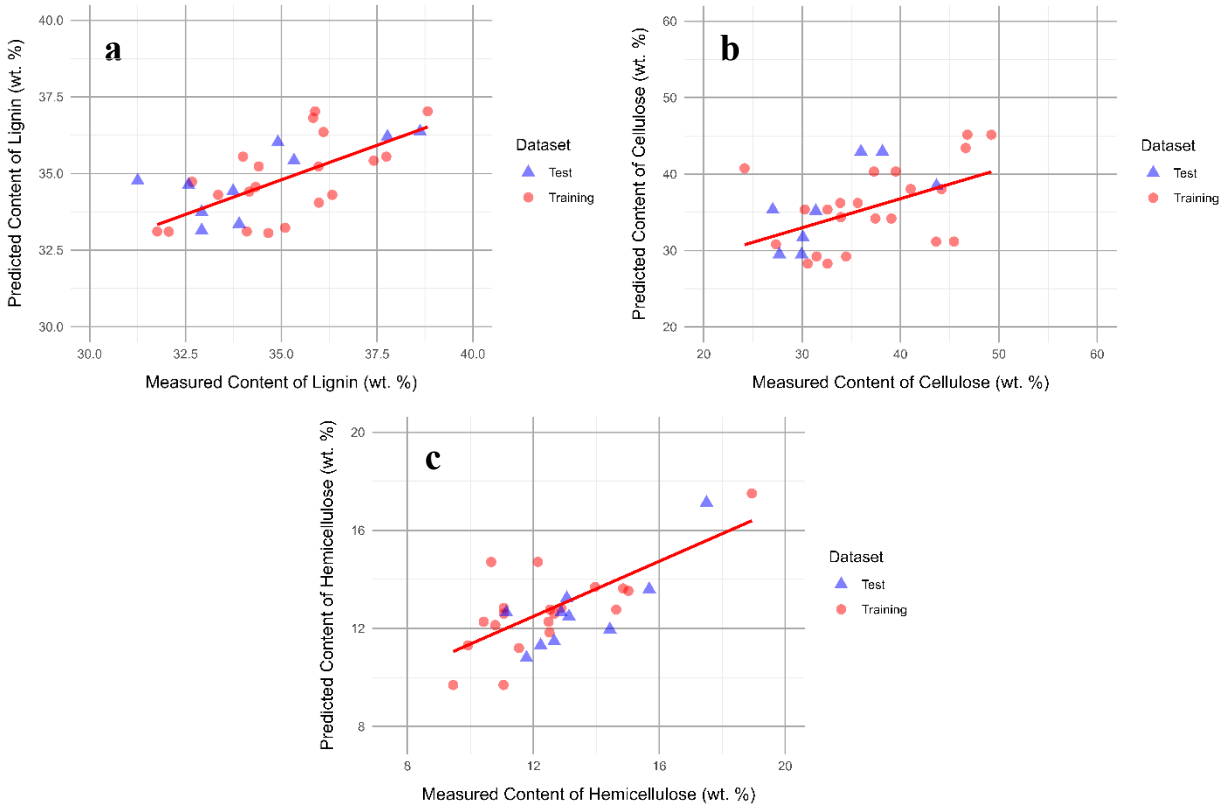

Figure 5.3. The results of support vector machine models showing the correlation between measured chemical compositions and the chemical compositions predicted with NIR spectra collected over the full spectral range (1,000 nm - 2,500 nm). a Lignin, b Cellulose, c Hemicelluloses.

Table 5.3. Wood NIR predictive modeling reported literature.

Tree # & species	# NIR Spectra [CAL:TEST]	NIR Range Measured [nm]	Number of Scans	Statistical Methodology	Correlation Coefficients Range [R^2]	RMSEC | RMSEP	Wood Geographic Origin	Reference
3 Loblolly pine	72 [45:27]	500 – 2,400	30	PLS	Lignin → 0.67 - 0.81 Glucose → 0.78 - 0.90 Xylose → 0.54 – 0.80 Mannose → 0.58 – 0.86 Galactose → 0.80 – 0.83	1.1 – 1.5 | 1.0 – 1.4 2.4 – 2.6 | 2.3 – 2.7 0.6 – 0.8 | 0.6 0.8 | 1.0 – 1.3 1.0 | 0.8 – 1.0	Southern Arkansas, USA	(Kelley et al. 2004)
17 Loblolly pine	40 [28:12]	1,100 – 2,500	100 - 150	PLS	Lignin → 0.85 Cellulose → 0.80 Hemicellulose → 0.59	0.48 | 1.21* 1.03 | 1.73* 0.92 | 1.04*	Georgia, USA	(Jones et al. 2006)
10 Longleaf pine	70	1,000-2,500	40	MLR – PLS - PCR	Lignin → 0.55	2.13 | NA	Mississippi, USA	(Via et al. 2007)
55 Larch 49 Eucalyptus 16 Poplar 27 Other	147 [100:47]	800 – 2,778	64	PLS	Lignin → 0.78 – 0.97	0.55 – 0.76 | 0.86 – 1.34	China	(He and Hu 2013)
4 Eucalyptus 9 Cotton wood 12 Aspen 12 Poplar	37 [13:3]	1,000-2,500	32	Linear & non-linear PLS	Lignin → 0.99 Cellulose → 0.96 Hemicellulose → 0.87	0.13 | 0.15 0.43 | 0.35 0.48 | 0.76	Varies	(Via et al. 2014)
30 Loblolly pine	176 [22:8]	1,000-2,500	128	PCR – BB - SVM	Lignin → 0.613 Cellulose → 0.963 Hemicellulose → 0.792	1.354 | 1.139 1.295 | 1.802 1.004 | 1.227	Southern Alabama, USA	This study

Partial Least Squares (PLS), Principal Components Regression (PCR), Multiple Linear Regression (MLR), Support Vector Machine (SVM), Not Available (NA)

*SEC and SEP

Similar improvements were observed for the hemicellulose model, with a wider range of high-R^2 regions (red) identified after SG pretreatment (Fig. 4c). The highest R^2 (0.974) was achieved with p = 1 and n = 97, but slightly lower values with less complexity were also promising (e.g., p = 3 and n = 51, R^2 = 0.961; p = 9 and n = 65, R^2 = 0.963). However, the optimized smoothing parameters were selected as p = 4 and n = 69, again considering optimization of RMSEC and RMSEP coefficients. These findings highlight the potential for fine-tuning the smoothing parameters to balance accuracy and model complexity.

As shown in **Figure 5.4**, Lignin prediction proved most sensitive to SG smoothing, with a more limited number of parameter combinations leading to improved R^2. The highest R^2 (0.99) was obtained with p = 9 and n = 55, but alternative combinations offered comparable accuracy with reduced complexity (e.g., p = 3 and n = 37, R^2 = 0.904; p = 5 and n = 9, R^2 = 0.865). Nonetheless, R2 could result in misleading performance of the models. The best RMSEC and RMSEP performance was obtained with p = 4 and n = 49. This suggests the need for careful optimization to avoid overfitting while maximizing accuracy for lignin prediction.

The reduced performance for the lignin model could root in several factors. For example, it has been suggested that extractive contents adversely affect the ability to estimate lignin due to the presence of phenolic compounds (B. K. Via et al., 2007). Since the NIR characterization of the cores was performed before the chemical characterization, bias due to extractives present in the cores is a plausible explanation. Moreover, the degradation experienced in the field could be a big contributor to errors in the models. For example, we detected samples with white rot and blue stain fungi after several weeks in the field. Living wood inherently houses dormant fungal inhabitants, and upon the tree's demise, a subset of these fungi promptly transitions into primary colonizers (Lustenhouwer et al., 2020; Parfitt et al., 2010). In the context of this study, the decay experienced

by the trees in the field serves as a pivotal factor influencing the construction of the NIR predictive model. The primary colonizers actively engage with wood components, including sap sugars and the resilient structures of lignocellulosic cell walls (Song et al., 2017). To fulfill this role, fungi must pass through the cell wall structure, breaking through the lignin barrier to reach cellulose and hemicellulose (Cline et al., 2018). The the enzymatic hydrolysis process, fungi play a crucial role by producing enzymes, such as cellulases, which facilitate the breakdown of cellulose into smaller sugar molecules (Payne et al., 2015). These molecules serve as a vital carbon source for the fungi, enabling them to access the energy and nutrients stored within the wood (Walker & White, 2017). Fungi with the capability to degrade lignin are categorized as white rot fungi (Fukasawa & Matsukura, 2021). These specialized organisms release a distinctive set of enzymes, including lignin peroxidases, manganese peroxidases, and laccases (B. Goodell et al., 2020). These enzymes work in concert to dismantle the intricate bonds within lignin. Through this enzymatic activity, white rot fungi modify and degrade lignin molecules, rendering the cellulose and hemicellulose components more accessible for subsequent stages of decomposition (Dashtban et al., 2010). The enzymatic hydrolysis of lignin in the wood core might have significantly influenced the model performance for lignin prediction, introducing additional complexities to the interplay of fungal colonization and wood decay considered in the NIR predictive modeling.

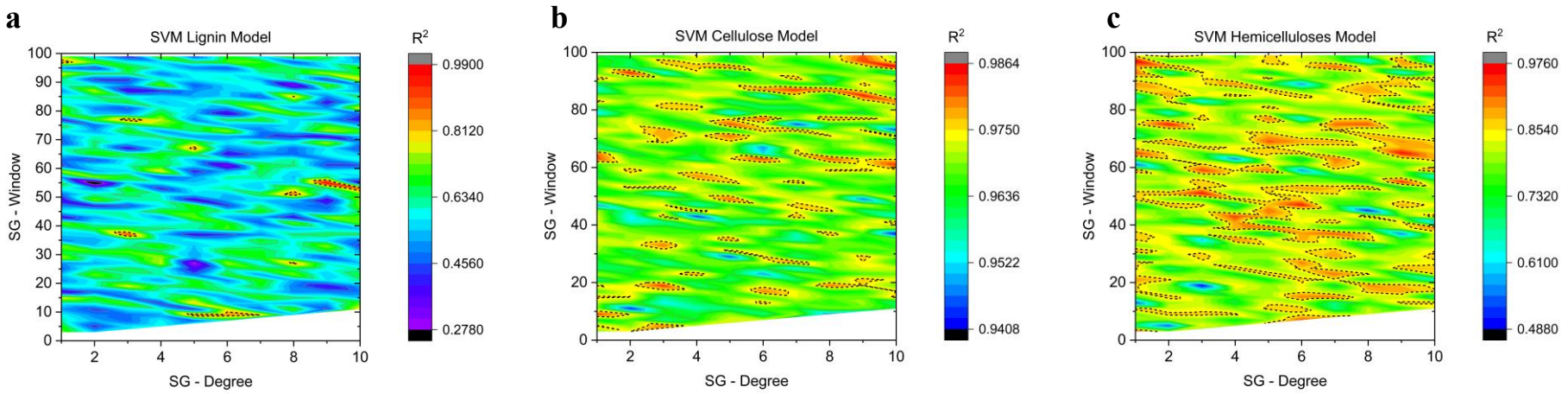

44

45 **Figure 5.4.** The sensitivity of support vector machine models with the polynomial kernel to Savitzky-Golay smoothing parameters (polynomial degree and window size) with

46 NIR spectra collected over the full spectral range (1,000 nm - 2,500 nm). **a** Lignin, **b** Cellulose, **c** Hemicelluloses. Red color indicates higher R2 statistic obtained by the model.

47 The region of the higher quarter R2 has been highlighted by dotted black lines.

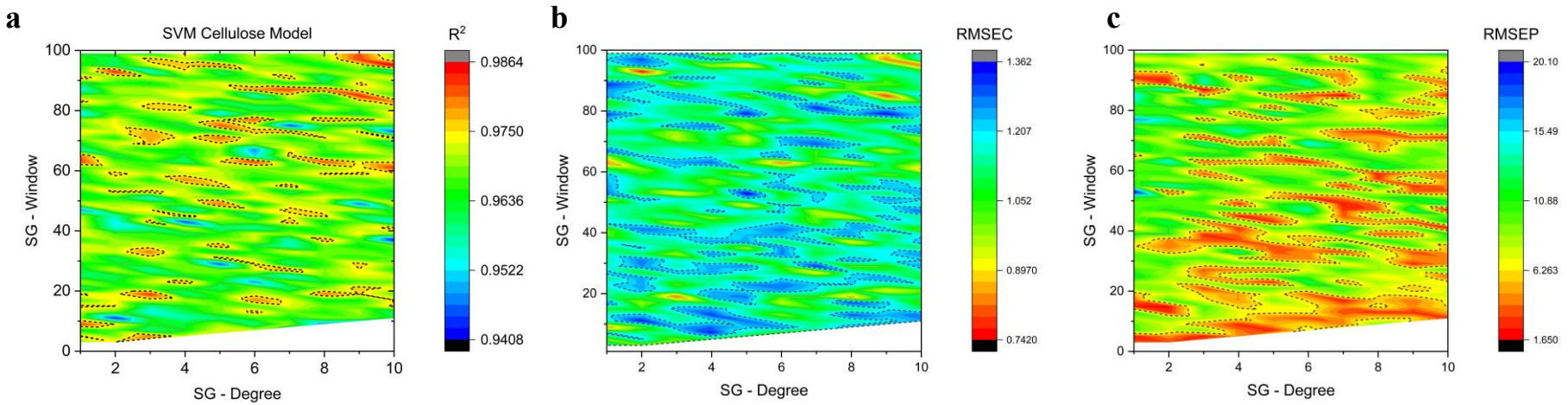

Figure 5.5. Optimized results for Lignin model. Statistical parameters: **a** R2, **b** RMSEC, **c** RMSEP. SG – Degree = 10, SG – Window = 47, R^2 = 0.963, RMSEC = 1.295, RMSEP = 1.802.

Several studies have highlighted the effectiveness of SG smoothing for NIR-based analysis, showcasing its versatility for different applications. Notably, Tuncer et al. explored its utility in distinguishing wood species like Scotch pine and black pine, which are notoriously difficult to separate using traditional methods. Employing SG parameters of 1 and 2 polynomial degrees with window sizes of 3, 5, and 15 alongside PLS-DA, they achieved a remarkable 95% classification accuracy, a significant improvement over the 84% without any preprocessing (Tuncer et al., 2023). Shi et al. implemented an "SG-PLS" optimization platform to systematically assess various parameter combinations and identify the optimal configuration for their specific dataset. Through this approach, they identified the most effective set of SG parameters – d = 2, p = 6 (3rd-degree polynomial), n = 23, and LV = 8 (8 latent variables) – leading to a promising RP,V of 0.722 (Shi et al., 2021). Finally, Chen et al. focused on optimizing SG smoothing in conjunction with another preprocessing technique, multiplicative scatter correction (MSC), for FT-NIR PLS models. Their investigation revealed that the most effective combination involved applying SG smoothing first, with parameters of p = 4 (4th-degree polynomial), derivative order of 2 (second-order derivative), and n = 67 smoothing points, followed by MSC. This combined approach yielded an impressive RMSEP of 0.3982 and Rp of 0.8862 (Chen et al., 2013).

5.3.5. Conclusions

The study's primary objective was to integrate nonlinear techniques with mathematical pretreatment (1st derivative) and a Box-Behnken design to reduce the sample size needed for predictive models related to loblolly pine downed timber characterization. The models were successfully created using 10% out of 176 core samples collected over a year of the trees enduring natural degradation on the field. The study explored the impact of various spectral pretreatments, including the use of first derivatives and Savitzky-Golay smoothing. The results indicated that

when appropriately treated, the first derivative achieved a balanced distribution of explained variance, showcasing its effectiveness in modeling. The models developed using Support Vector Machines (SVM) with different kernels demonstrated varying predictive performances, with the polynomial kernel as the most robust. The models' quality was assessed using coefficients of determination (R2) and root mean square errors (RMSEC and RMSEP). The cellulose model exhibited the best overall performance, followed by hemicellulose and lignin models. The best-performing kernel for SVM was the polynomial kernel with R2 values of 0.61, 0.96, and 0.79 (Lignin, Cellulose, and Hemicellulose, respectively). The RMSEC were 1.354, 1.295, and 1.004, respectively. Finally, the RMSEP were 1.139, 1.802, 1.227, respectively.

The study's innovative approach, utilizing a reduced sample size and simplified spectral treatment, yielded competitive results compared to traditional methods, showcasing its potential for efficient wood composition prediction and even facing the challenges of samples enduring extended degradation times on the field. The findings of this study open avenues for more streamlined and resource-efficient approaches to wood characterization, with implications for both research and practical applications, for example in biorefineries and circular economy. Future research could explore the application of the developed models to fresh samples and further refine the methodology for broader use in forestry and wood industry applications. Additionally, exploring reduced spectral ranges to achieve higher fitting models for wood components. This could include exploring the lower spectral range from (650 nm - 1000 nm) to improve further the lignin model.

6. Utilization Window of Downed Timber: Deterioration Detection with Field Friendly Technologies, Near Infra-Red Spectroscopy and Acoustics, and Correlations With Chemical Composition Changes Over Time

6.1. Abstract

This study investigates the degradation of hurricane-downed timber, a crucial concern for the timber industry post-natural disasters, using rapid Near-Infrared Spectroscopy (NIR) and acoustic technology, and its correlation with timber chemical composition. A model study, based in Alabama, utilized 30 loblolly pine trees from three locations, spanning various ages. Over a year, sound-wave propagation and NIR measurements were conducted, revealing distinct temporal patterns. Principal Component Analysis (PCA) of NIR data captured 97.4% of the variance, showcasing temporal phases. Transverse sound-wave measurements indicated consistent stress wave velocity variations, displaying a multi-phase pattern. Thermogravimetric Analysis (TGA) demonstrated significant shifts, emphasizing temporal dynamics. Chemical characterization of the woody biomass using HPLC highlighted variations in lignin and carbohydrate fractions. Acid-insoluble lignin content increased 4% while acid-soluble lignin decreased. This could be potentially valuable in biorefinery applications. These findings unveil the dynamic degradation process of hurricane-downed timber and the potential of advanced analytical methods for timber quality assessment and biorefinery applications. The research contributes to resilient and sustainable timber utilization post-catastrophic weather events, offering insights into composition changes over time and enhancing understanding of the weathering process.

Keywords: Acoustic Technology, Chemical Characterization, Deterioration, Downed Timber, Near-Infrared Spectroscopy (NIR)

6.2. Methodology

The methodology for the downed timber model study is addressed in section 3.5. The sound wave propagation measurement plan is detailed in section 3.6. The sampling protocol is explained in section 3.7. Near infrared spectroscopy methodology is further explained in section 3.9. The experimental design and machine learning approach for the model calibrations is detailed in section 3.10. Finally, the chemical characterization of the downed timber is noted in section 3.11. Finally, the thermogravimetric analysis is depicted in section 3.12.

6.3. Results and discussion

6.3.1. Near-infrared spectroscopy

The infrared (IR) region is situated between the visible and microwave sections of the electromagnetic spectrum. In the context of this study, the near-infrared (NIR) technique quantifies the absorption, transmission, or reflection of near-infrared light by a sample, based on its chemical composition. In the near infrared region, absorbance peaks occurring from 4000 cm^{-1} to 5000 cm^{-1} are a result of the interactions of O-H, C-H and N-H functional groups interacting with one another. Peaks have also been ascribed to specific chemical constituents of lignocellulosic biomass: 4765 cm^{-1} results from O-H and C-H stretching and deformation vibration of cellulose and xylan; 5205 cm^{-1} is due to the asymmetric stretching and/or deformation of O-H in water; and 5845 cm^{-1} credited to the first overtone stretching of C-H in hemicelluloses (Kelley, Rials, Snell, et al., 2004; Lupoi et al., 2014; Manley, 2014). In addition, the peak at 6875 cm^{-1} has been attributed to the first overtone of O-H stretching of phenolic groups in lignin (Acquah et al., 2016; Meier, E.W., 2015). . In this context, NIR has emerged as a valuable tool for predicting key properties of wood samples, for example; extractives, holocellulose, and lignin content in solid wood blocks of *Liriodendron tulipifera* (Acquah, Via, et al., 2018).

In the context of the study, the application of PCA on the NIR measurement of cores has yielded insightful results from these bands in a comprehensive manner. PCA is a powerful multivariate statistical technique used to reduce the dimensionality of data while retaining its essential variability (Jolliffe & Cadima, 2016; Nørgaard et al., 2012). PCA enables the identification of dominant patterns within the data. This approach facilitates the extraction of key information from the NIR spectra, aiding in the identification of chemical traits and wood properties associated with the samples (Medeghini et al., 2016).

The analysis revealed the presence of three principal components, with distinct levels of explanatory power for the observed variance (Figure 6.1). Notably, PC1 emerged as the most influential component, accounting for a substantial 89.5% of the total variance within the dataset. This high percentage underscores the significance of PC1 in capturing the primary patterns and trends inherent in the NIR core data. Furthermore, PC2 and PC3 contributed 6.4% and 1.5% of the variance, respectively, collectively representing additional dimensions of information within the dataset. The cumulative effect of these three principal components accounts for 97.4% of the total variance present in the NIR coresThe best-performing models, calibrated with the full NIR range, reported favorable R2 values of 0.84 for extractives, 0.68 for holocellulose, and 0.64 for lignin (Nkansah et al., 2010). The dominance of PC1, followed by the relatively modest contributions of PC2 and PC3, emphasizes the efficacy of PCA in compressing the original multidimensional data into a reduced set of components that retain the most critical information.

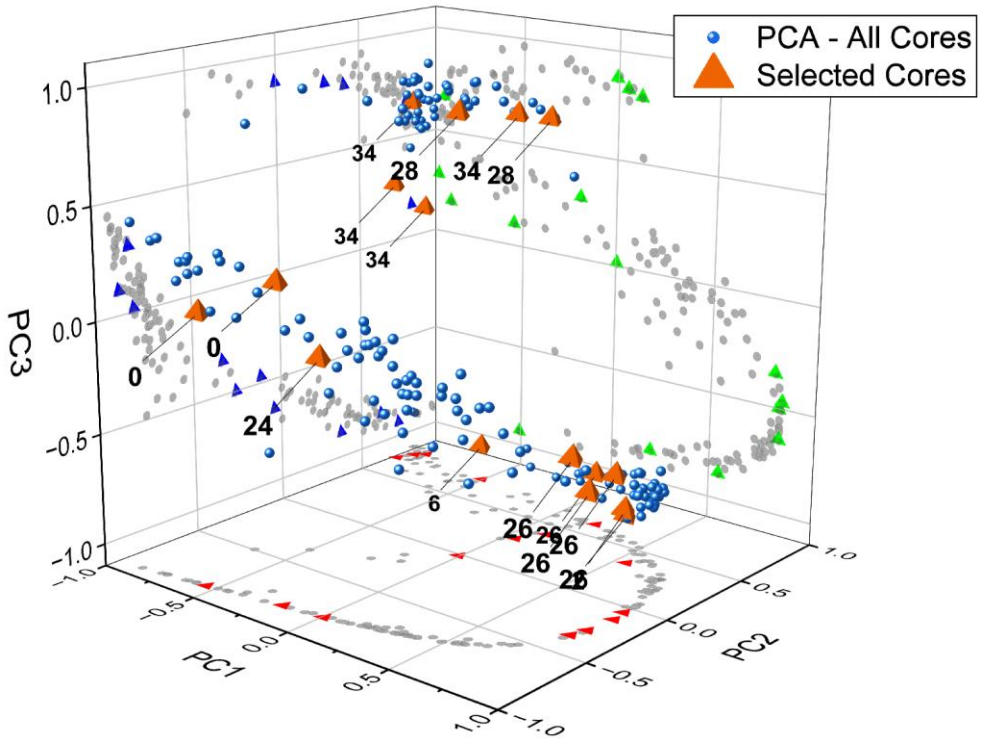

Figure 6.1. PCA of NIR first derivative of cores collected. Tetrahedron (orange) corresponds to Box-Behnken design selected cores, labels show the core collection week.

These outcomes have been further refined through the integration of the Box-Behnken experimental design, where a total of 15 core samples were strategically selected from the PCA. The Box-Behnken design, aimed at streamlining further characterization processes, efficiently explores the effects of multiple variables related to chemical composition and properties (Silva et al., 2022). Furthermore, the PCA analysis has revealed an intriguing pattern within the dataset. Specifically, a notable segregation of samples becomes apparent, with the divergence predominantly initiating around the 26th weeks. This segregation was more clearly defined after week 28th. This temporal segmentation highlights a potentially significant shift in the underlying factors influencing the NIR core measurements over time. The observed separation underscores

the sensitivity of the PCA technique paired with the Box-Behnken design in capturing subtle variations and suggests the presence of distinct phases or trends within the dataset.

Moreover, as seen in **Table 6.1**, the PCA and BB design resulted in the set of 15 cores meticulously chosen from a total of 9 distinct downed timbers. For the first DT planted in 1981, core samples were selected at two critical time points: week 0 and week 28 (specifically at 13.4 meters and 1.2 meters above the ground, respectively). From the group that were planted in the year 1990, three (1, 5, and 6) were chosen at three crucial times: weeks 0, 26, and 34 respectively, specifically at heights of 13.4, 1.2 and 1.2 meters above the ground, respectively. For the DT that were planted in the year 2005 five specific cores were selected (1, 2, 4, 5, and 8). The time points resulted in weeks 2, 6, 24, 26, 28, and 34 sampled with heights 1.2, 7.3, and 13.4 meters above the ground.

Finally, from the initial set of 15 core samples, four from week 26 underscore the significance of this sampling period, possibly indicating a period of time of particular dynamics. Similarly, two core samples from week 28 and four core samples from week 34 provide a snapshot of the later stages of the core sampling.

Table 6.1. Details and characterization results of selected cores.

											Lignin		Carbohydrates				
Sample Number	**NIR ID**	**Collection week**	**Site year planted**	**Site tree number**	**Tree height [ft (m)]**	**Tree diameter [in (m)]**	**Core height [ft (m)]**	**Moisture [%]**	**Ash [%]**	**Extractives [%]**	**Klason [%]**	**Acid Soluble [%]**	**Glucan [%]**	**Xylan [%]**	**Galactan [%]**	**Arabinan [%]**	**Mannan [%]**
1	F	0	1990	T01	66 (20.1)	16.5 (0.419)	44 (13.4)	6.7 ± 0.3	1.3 ± 0.2	2.9 ± 0.3	28.8 ± 0.8	4.2 ± 0.8	46.5 ± 1.2	6 ± 0.6	1.9 ± 0.3	1.6 ± 0.7	10.1 ± 0.1
2	K	0	1981	T01	89 (27.1)	21 (0.533)	44 (13.4)	5.7 ± 1	0.4 ± 0.2	3 ± 0.2	28.8 ± 0.6	3.2 ± 0.7	43.5 ± 0.2	7.9 ± 0.1	2.5 ± 0.2	1.4 ± 0.1	11 ± 1.3
3	AC	2	2005	T01	64 (19.5)	10 (0.254)	24 (7.3)	5.6 ± 0.6	1.5 ± 0.2	2.7 ± 0.2	32.5 ± 0.9	3.9 ± 1.2	42.5 ± 0.4	6.8 ± 0.7	2.6 ± 0.4	1.2 ± 0.1	8.5 ± 0.2
4	AR	6	2005	T01	64 (19.5)	10 (0.254)	24 (7.3)	5.1 ± 0.8	0.4 ± 0.1	4 ± 0.3	30 ± 0.3	5.4 ± 0.9	42.9 ± 0.4	6.5 ± 0.4	2.7 ± 0.2	1.1 ± 0.1	8.5 ± 0.4
5	BZ	24	2005	T02	74 (22.6)	10.5 (0.267)	4 (1.2)	5.8 ± 0.8	0.8 ± 0.7	4.7 ± 0.5	29.7 ± 0.3	3.8 ± 0.7	42.5 ± 0.3	7.2 ± 0.2	2.9 ± 0.1	1.1 ± 0.1	8.4 ± 0.3
6	CV	26	1990	T05	73 (22.3)	15 (0.381)	4 (1.2)	5.7 ± 0.3	0.9 ± 0.1	14.9 ± 0.4	25.3 ± 0.6	3.1 ± 0.5	38.3 ± 2.1	5.8 ± 0.8	2.6 ± 1	1.1 ± 0.3	8.8 ± 0.7
7	DE	26	2005	T04	69 (21)	8.5 (0.216)	4 (1.2)	5.3 ± 0.3	1.2 ± 0.3	3.8 ± 0.1	32.8 ± 0.7	2 ± 1	45.6 ± 1.2	4.6 ± 0.8	1.5 ± 0.1	1.1 ± 0.1	9.2 ± 0.4
8	DC	26	2005	T02	74 (22.6)	10.5 (0.267)	4 (1.2)	6 ± 0.1	1.1 ± 0.5	2.6 ± 0.1	28.9 ± 0.1	4 ± 0.9	45.5 ± 1.2	7.3 ± 0.8	1.5 ± 0.1	1.1 ± 0.1	9.9 ± 0.1
9	DF	26	2005	T05	73 (22.3)	12 (0.305)	4 (1.2)	4.9 ± 0.1	0.5 ± 0.3	3.2 ± 0.4	30.3 ± 0.7	1.5 ± 0.9	43.4 ± 1.4	7.4 ± 0.1	2.6 ± 1.1	1.2 ± 0.4	9.3 ± 1
10	DQ	28	1981	T01	89 (27.127)	21 (0.533)	4 (1.2)	4.5 ± 0.2	0.8 ± 0.3	2.4 ± 0.2	30.5 ± 1.1	1.6 ± 1.1	47.8 ± 0.3	5.7 ± 0.9	1.8 ± 0.6	0.8 ± 0.1	11.4 ± 0.5
11	EE	28	2005	T01	64 (19.5)	10 (0.254)	44 (13.4)	5.8 ± 0.5	0.6 ± 0.3	1.7 ± 0.2	32.5 ± 0.8	1.7 ± 1.2	45.8 ± 1.1	6.3 ± 1.7	2.2 ± 1	1.1 ± 0.1	9.2 ± 0.5
12	EX	34	1990	T06	59 (18)	16.5 (0.419)	4 (1.2)	5.5 ± 0.7	0.7 ± 0.4	2.4 ± 0.3	31.3 ± 0.6	1.9 ± 1.2	45.9 ± 0.2	6.2 ± 0.5	1.6 ± 0.1	0.8 ± 0.1	10.8 ± 0.8
13	FC	34	2005	T01	64 (19.5)	10 (0.254)	4 (1.2)	6.5 ± 0.3	0.8 ± 0.3	2.5 ± 0.1	34.5 ± 0.6	1.9 ± 1.1	43.2 ± 1.1	6.9 ± 1.1	2.4 ± 0.2	0.9 ± 0.1	8.6 ± 0.9
14	FG	34	2005	T01	64 (19.5)	10 (0.254)	44 (13.4)	5.6 ± 0.2	0.5 ± 0.2	1.6 ± 0.2	33.5 ± 1.2	1.9 ± 1.5	44.6 ± 0.3	6.7 ± 0.3	1.9 ± 0.8	1.1 ± 0.1	9.4 ± 0.3
15	FN	34	2005	T08	74 (22.6)	12.5 (0.318)	4 (1.2)	5.6 ± 0.6	0.9 ± 0.4	8.1 ± 0.3	30.6 ± 0.3	1.4 ± 1.1	40.3 ± 0.2	6.7 ± 0.6	2.4 ± 0.4	1.4 ± 0.5	8.4 ± 0.3

6.3.2. Sound-wave propagation

Across all DT measurements, the sound-wave propagation exhibited a discernible positive slope trend in transverse measurements, indicating consistent variations in stress wave velocities. Conversely, the slope trend in longitudinal measurements remained close to 0, suggesting minimal variation in this orientation. The transverse measurement yield the most prominent and noteworthy outcomes (**Figure *6.2***). In previous reports, a good correlation between transverse position and NIR measurements was observed (Musah et al., 2022). A complete figure of the measurements can be found in supplementary.

The behavior of the measurements was notably characterized by distinct phases. The initial phase, extending from week 0 through weeks 10-14, showcased a period of initial adjustment marked by fluctuations both upwards and downwards in the sound-wave propagation values. Subsequently, a phase ensued in which sound-wave propagation within the different sections of the downed timbers demonstrated increased stability over time, observed until weeks 24-26. The third and final phase was marked by substantial variations and a lack of consistency between the measured sections. The relationship between time of flight and stability is crucial in understanding the mechanical properties of the woody biomass. In the study, stability refers to the consistency in the velocity of propagation of sound waves over time. A stable woody biomass would exhibit minimal variations in sound wave velocity. In the majority of cases, the time-of-flight increases, indicating a decrease in velocity. This decrease in velocity over time may be associated with factors such as moisture content, decay, or structural changes within the woody biomass.

Previous reports on 14-year-old loblolly pine acoustic response, has shown that cellulose acts as the primary contributor to sound wave velocity, while lignin plays the opposite role as a dispersant of sound waves at the molecular level (Essien et al., 2017). Considering the increase in

time of flight, cellulose, being a major contributor to wave velocity, might be undergoing a reduction. This could imply potential degradation, possibly initiated by insects, fungal or microbiological activity. The initial phase of stabilization, likely due to water loss, could be followed by subsequent phases where cellulose depolymerization contributes to the gradual decrease in wave velocity. This could be indicative of structural changes within the cell wall, with cellulose potentially being degraded by external factors.

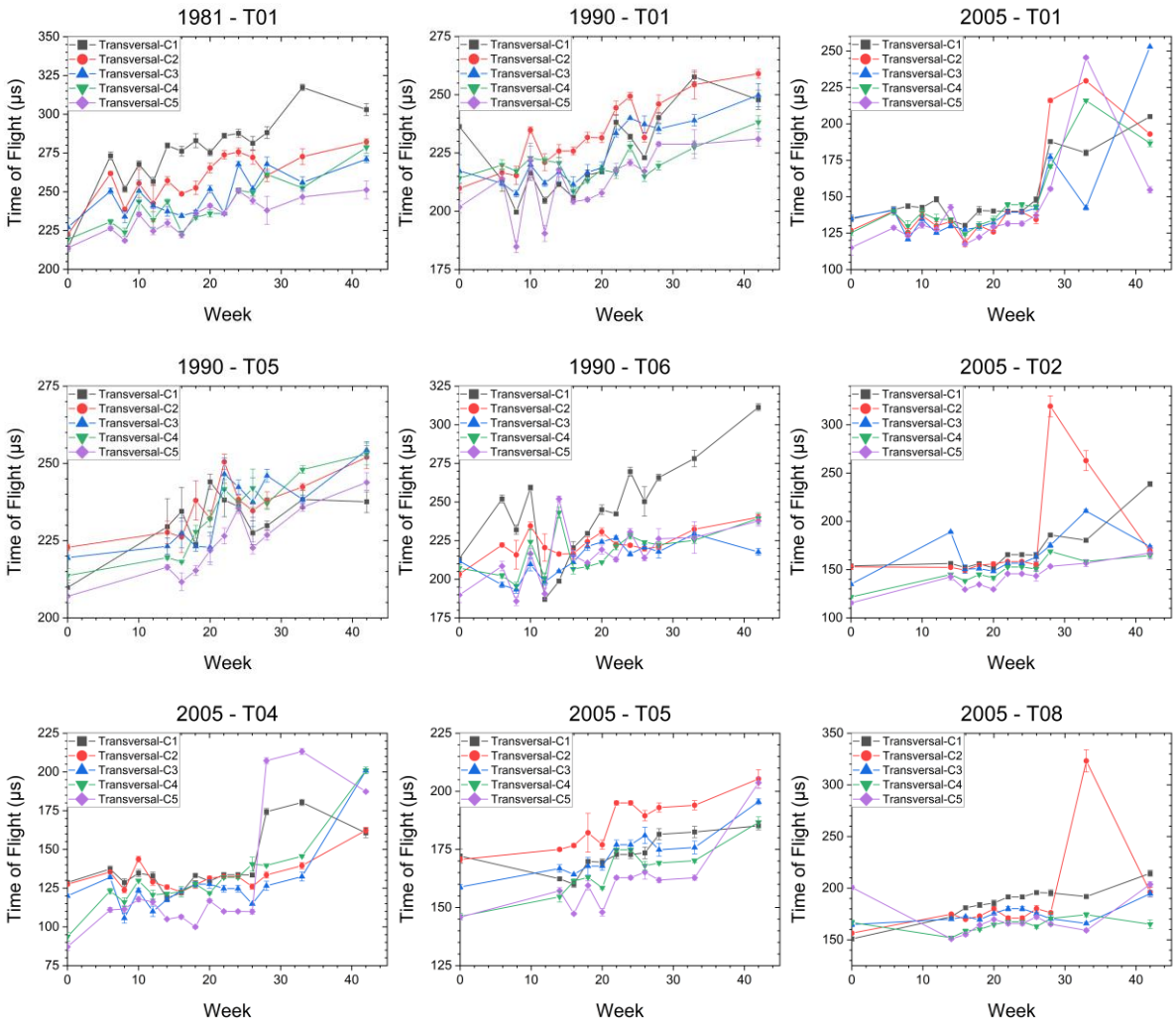

Figure 6.2. Transversal sections sound-wave propagation results for selected downed timbers by BB design.

6.3.3. Thermogravimetric Analysis (TGA)

Thermogravimetric analysis of the core samples revealed similar behaviors for the cores collected around the first 24 weeks, after that time frame the TGA curves of the cores collected in the same week were averaged (**Figure *6.3***). Distinct trends became evident upon observation. Notably, there is a significant shift in the first peak of the first derivative around 350°C during week 28, indicating a noteworthy alteration in thermal degradation behavior at this specific point. It has been reported that within the temperature range of 150°C to 425°C mass loss is mainly due to the decomposition of hemicelluloses and cellulose fractions, with lignin decomposition occurring at higher temperatures (Owen et al., 2015; Xu et al., 2021). Additionally, a discernible reduction in the lignin peak around 475°C during week 26 is followed by a subsequent shift to higher temperatures around 500°C in the following weeks, highlighting the transformation in the lignin degradation pattern, which underscores intricate temporal dynamics. Within this figure, the maximum temperature of mass loss (MTML) of cellulose for each week shows peculiar characteristics. Notably, it exhibits a phase characterized by a slight upward slope until week 24, with the MTML increasing from 355 ± 4°C at week 0 to 358 ± 3°C at week 24. This phase is followed by a decrease at week 26 (354 ± 2°C) and then an increase at week 28 (362 ± 8°C), accompanied by an elevated standard deviation. The final phase demonstrates a gentle negative slope, eventually converging back to values similar to the initial phase by week 34 (356 ± 5°C), albeit with a slightly elevated standard deviation. For MTML of the lignin fraction for each week, the TGA data reveals an elevation in the maximum degradation temperature at week 6 (from 475 ± 1°C to 492 ± 1°C), followed by a decline at week 24 (462 ± 8°C). Week 26 stands out with a significant increase in standard deviation and a positive slope (481 ± 20°C), persisting until week 28 (493 ± 6°C). The last phase showcases a gentle negative slope, characterized by a lower

standard deviation on week 34 (488 ± 5°C). The thermoxidation process over the range 400°C - 500°C has been reported in literature (Emandi et al., 2011; Mandalika et al., 2019).

Summarizing the analysis, the potential impact of cellulose-consuming biological agents activity on the degradation pattern aligns well with these findings. The observed increase in the maximum temperature of mass loss (MTML) of cellulose until week 24 could indeed be attributed to the selective consumption of shorter amorphous cellulose chains by the fungi. This might result in an enrichment of the remaining cellulose with larger degree of polymerization, leading to a higher degradation temperature. The subsequent decrease in MTML at week 26, followed by an increase at week 28, as well as the variations in the standard deviation, could be indicative of a more complex degradation process. Having extended sufficiently by the later weeks, the biological agents may start degrading longer cellulose chains or fractionating them. The elevation in the maximum degradation temperature at week 6, followed by a decline at week 24, and the subsequent variations in weeks 26 to 28, support the idea of a dynamic fungal degradation process affecting both cellulose and lignin fractions.

Moreover, the initial degradation by the biological agents may target the ASL with lower molecular weight, leading to an increase in the degradation temperature of the remaining lignin in the DT.

.

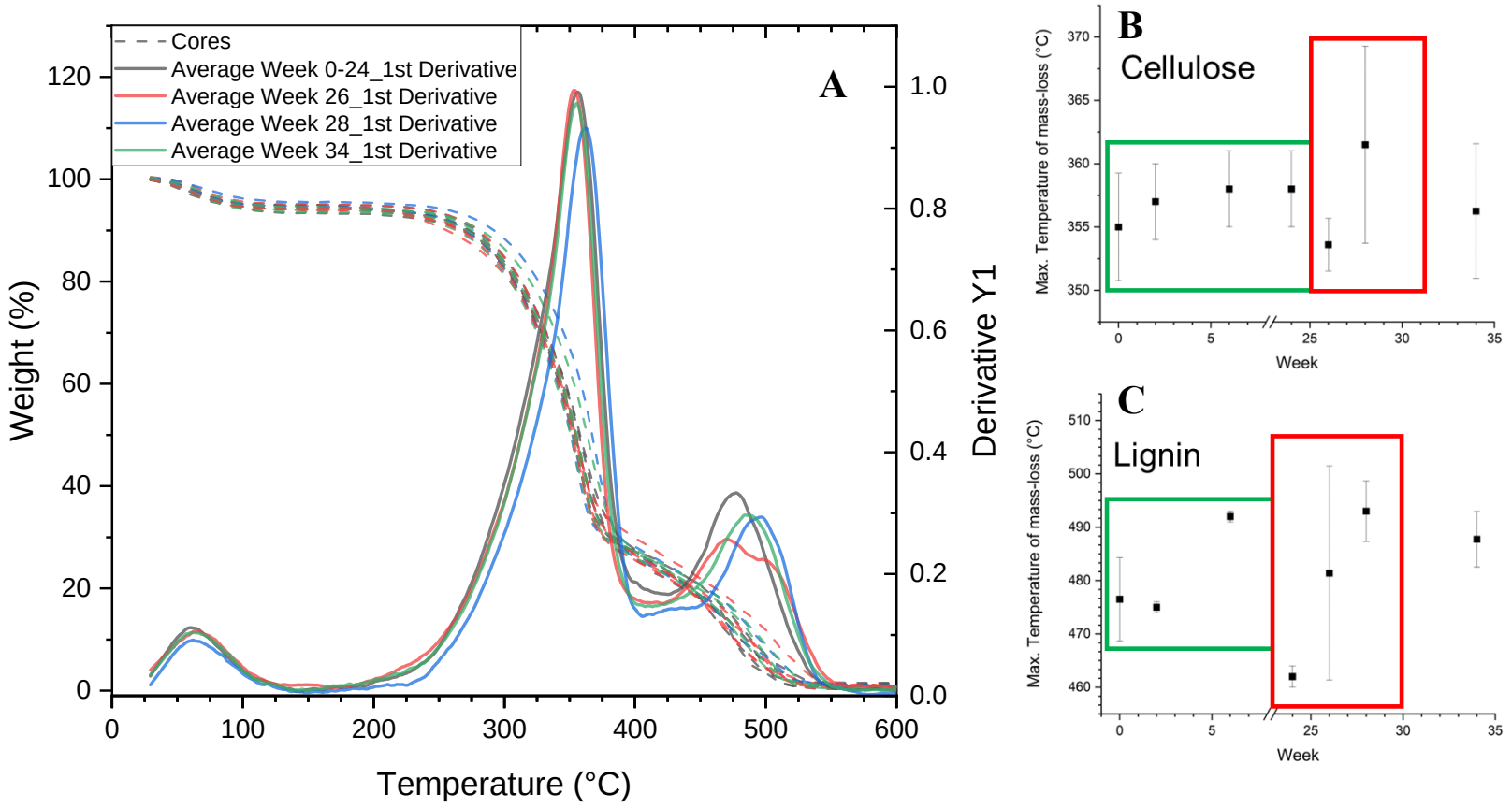

Figure 6.3. TGA analysis of NIR selected core samples. A) TGA curves and averaged first derivatives for week ranges. B) Maximum temperature of degradation for cellulose fraction. C) Maximum temperature of degradation for Lignin fraction.

6.3.4. Compositional analysis

The overall moisture content of the cores was within a range of 5.6 ± 0.6 %. The consistent moisture levels observed indicate that the cores were relatively stable and well-preserved during the sampling process (Table 1). The ash contents were low in all the cores, average at 0.8 ± 0.3 %. These results are in accordance with reported literature values for loblolly pine; i.e. 0.1 % - 0.6 % (Acquah, Via, et al., 2018), 0.5 % (Kim et al., 2021), and 0.1 % - 4 % (Saha et al., 2017). The low ash content across all samples suggests that the influence of inorganic materials was minimal. This is favorable for conducting precise compositional analysis. Extractives showed a higher variation within the samples, from 4 ± 3.4 %. Literature also shows a high variability (0.4 % to 9.4 %) in extractive content within the same species (Acquah, Via, et al., 2018) with other reports stating ranges from 5.8 % to 11.3% depending on the silvicultural treatments employed (Shupe et al., 1996). Extractives are compounds that can significantly influence the properties of wood and its subsequent applications. The cores with higher extractives (14.9%) corresponded to DT 1990-T05 obtained in week 26 at 1.2m core height. The other notable tree was 2005-T08 (8.1%) obtained at week 34 at 1.2m height. This is in agreement with previous research which demonstrated extractive content decreased with age and height for loblolly pine (B. K. Via et al., 2007). In this analysis the lower content of extractives is related to the older trees sampled.

The acid insoluble lignin (AIL) average was 30.7 ± 2.3 %. This is in agreement with previous literature reporting loblolly pine lignin content in ranges from 26.7 % to 35 % (Acquah, Via, et al., 2018), 29.2 % (S. Wu et al., 2010), and 30.7 % (Rana et al., 2012). This fraction shows a tendency to relative enrichment of content as the time of the sampling increases, from an average of 28.8 % on week 0 to 31.5 % on week 34. In previous literature, the expected behavior was a decrease of lignin content for loblolly pine owing to maturation (age of the tree) (L. R. Schimleck

et al., 2021). In this study even though the older downed timbers have relatively lower lignin content, the relative enrichment over degradation time is still noticeable. Meanwhile, the acid soluble lignin (ASL) fraction range was within 2.8 ± 1.3 %. Contrary to the previous case, this fraction showed a decreased tendency from an average 3.6 % on week 0 to 1.8 % on week 34. As ASL is more easily degraded than AIL lignin due to lower molecular weight, the decrease in ASL over time may be due to the action of biological agents (Janusz et al., 2017). The increase of acid insoluble fraction could be of interest in some biorefinery applications to optimize the value of polymer isolation process (Atiwesh et al., 2022; Grgas et al., 2023; Leskinen et al., 2015, 2015; Shapiro et al., 2023, 2023; Thevenot et al., 2010).

For the carbohydrate fractions, the ranges of glucan were between 43.9 ± 2.5 %, for galactan 2.2 ± 0.5 %, mannan 9.4 ± 1 %, xylan 6.5 ± 0.8 %, and arabinan 1.1 ± 0.2 %. Other research reports have provided values for sugar monomers: glucan (46 - 47.7 %), xylan (4.8 - 7.5 %), galactan (1.5 - 2.5 %), arabinan (0.9 - 1.6 %), and mannan (8.2 – 11.7 %) (Eberhardt & Samuelson, 2022; Rana et al., 2012). In this research, no significant trend was shown by glucan, from the average of week 0 (43.6 ± 0.2 %) to week 34 (43.4 ± 0.1 %). Galactan showed a relative depletion from the average of week 0 (2.3 ± 0.2 %) to week 34 (1.8 ± 0.1%). Variation on mannan also showed some decrease from week 0 (10.1 ± 0.1 %) to week 34 (9 ± 0.2 %). Xylan was also depleted from week 0 (7.8 ± 0.1 %) to week 34 (6.6 ± 0.2 %). Finally, arabinan decreased similarly from week 0 (1.4 ± 0.1 %) to week 34 (0.9 ± 0.1 %). The relatively depletion of hemicelluloses suggest potential changes in the cell wall composition as the DT weathered. This could be attributed to various factors, such as microbial agents' activity. Other literature reports have analyzed the decay of different woods to single organisms in laboratory conditions. For example, Eucalyptus grandis was inoculated with the decay fungus *P. sanguineus* and showed 34% of weight

loss after 12 weeks for untreated wood (Calonego et al., 2010). In uncontrolled situations, such as this study, the decay colonies of biological agents would vary greatly. Living wood harbors dormant biological agents, and upon the tree's death, a subset of these promptly transitions into primary colonizers (Lustenhouwer et al., 2020; Parfitt et al., 2010). The primary colonizers actively connect with wood components, including sap sugars and the resilient structures of lignocellulosic cell walls (Song et al., 2017). The biological agents must get through the cell wall structure, breaking the lignin barrier to reach hemicelluloses and cellulose (Cline et al., 2018).

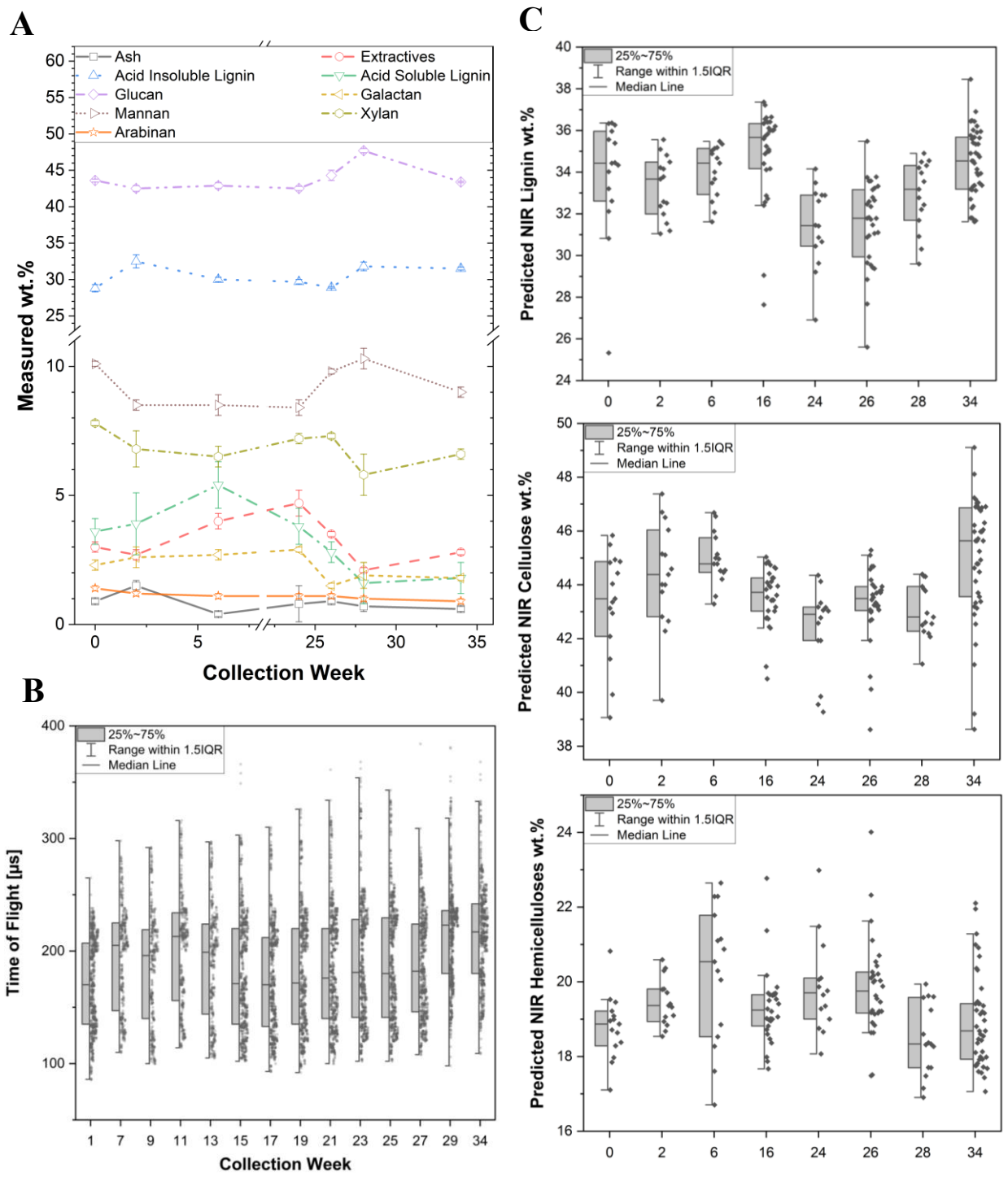

Figure 6.4. (A) weight averaged wet chemistry measurements on selected BB-design, representative of highest variation wood cores. (B) Transversal acoustics measurements on all trees over the experiment period. (C) NIR predictive modeling of main components of wood.

6.4. Conclusions

This study is a significant contribution to assessing the deterioration rate of DT resulting from catastrophic weather events such as hurricanes. The study employed a multidisciplinary approach combining rapid Near Infra-red Spectroscopy (NIR) and acoustic technologies to correlate the observed changes with chemical alterations over time. Furthermore, the manuscript emphasized the importance of developing innovative approaches to assess timber quality post-storm and identify new avenues for utilizing salvaged timber. Biorefineries and extracting natural polymers from biomass were introduced as potential solutions, providing economic opportunities and aiding in the development of a circular economy.

The study's findings shed light on the intricate temporal and chemical dynamics of DT degradation through rigorous methodologies, including sound-wave propagation analysis, near-infrared spectroscopy, thermogravimetric analysis, and chemical characterization. Key trends emerged, including shifts in sound-wave propagation behavior, alterations in chemical composition, and changing thermal degradation patterns. Notably, acid-insoluble lignin content showed a 4% relative enrichment over degradation time, offering insights into the potential for optimizing lignin isolation processes in biorefinery applications. Meanwhile, acid-soluble lignin content showed a relative 2% depletion. Conversely, the high variability of extractive content could represent a challenge in biorefinery processes and should be considered while designing future projects. Sugars related mostly to hemicelluloses showed similar lower content over the study time frame, thus signaling how biological agents use them as energy at the first stages of the degradation process of DT.

Finally, this report has shown how all the proposed methodologies were able to detect the signs of degradation of DT in the field. This has significant applications in the future of

biorefineries; recollecting the data and submitting it to the processing facility can be executed by field crews (portable-NIR or acoustics). Moreover, the techniques employed at the lab scale are applicable in different scenarios and capabilities. Depending on business plans, biorefinery facilities could implement their combination of preferred methodologies for quality control (NIR, TGA, HPLC). This research has provided valuable insights into storm-DT's potential recovery and utilization time windows for polymer recovery.

7. Lignin Recovery from Weathered Downed Timber: Insights from Co-Solvent Enhanced Lignocellulosic Fractionation (CELF) and Biomass Resource Utilization

7.1. Abstract

This study investigates the weathering effects on downed timber over a 12-month period, with a focus on lignin and carbohydrate composition changes. A model study was conducted using freshly harvested loblolly pine trees subjected to deliberate felling. Stump samples collected at 0, 6, and 12 months were processed and analyzed to assess variations in composition, especially lignin, and carbohydrates. The results reveal that Klason lignin content gradually increased over time, with values of 30.9% at 0 months, 30.7% at 6 months, and 33.2% at 12 months. A consistent escalation in lignin recovery yields was observed. The 0-month samples yielded an average of 22.6 grams (65%), 23 grams (68%) at 6 months, and the most significant shift in yield occurred at the 12-month, with samples yielding an average of 24.7 grams (70%) indicating potential improvements in lignin recovery operations. The changes in Fourier-transform infrared spectroscopy (FTIR) spectra, with distinctive peaks observed in 1700, 1670, 1452, and 1080 cm^{-1}, are indicative of changes in the chemical composition, structure, and aging of the lignin samples. Thermogravimetric analysis (TGA) demonstrates that the CELF lignin samples possess excellent thermal stability, with maximum degradation temperatures of 388°C (0 months), 417°C (6 months), and 413°C (12 months). Differential scanning calorimetry (DSC) analysis provides specific glass transition temperature (Tg) values, with the 0-month sample exhibiting a Tg of 102.2°C, the 6-month sample at 100.5°C, and no discernible Tg for the 12-month sample. Molecular weight distribution analysis (GPC) indicates that the 0-month sample exhibits higher Mn (4,700 g/mol), Mw (7,080 g/mol), and Mz (10,340 g/mol) compared to the 6-month and 12-month samples. The polydispersity index (PDI) values for the CELF lignin samples show moderate

polydispersity, with a PDI of 1.51 (0 months), 1.44 (6 months), and 1.48 (12 months). These results are consistent with expected natural degradation, with the differences in molecular weight distribution being relatively small.

7.2. Methodology

This chapter methodology for downed timber chemical characterization is detailed in section 3.11. Thermogravimetric analysis experimental settings are depicted in section 3.12. The lignin isolation methodology es further explained in section 3.13. Characterization via FTIR was done following the experimental details in section 3.14. Differential scanning calorimetry performed in the isolated lignins is described in section 3.15. Gel-permeation chromatography for isolated lignins is further detailed in section 3.16. Characterization of the downed timber cell walls and recovered lignin via nuclear magnetic resonance chromatography is explained in section 3.17. CELF Lignin particle production method is explained in 3.18. Zeta potential and particle size measurements via dynamic light scattering are detailed in section 3.19. Finally, scanning electron microscopy and image processing of CELF lignin particles is described in section 3.20.

7.3. Results and discussion

7.3.1. Downed timber characterization

The ash content, indicative of the inorganic mineral content in the samples, shows a slight decrease from 0 to 12 months. In other literature for loblolly pine; ash content has been reported between 0.1 % and 0.6 % (Acquah, Via, et al., 2018), 0.5 % (Kim et al., 2021), and 0.12 % to 3.96 % (Saha et al., 2017). The amount of extractives in the samples increased slightly from 0 to 6 months but decreased again at the 12-month mark. The increase at 6 months could be due to the accumulation of extractable compounds during specific degradation processes, while the

subsequent decrease at 12 months may suggest that some of these compounds were further removed or degraded. Literature also shows a irregularity within the same species of tree: 0.4 % to 9.4 % (Acquah, Via, et al., 2018), ranges from 5.8 % to 11.3% were also reported depending on the silvicultural treatments employed (Shupe et al., 1996). **Table 7.1** details the chemical composition of collected downed timber.

The Klason lignin content, which represents the acid-insoluble lignin, shows a steady increase from 0 to 12 months. This is a crucial finding, as it indicates the gradual enrichment of lignin in the samples over time. In the other hand, the carbohydrate composition, including glucan, galactan, mannan, xylan, and arabinan, varies slightly over the collection months. There is no consistent pattern of change for these components, with some showing minor increases and decreases. Overall, the values are in agreement with literature: lignin content in ranges from 26.7 % to 35 % (Acquah, Via, et al., 2018), 29.2% (S. Wu et al., 2010), and 30.65% (Rana et al., 2012). Meanwhile, the acid soluble lignin fraction showed a decreased tendency. The increase of acid insoluble fraction could be of interest in some biorefinery applications to optimize the value of polymer isolation (Leskinen et al., 2015; Shapiro et al., 2023). On the other hand, the decrease in acid soluble lignin suggests a potential degradation or transformation of this fraction during the weathering process (Atiwesh et al., 2022; Grgas et al., 2023; Thevenot et al., 2010).

Table 7.1. Characterization results of collected downed timber.

				Lignin		Carbohydrates				
Month	**Moisture**	**Ash**	**Extractives**	**Klason**	**Acid Soluble**	**Glucan**	**Galactan**	**Mannan**	**Xylan**	**Arabinan**
0	6 ± 1.2	1.1 ± 0.3	2.9 ± 0.4	30 ± 1.3	3.8 ± 1.6	43.4 ± 1.8	3.2 ± 0.3	11.5 ± 0.1	4.9 ± 0.4	1.3 ± 0.1
6	5.3 ± 0.9	0.8 ± 0.8	7.3 ± 0.7	28.5 ± 1.3	2.9 ± 1.4	44.2 ± 0.8	3.2 ± 0.1	11.2 ± 1.2	4.7 ± 0.1	1.3 ± 0.2
12	5.5 ± 0.8	0.7 ± 0.6	2.2 ± 0.4	32.5 ± 1.8	1.8 ± 2.4	44.8 ± 2.5	3.7 ± 0.4	10.2 ± 0.4	5.9 ± 0.5	1.4 ± 0.2

Values in %

7.3.2. CELF lignin characterization

The yield data from the CELF lignin process over a span of 0, 6, and 12 months reveal intriguing trends. The 0-month samples demonstrated an average yield of 22.6 ± 3.3 grams, reflecting a certain degree of variability. As time progressed, the 6-month samples showed a slight improvement, yielding an average of 23 ± 1 grams a reduced standard deviation. However, the most striking shift in yield occurred at the 12-month mark, with samples yielding an average of 24.7 ± 1.5 grams. These figures translate to an increase in yield, evolving from 65% at the initial stage to 68% after 6 months, and eventually reaching 70% at the 12-month mark. Some studies have reported higher yields (excess mass) at harsh conditions, which results from likely due to cross-polymerization reactions between soluble sugars and lignin during pretreatment and the formation of pseudo-lignin (Y.-Y. Wang et al., 2020). In our case, via FTIR we have discarded the presence of residual sugars. This progressive escalation in yield holds significant promise for biorefinery operations with a primary focus on lignin recovery. The consistent improvement in yield over time underscores the potential benefits of long-term lignin extraction processes, making them increasingly attractive for industrial applications. Enhanced lignin recovery rates not only contribute to the economic viability of biorefineries but also promote the sustainable utilization of lignocellulosic biomass resources such as downed timber.

7.3.3. Fourier transform infrared spectroscopy (FTIR)

Figure 7.1 shows the FTIR spectra for the CELF lignin samples obtained. In previous studies examining softwood lignin spectra absorption bands have been identified at the wavenumbers: 1720, 1670, 1590, 1500, 1463, 1423, 1360, 1330, 1270, 1215, 1140, 1125, 1087, 1031, 970, 855, and 815 cm^{-1} (Derkacheva & Sukhov, 2008). In our case the distinctive peaks identified start with the prominent absorption bands included those in 1720 and 1670 cm^{-1},

suggesting the presence of carbonyl (C=O) stretching vibrations, possibly originating from various carbonyl groups within the lignin structure. Peaks at 1590 and 1500 cm^{-1} likely corresponded to aromatic ring stretching vibrations (C=C), indicative of the aromatic nature of lignin. Additionally, peaks at 1463 and 1423 cm^{-1} might be associated with C-C or aromatic ring vibrations within the lignin molecules. The peaks at 1360 and 1330 cm^{-1} could relate to deformations or vibrations of CH_2 or CH_3 groups in aliphatic side chains. **Figure 7.1** shows that over the course of the study, minimal variations were observed between the FTIR spectra of the samples at 0 months and 6 months. However, some changes in peak intensities became evident at the 12-month mark. The alterations in the 1700 and 1670 cm^{-1} peaks may be indicative of changes in carbonyl (C=O) groups within the lignin structure. This could result from oxidation, cross-linking, or other chemical reactions occurring as the samples aged. Variations in the 1452 cm^{-1} peak could reflect changes in the lignin's structural components, possibly related to alterations in aromatic ring vibrations (C=C) or side-chain conformations. Peaks at 1266 and 1080 cm^{-1} may be influenced by degradation or polymerization processes in the lignin. These processes can lead to the formation or breakdown of chemical bonds within the lignin matrix, affecting the FTIR spectrum.

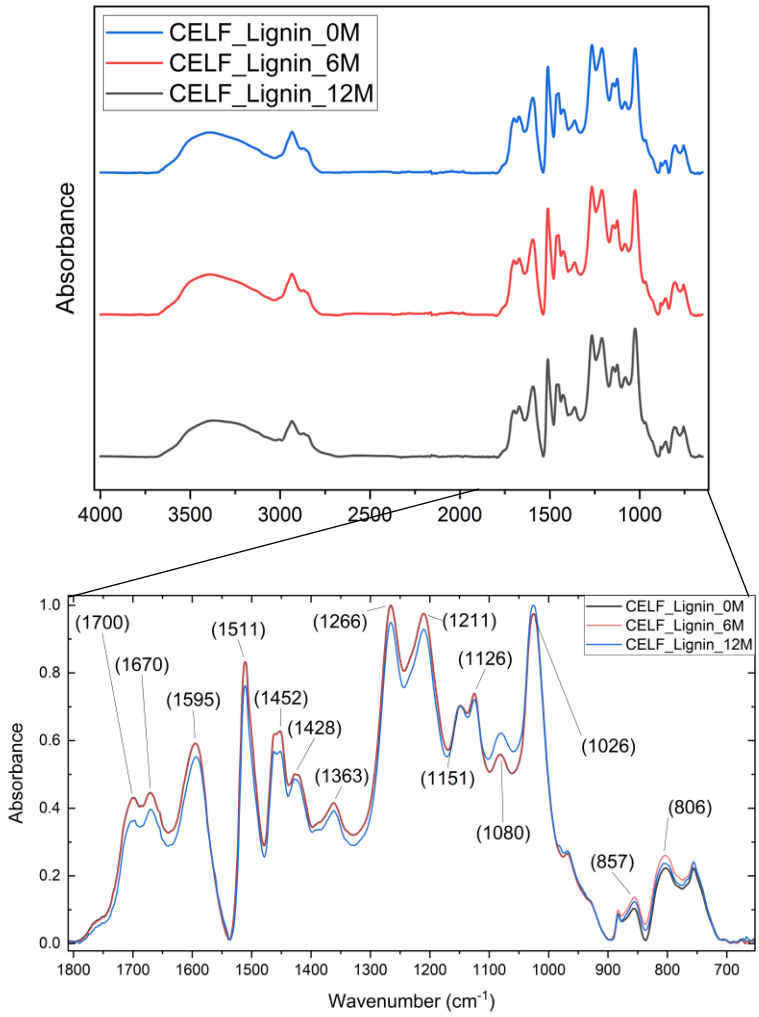

Figure 7.1. FTIR of CELF lignin samples.

7.3.4. Thermogravimetric Analysis (TGA)

The maximum degradation temperature for the 0-month sample was 388°C and a degradation range spanning from 270°C to 560°C. Meanwhile, the maximum degradation temperature was 417 and 413°C for the 6-month and 12-month samples, respectively. The ranges for those samples were from 280°C to 560°C and 280°C to 580°C. The maximum degradation temperatures for all three samples (0M, 6M, and 12M) were relatively high, suggesting the thermal

stability of the lignin samples. The maximum degradation temperature shows a slight increase from the 0-month sample (388°C) to the 6-month sample (417°C) and then a slight decrease in the 12-month sample (413°C). The degradation range, which represents the temperature range over which degradation occurs, is quite consistent across the samples. This indicates that the lignin samples exhibit similar patterns of thermal decomposition. The degradation temperature ranges for all three samples encompass a broad range from 280°C to 580°C, implying that these lignin samples can withstand high temperatures before undergoing significant decomposition. **Figure 7.2** illustrates the degradation temperature characteristics for CELF lignin samples collected at different time points (0, 6, and 12 months). Detailed information has been provided in **Table 7.2**.

Table 7.2. Maximum degradation temperature of CELF lignins.

	Degradation temperature	
ID	**Max.**	**RANGE**
CELF Lignin 0M	388	270 – 560
CELF Lignin 6M	417	280 – 560
CELF Lignin 12M	413	280 – 580

A highly noticeable peak, resulting from the disruption of C–C interconnections and the removal of methoxy groups from aromatic rings, is consistently observable in all CELF lignin samples within the temperature range of 350 to 400°C (Y.-Y. Wang et al., 2019). Although, the peak shifted as the downed timber degrades (6 and 12 months), and such phenomenon is consistent with the decreasing S/G ratio caused by demethylation (Y.-Y. Wang et al., 2020).

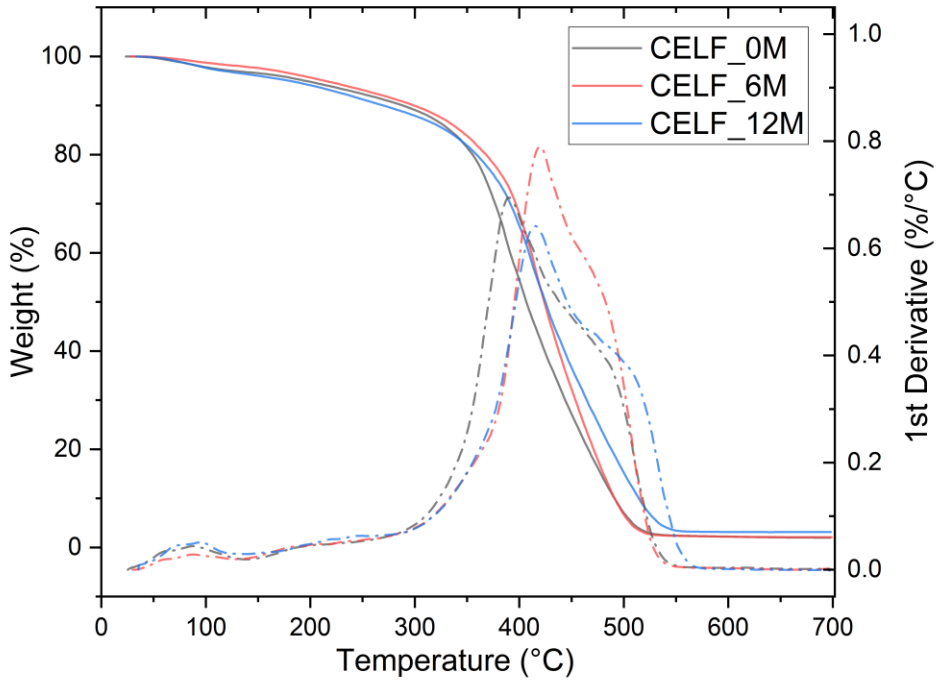

Figure 7.2. TGA analysis of CELF lignins.

7.3.5. Differential scanning calorimetry (DSC)

Differential Scanning Calorimetry (DSC) analysis performend on the CELF Lignin revealed insights into the thermal behavior of CELF lignin samples collected at different time points. Specifically, the data indicates that the glass transition temperature (Tg) for the 0-month sample was detected at 102.2°C, while for the 6-month sample, it was slightly lower at 100.5°C. Notably, no discernible Tg was observed for the 12-month sample. In previous reports, the glass transition temperature of CELF lignin was found to be positively correlated with molecular weight (Y.-Y. Wang et al., 2020). Moreover, the researchers found that a clear Tg could were characterized by a high degree of condensation and crosslinking through rigid C–C bonds, as opposed to C–O bonds even with lower molecular weights. On the other hand, other molecular structures or crosslinking patterns can lead to no discernible Tg (**Figure 7.3**).

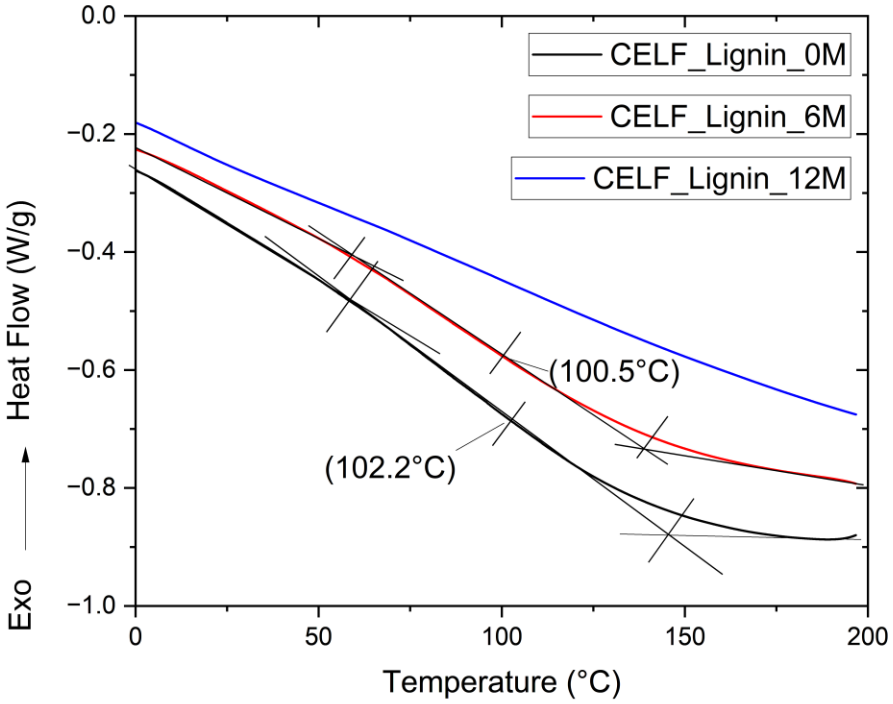

Figure 7.3. DSC of CELF lignins.

7.3.6. Molecular weight

Weight distribution of CELF lignin samples was analyzed using GPC/SEC. Elution profiles presented in **Figure 7.4** and detailed results are given in **Table *7.3***. The 6-month sample has the lowest Mn value (3,401 g/mol), followed by the 0-month sample (3,675 g/mol), and the 12-month sample has the highest Mn (4,548 g/mol). The 12-month sample has the highest Mw (6,747 g/mol), followed by the 0-month sample (5,623 g/mol), and the 6-month sample has the lowest Mw (4,960 g/mol). The 12-month sample has the highest Mz (9,720 g/mol), followed by the 0-month sample (8,369 g/mol), and the 6-month sample has the lowest Mz (7,024 g/mol). Other researches have reported molecular weights for organosolv lignin from loblolly pine in ranges from M_n =

3,000 to 7,600 (g/mol), Mw = 5,400 to 13,500 (g/mol), and PDI's from 1.77 to 2.57 (Sannigrahi et al., 2009). Results are in accordance with ranges in previous literature.

Table 7.3. Molecular weight of CELF Lignins.

SAMPLE ID	SEC/GPC			
	Mn	**Mw**	**Mz**	**Mw/Mn**
CELF_0M	3,675	5,623	8,369	1.53
CELF_6M	3,401	4,960	7,024	1.46
CELF_12M	4,548	6,747	9,720	1.48

The Polydispersity Index (PDI) is a dimensionless value that provides insights into the breadth of the molecular weight distribution in a sample. It is used to characterize the heterogeneity of polymer chains in the sample (Rane & Choi, 2005). For the CELF Lignin 0M sample, the PDI is 1.53. A PDI greater than 1.0 indicates that the molecular weight distribution is relatively broad. The CELF Lignin 6M sample has a PDI of 1.46. This value indicates a slightly narrower molecular weight distribution compared to the 0-month sample. While there is still polydispersity, the range of molecular sizes appears to be somewhat narrower. The CELF Lignin 12M sample has a PDI of 1.48. These values suggest that the molecular weight of CELF lignin of 0-month samples and 6-month samples are similar. Meanwhile, t he CELF lignin from DT resulting from 12 months of degradation exposure has experienced a small change in properties.

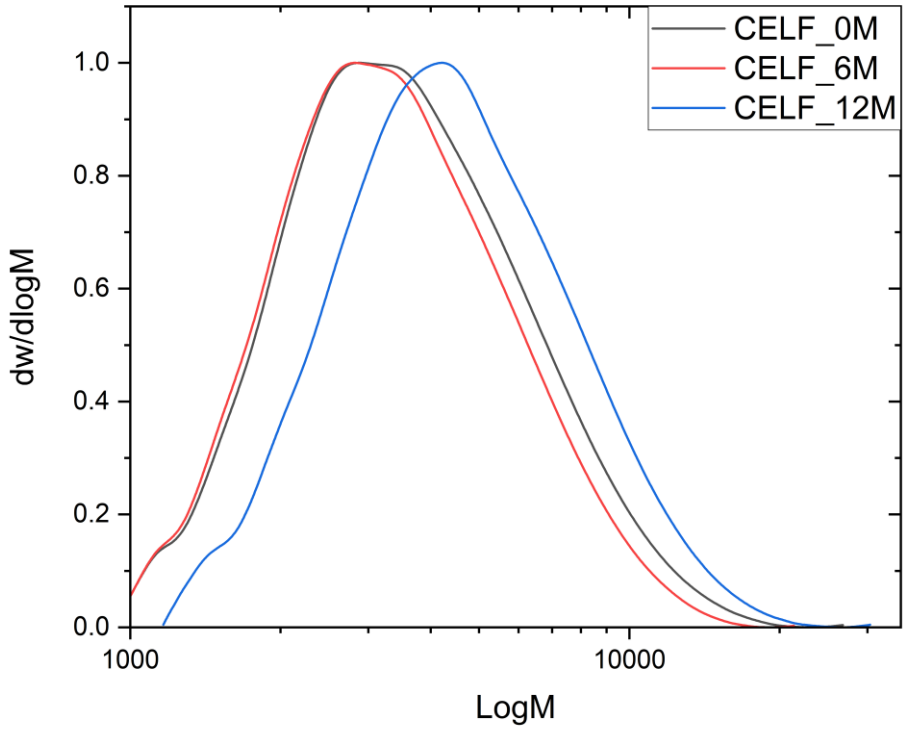

Figure 7.4. GPC of CELF lignins.

7.3.7. NMR

The NMR analysis of the cell wall structure revealed interesting trends in lignin and polysaccharide content over time. Initially, at 0-months, the lignin content was measured at 21.8%, while polysaccharides constituted 78.2% of the cell wall composition. Over the course of the study, there was a noticeable increase in lignin content. At 6-months, the lignin content rose to 24%, indicating a relative enrichment of lignin within the downed timber cell wall structure. This trend continued, with lignin content further increasing to 25.4% at 12-months. Conversely, the polysaccharide content exhibited a decreasing trend over the study period. At 6-months, polysaccharides decreased to 76%, and further declined to 74.6% at 12-months. This reduction in

polysaccharide content suggests potential degradation or modification of polysaccharide components within the cell wall structure **Figure *7.5***. Detailed signal assignments are discussed in detail in other literature (Kim et al., 2008; Kim & Ralph, 2010).

Further analysis of lignin aliphatic structures within the cell wall of downed timber revealed intriguing insights into the distribution of various interunit structures **Figure *7.6***. Among these, the β-Ether (β–O–4) units (BE) emerged as the predominant interunit structure throughout the study period. At the outset, the presence of β-Ether units constituted 73.4% of the lignin aliphatic structures. Remarkably, this dominance persisted over time, with minimal fluctuations observed at 6 months (73.7%) and 12 months (73.7%). The structural composition of the lignin within downed timber suggest these BE units' resilience to environmental factors or degradation processes.

In contrast, phenylcoumaran (β–5) units (PC) exhibited a relatively lower abundance compared to β-Ether units but still represented a significant proportion of the lignin aliphatic structures. From the initial measurement of 21.1% at 0-months, there was a slight decrease observed at 6 months (20.3%), followed by a marginal increase at 12 months (20.8%). While the fluctuations in phenylcoumaran units were modest, they indicate potential alterations in the lignin polymerization processes or structural rearrangements over time. Minor amounts of pinoresinol (β–β) units (R) were detected within the lignin aliphatic structures, albeit in lesser quantities compared to other interunit structures. The presence of pinoresinol units showed minimal variation across the study period, with measurements of 5.5% at 0-months and 6% at 6 months, before returning to 5.5% at 12 months.

Additionally, cinnamyl alcohol endgroups (E1 units) were identified as part of the lignin aliphatic structures, albeit declining in abundance over time. Initially, E1 units accounted for 9.2%

of the composition at 0-months, which decreased to 7.7% at 6 months, and further diminished to 6.4% at 12 months. The decreasing trend in cinnamyl alcohol endgroups may indicate their susceptibility to degradation or modification processes occurring within the cell wall matrix. Overall, the detailed analysis of lignin aliphatic structures provides valuable insights into the dynamic nature of lignin composition within downed timber over time. These findings contribute to a deeper understanding of the structural stability, degradation mechanisms, and potential applications of lignocellulosic materials in various bio-based industries.

The analysis of lignin aromatic structures within the cell wall of downed timber revealed intriguing dynamics in the distribution of guaiacyl (G) and p-hydroxyphenyl (H) units over time **Figure *7.6***. Guaiacyl units, denoted by G, emerged as the predominant aromatic structure throughout the study period. Initially, at 0-months, guaiacyl units accounted for a substantial proportion, comprising 98.4% of the lignin aromatic structures. This dominance persisted with minor fluctuations at 6 months (98.6%) and 12 months (96.8%). In contrast, p-hydroxyphenyl units, denoted by H, were present in comparatively lower quantities within the lignin aromatic structures. From the initial measurement of 1.6% at 0-months, there was a slight decrease observed at 6 months (1.4%), followed by a notable increase at 12 months (3.2%). The fluctuations in p-hydroxyphenyl units suggest lignin structural modifications over time, possibly influenced by weathering processes.

The Co-solvent Enhanced Lignin Fractionation (CELF) process, employed for the isolation of lignin from the cell wall matrix, yielded highly condensed lignin with distinctive structural characteristics, as revealed by NMR analysis. The NMR results indicate a significant loss of signals, suggesting extensive condensation of lignin during the isolation process. Despite the loss of some signals, the main aliphatic structures that remained prominent within the isolated lignin

fraction were identified as β-Ether (BE) units, phenylcoumaran (PC) units, and pinoresinol (R) units. The CELF process demonstrated remarkable consistency in yielding lignin of the same quality, irrespective of the degradation undergone by downed timber over the 12-month experimental period. Despite the varying degrees of degradation experienced by the timber samples during the course of the experiment, the quality of the lignin isolated through the CELF process remained consistent. The ability of the CELF process to yield lignin of consistent quality is of significant importance for various industrial applications. It ensures a reliable and predictable supply of lignin with desirable properties, facilitating its utilization in sectors such as bioenergy, biopolymers, and biochemicals. Moreover, this consistency may simplify downstream processing and product formulation, streamlining production processes and enhancing overall efficiency.

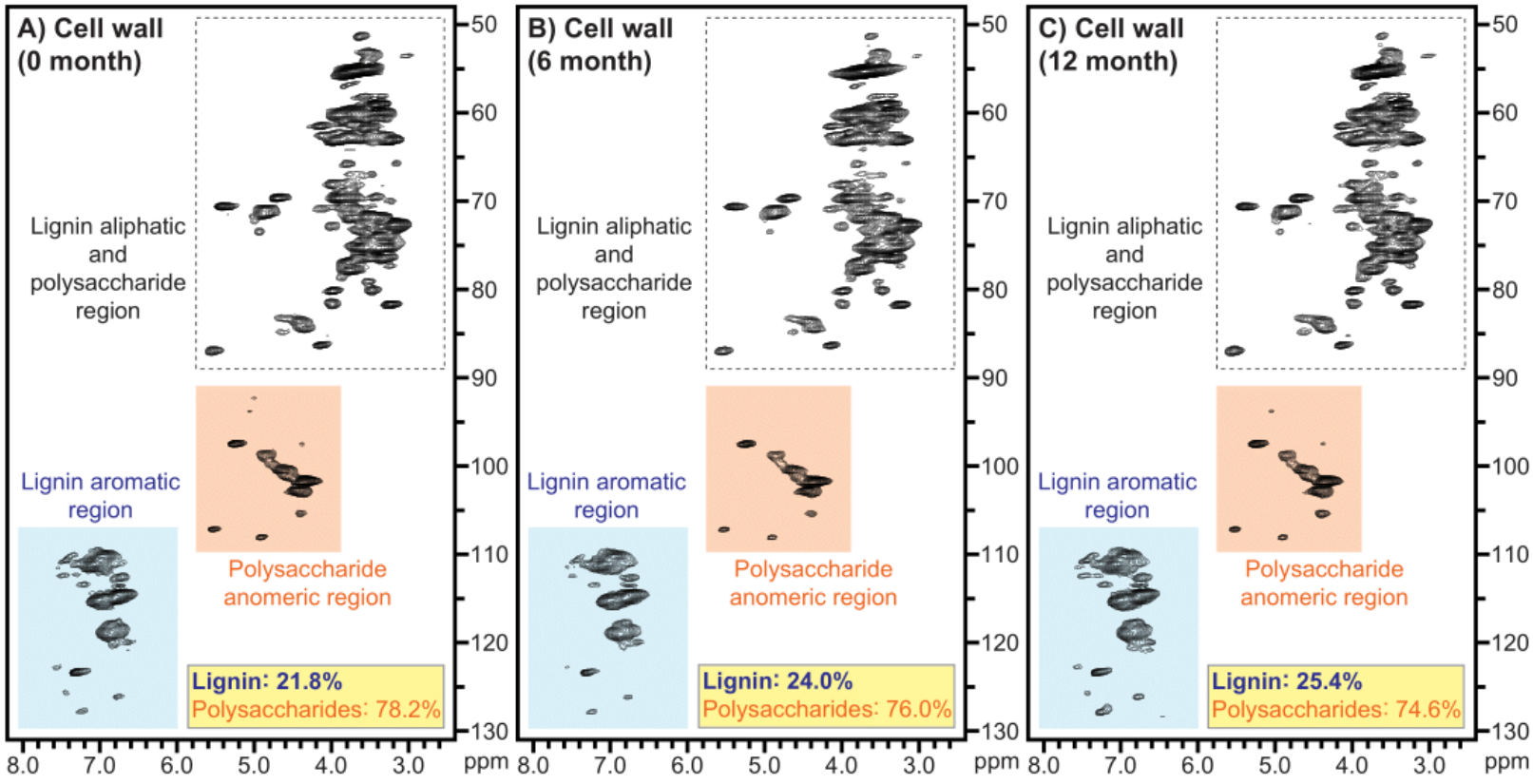

Figure 7.5. NMR of downed timber cell walls.

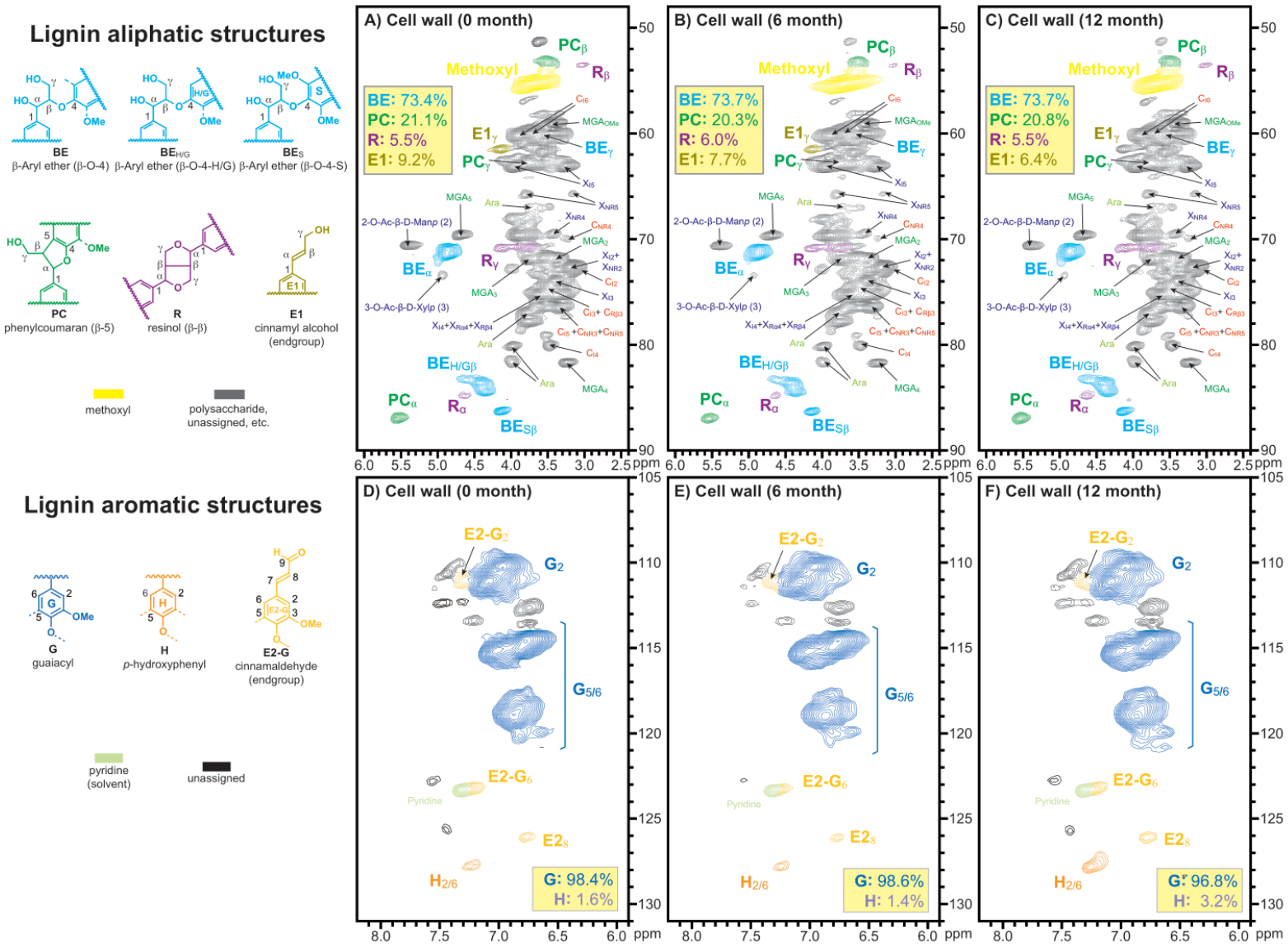

Figure 7.6. NMR of downed timber cell walls. Detailed lignin structures.

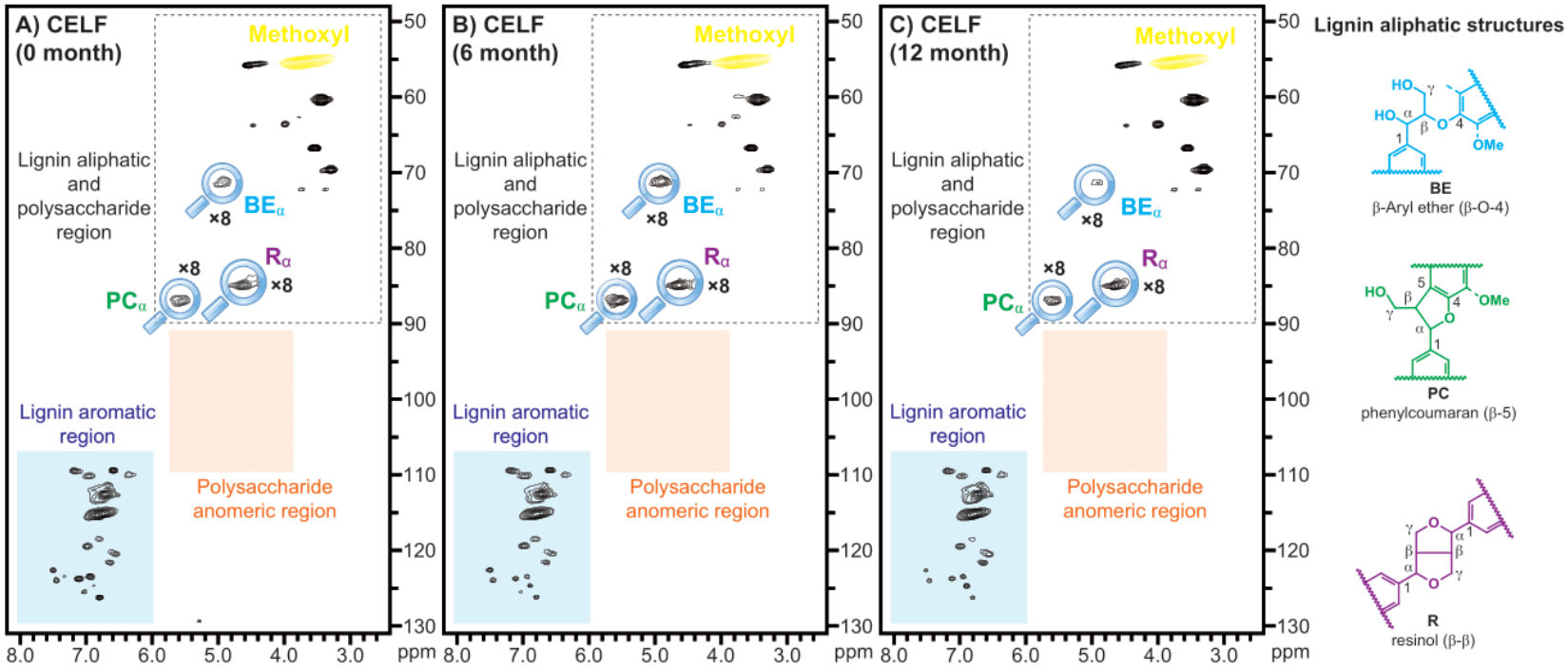

Figure 7.7. NMR of CELF Lignin estructures.

7.3.8. CELF Lignin Particles Production

In this study, CELF Lignin samples were dissolved in a solvent system consisting of tetrahydrofuran/water-salt (THF:0.1M NaNO3) at 3:1 ratio with incremental solid contents. The dissolution process aimed to achieve complete solubilization of the lignin samples, regardless of the initial concentration. Through systematic testing, it was determined that a ratio of 3:1 of THF to the water-salt solution provided the most efficient dissolution of CELF Lignin samples. This ratio resulted in complete solubilization of the lignin samples regardless of initial % wt. for the studied range (2, 4, and 6 % wt.). CELF Lignin samples were dissolved by mixing them with the solvent system and then subjecting them to gentle agitation on a laboratory rotator at room temperature for 12 hours **Figure 0.2**. Subsequently, the dissolved samples were mixed dropwise with deionized water under magnetic stirring, resulting in the formation of homogeneous solutions. Particles suspensions produced showed promising stability over a period of 5 months as shown in **Figure 0.3**. Recent reports have used antisolvent (acetone-water) precipitation systems with ratios of 7:3 aided with mechanical treatments such as homogenization (12,000rpm) or ultrasonication (600 W) to help stabilize the negative surface charge (-36.6±0.4 mV) to prepare stable aqueous solutions for 3 months (Aryana et al., 2023). Another report compared three approaches: acid precipitation, 70% ethanol dissolution, and acetone:water (3:1) system (Figueiredo et al., 2021). The authors from this study utilized the mixture of acetone water to dissolve 10mg/mL of lignin (1 % wt.), further precipitation in water under stirring. Their final yield was 86%. Which could signal that the full dissolution of the lignin in the system was not complete. Nevertheless, their conclusion was that the acetone-water systems were a clear winner for effectiveness and properties obtained from lignin particles with three different technical lignins.

7.3.9. SEM

Scanning electron microscopy (SEM) coupled with ImageJ software was employed to analyze the particle size distributions of Co-solvent Enhanced Lignin Fractionation (CELF) lignin particle samples at different time points and initial concentrations. The particle sizes produced with the initial 0-month samples ranged in mean values from 321 to 475 nm, with standard deviations from 73 to 177 nm. Intriguingly, the highest mean was observed for the 4% wt. concentration (**Table *7.4***). Meanwhile, the 2 and 6 % wt. values obtained were very close. The gaussian distribution was very similar in the two samples, while the 4 % wt. exhibited a small right tailed deformation of the distribution as shown in **Figure 7.8**. The particle sized produced with the 6-month downed timber showed an increased mean particle size across all the initial concentrations, ranging from 442 to 592 nm with higher standard deviations ranging from 141 to 185 nm. Interestingly, in this case the initial % wt. increase resulted in increased mean particle size. The three concentrations yielded right tailed gaussian particle size distributions as shown in **Figure 7.9**. Finally, the samples of downed timber obtained after 12-months produced lignin particles with closer mean particle sizes not dependent on the initial concentration of lignin. The mean range was from 409 to 449 nm with standard deviations ranging from 103 to 156 nm. Again, the three concentrations showed right-tailed gaussian distributions. Notably the 6 % wt. concentration was closer to normal distribution as shown in **Figure 7.10**.

Table 7.4. SEM particle size of CELF Lignins.

Initial	**Mean particle diameter [nm]**		
%wt.	**0 - Months**	**6 - Months**	**12 - Months**
2%	321 ± 77	442 ± 141	430 ± 147
4%	475 ± 177	503 ± 164	449 ± 156
6%	329 ± 73	592 ± 185	409 ± 103

*Means of 200 particles measured using ImageJ software.

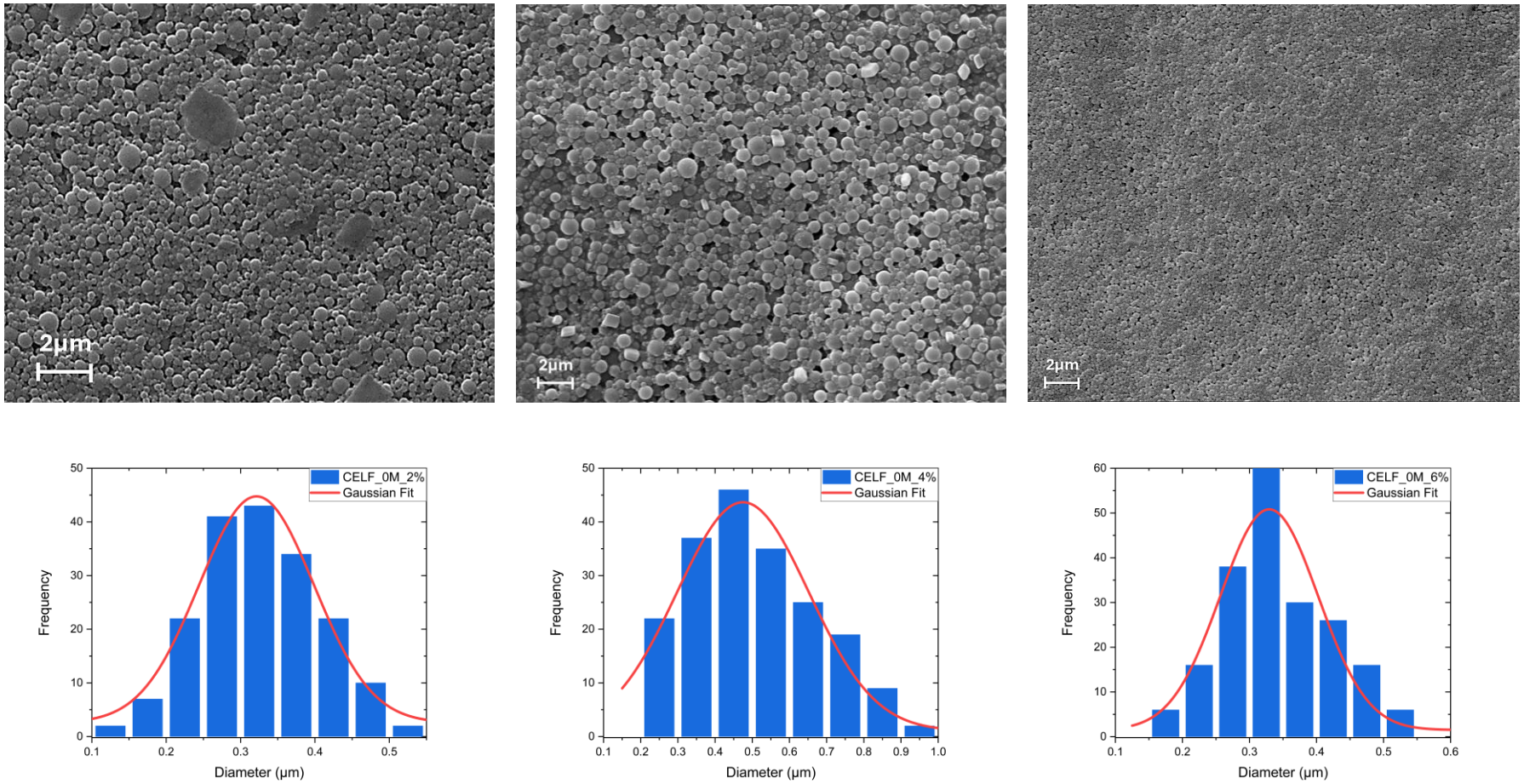

Figure 7.8. SEM images of CELF lignin particles obtained from the initial (0 months) downed timed (top). Particle size (diameter) distribution measured using ImageJ software over 200 individual particles (bottom).

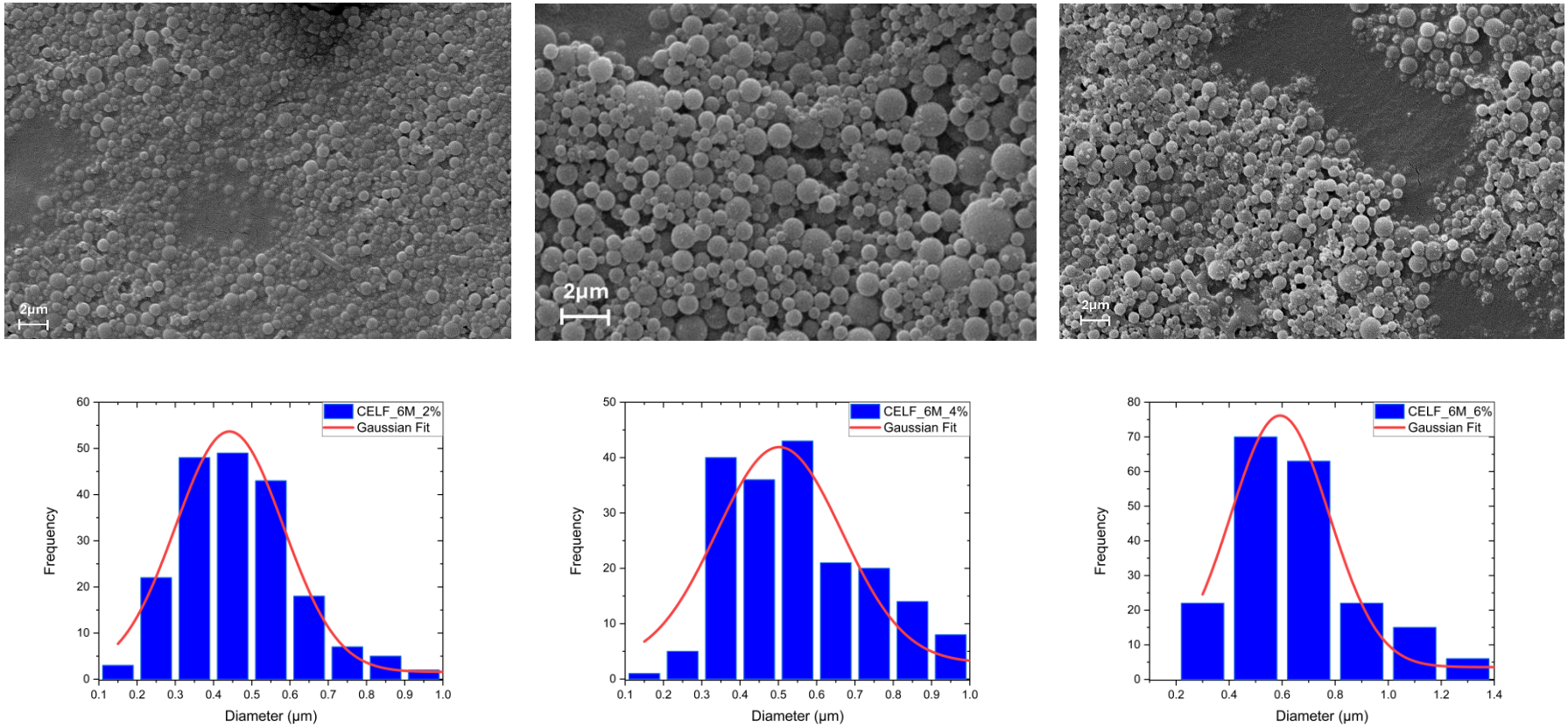

Figure 7.9. SEM images of CELF lignin particles obtained from the middle time frame (6 months) downed timed (top).

Particle size (diameter) measured using ImageJ software over 200 individual particles (bottom).

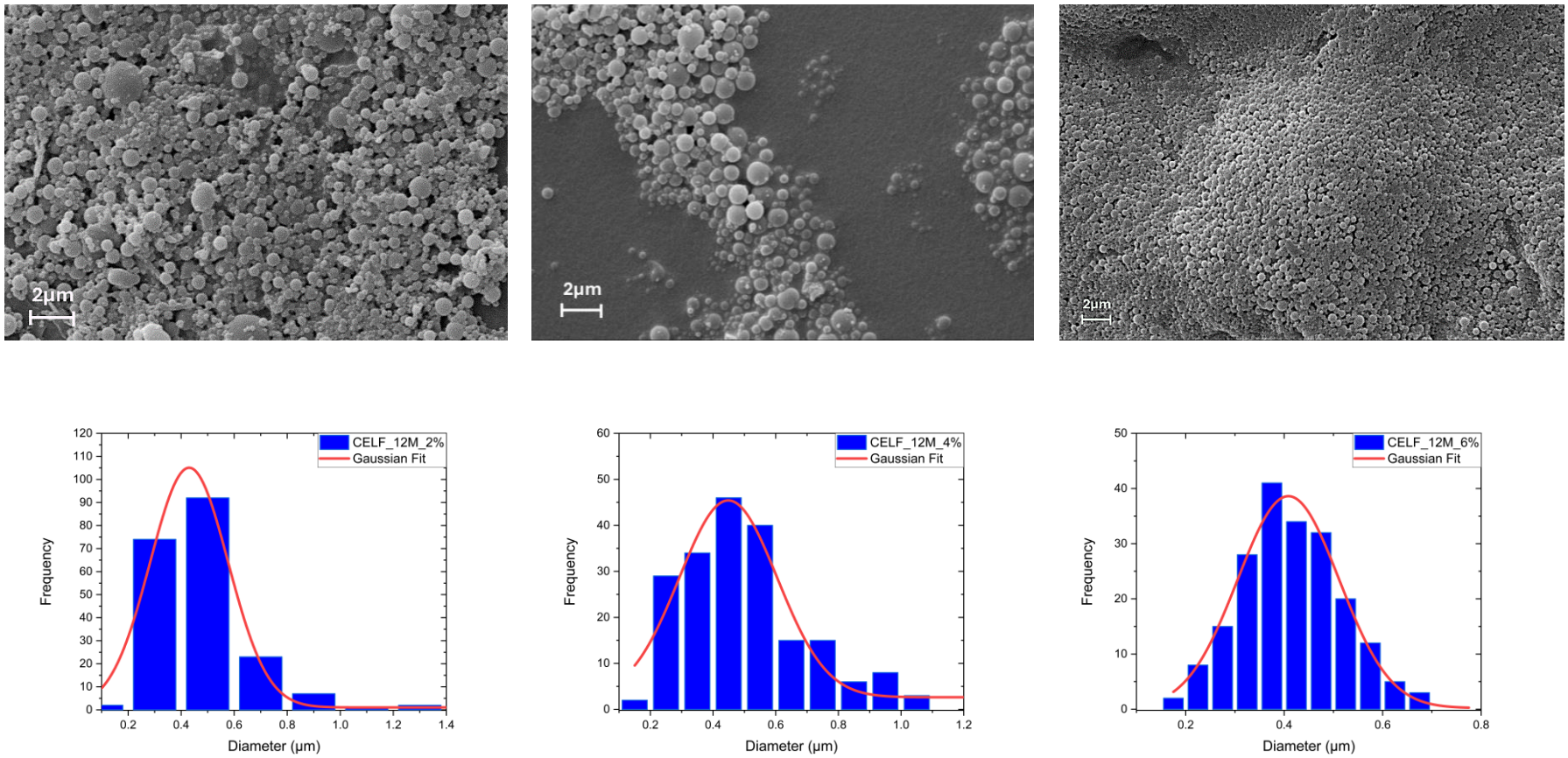

Figure 7.10. SEM images of CELF lignin particles obtained from the last time frame (12 months) downed timed (top). Particle size (diameter) measured using ImageJ software over 200 individual particles (bottom).

7.3.10. DLS

The optimal concentration for measurement of CELF lignin particles in the Litesizer 500 was determined to be 500 ppm by previous runs. From the data obtained, the higher initial concentration tends to correlate with larger hydrodynamic diameters **Table *7.5***. The overall range is relatively small from 208 to 344 nm. The smallest mean particle being observed by the particles prepared from the 6-months CELF lignin samples at the lowest 2 % wt. initial concentration. Meanwhile, the highest mean particle size was observed by the 0-months CELF lignin samples at the 4 % wt. initial concentration. Overall, the narrow distribution of the results could indicate that the CELF processing technique can recover lignin with similar characteristics independently of the degradation undergone for 6 or 12 months of the downed timber. These results are slightly higher than the ~100-200 nm reported by (Figueiredo et al., 2021). Nevertheless, the report utilized 1 % wt. for lignin particle preparation and reached a yield of 86%. In this report, the complete dissolution of initial lignin 2, 4, and 6 % wt. was achieved.

Table 7.5. Particle size and zeta-potential of CELF Lignins by dynamic light scattering (DLS).

Time	Initial %wt.	Hydrodynamic diameter [nm]	PDI	Zeta potential [mV]
0-Months	**2%**	215 ± 4	21 ±3	-47 ± 0.2
	4%	344 ± 5	26 ± 2	-48 ± 0.3
	6%	280 ± 3	25 ± 2	-48 ± 0.4
6-Months	**2%**	208 ± 3	16 ± 3	-48 ± 0.3
	4%	331 ± 6	25 ± 1	-49 ± 0.2
	6%	251 ± 5	24 ±3	-50 ± 0.2
12-Months	**2%**	236 ± 3	22 ± 4	-43 ± 0.1
	4%	324 ± 6	23 ± 1	-45 ± 0.3
	6%	266 ± 5	26 ± 1	-45 ± 0.2

*Means of five series measurements performed at 500ppm dilution in DI water.

The initial concentration of CELF samples appears to influence the PDI values, with higher concentrations generally associated with higher PDI values. This suggests that higher concentrations may lead to greater heterogeneity in particle size distribution. Notably the lower PDI value was observed for the 6-months CELF lignin samples at the 2 % wt. initial concentration. Tukey test was performed on the results as shown in **Figure 7.11**. Regarding PDI the only significative different sample were the particles produced by 0-Month CELF Lignin at 2 % wt. concentration.

Zeta potential is a measure of the electrostatic potential at the slipping plane of a particle and reflects the stability of colloidal dispersions. A higher absolute zeta potential value indicates greater repulsion between particles, leading to increased stability. In the case of lignin particles, the zeta potential is negative mV. The initial concentration of CELF samples appears to influence the zeta potential values, with higher concentrations generally associated with more negative zeta potentials. The lowest absolute values in general were observed with the CELF lignin particles produced with the 12-Months downed timber. Nevertheless, the range is clearly small, varying from -43 to -50 mV in the whole sample set. The negative surface charge of LNPs can be attributed to the abundance of phenolic, aliphatic hydroxy, and carboxylic groups on their surface. These groups facilitate the stabilization of LNPs in colloidal dispersion by inducing electric double-layer repulsion (Figueiredo et al., 2021). These results reinforce the hypothesis that the CELF process can produce lignin suitable for particles production even after 12 months of degradation from downed timber. These results surpass the best values obtained by (Aryana et al., 2023), which obtained -36.6±0.4 mV. Similarly, with the acetone:water system explored by (Figueiredo et al., 2021) one sample did not achieved values under -25mV, and the other two were similar to our results around -45mV.

The zeta potential, a critical parameter influencing the stability of colloidal dispersions, was investigated for lignin particles at a concentration of 1000 ppm in deionized (DI) water solution across a pH range from 2 to 12 with 0.5 pH steps. Five series repetitions were conducted for each sample to ensure statistical significance, and the results were averaged. The results of the zeta potential measurements revealed consistent behavior across all experimental conditions for lignin particles production. Lignin particles at different aging time points exhibited subtle variations in their zeta potential behavior. The 0-month samples displayed the most consistent behavior, while slight deviations were observed in the 6-month and 12-month samples. Notably, in the report from (Figueiredo et al., 2021) the pH range explored was limited to the range 3-8.

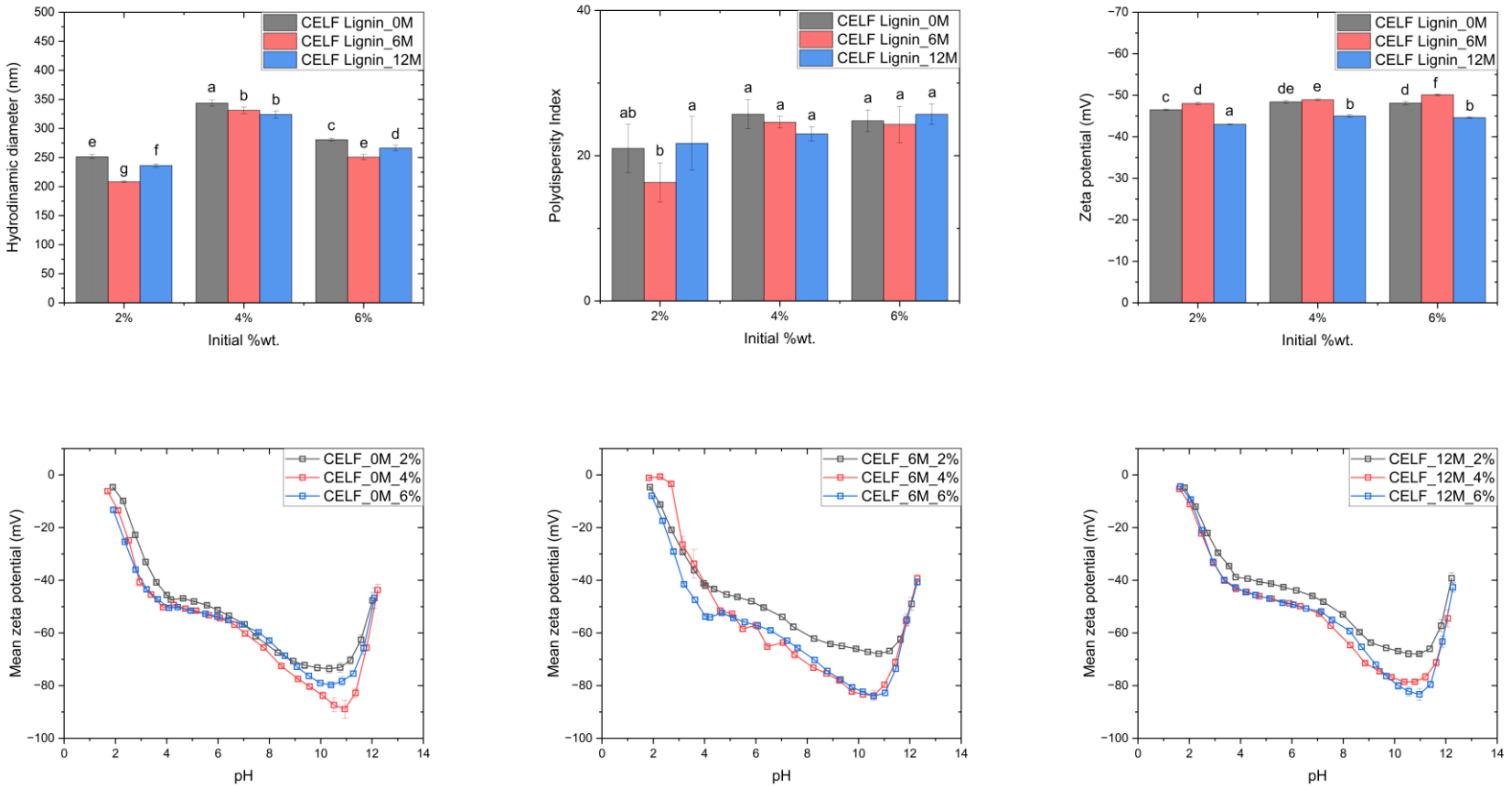

Figure 7.11. Hydrodynamic diameter, polydispersity index and zeta-potential results from CELF Lignin particles (top). Tukey's test was performed to help identify significant differences in the results and are labeled with letters. Zeta-potential over pH range results from CELF Lignin particles (bottom).

The zeta potential of lignin particles showed a noticeable change, or "elbow," in behavior around pH 3.5 for the 0-month and 12-month samples, while it occurred closer to pH 4 for the 6-month samples. Additionally, the lowest zeta potential values were consistently observed at pH 11, followed by a sharp decrease in zeta potential absolute value indicating destabilization of particles at alkaline pH.

7.4. Conclusions

In summary, the data suggests a dynamic transformation in the composition of lignin and carbohydrates during the weathering process. Notably, there is an increase in Klason lignin content over time, which is a positive outcome for lignin recovery. The variations in other components, such as extractives and soluble lignin, may be attributed to the intricacies of the natural degradation processes occurring in downed timber.

The alterations in the FTIR spectra at 12 months, particularly in 1700, 1670, 1452, and 1080 cm^{-1} peaks, indicate changes in the chemical composition, structure, and possibly the aging of the lignin samples. These variations may result from chemical, structural, and environmental factors affecting lignin's spectral characteristics over time. Further analysis and additional experiments may be necessary to elucidate the specific mechanisms behind these changes.

The TGA analysis demonstrates that the CELF lignin samples possess excellent thermal stability, as indicated by the high maximum degradation temperatures and consistent degradation temperature ranges. The minor fluctuations in maximum degradation temperature may be attributed to slight variations in sample composition or preparation. These results are promising for applications where lignin needs to withstand high-temperature conditions, such as in the production of biopolymers and composites.

The DSC analysis not only provided specific Tg values for different CELF lignin samples but also underscored the influence of molecular structure and crosslinking on the thermal behavior of lignin. These insights are essential for tailoring lignin properties for its intended applications, particularly in polymeric materials, and highlight the significance of weathering in downed timber for lignin valorization.

The 0-month sample exhibits slightly higher molecular weights (both M_n and M_w) and larger lignin molecules (M_z) than the 6-month and 12-month samples. The PDI values for the CELF lignin samples show a consistent pattern of moderate polydispersity. The PDI values for the 6-month and 12-month samples indicate slightly narrower molecular weight distributions than the 0-month sample. These results are consistent with expected natural degradation. Nevertheless, the differences are relatively small and biorefinery industries could have little impact on the final properties of lignin produced after an extended period of degradation of downed timber.

The consistency in lignin quality suggests the robustness and reliability of the CELF process in effectively isolating lignin from different stages of timber degradation. The process appears to be resilient to variations in the structural integrity and chemical composition of the starting material, ensuring that the resulting lignin maintains similar characteristics regardless of the initial state of the downed timber.

General conclusions, recommendations, and future work

For the price prediction utilizing wavelet methodologies, work has been started on applying the same methodology for other hurricane seasons (starting from year 2000) to create a comparative study. Moreover, utilization of other techniques, such as Machine Learning or Artificial Intelligence, could be explored to manage the high quantity of data and models. Ultimately, these price prediction models could benefit the input for feasibility analysis of biorefinery business plans to promote the implementation of technology investment in the US Southeast.

In future work, downed timber degradation studies should be extended to cellulose and hemicellulose fractions since this work have focused mainly on lignin recovery and utilization. Moreover, the degree of polymerization for cellulose fraction over the degradation time frame would be of special interest to biorefinery concepts. The degradation studies could benefit from exploring other experimental design methodologies to verify the robustness of the Box-Behnken design coupled with machine learning as applied in this research.

The CELF process conditions used for this study focused on maximizing lignin recovery, resulting in condensed lignin structures. Future work could benefit from studying different conditions to balance the yield of other natural polymers from downed timber.

Further research could explore the underlying mechanisms responsible for the efficacy of the THF:water-salt solvent system in dissolving lignin and investigate its applicability to other lignin sources and concentrations. Additionally, this solvent system could be investigated as a medium for measuring the molecular weight of other technical lignin sources.

References

A Bird's Eye View: Aerial surveyors map timber damage from Hurricane Florence | In the Field. (2018, October 1). https://blog.ncagr.gov/2018/10/01/a-birds-eye-view-aerial-surveyors-map-timber-damage-from-hurricane-florence/

Aber, J. D., Bolster, K. L., Newman, S. D., Soulia, M., & Martin, M. E. (1994). Analyses of forest foliage II: Measurement of carbon fraction and nitrogen content by end-member analysis. *Journal of Near Infrared Spectroscopy*, *2*(1), 15–23.

Acquah, G. E., Essien, C., Via, B. K., Billor, N., & Eckhardt, L. G. (2018). Estimating the Basic Density and Mechanical Properties of Elite Loblolly Pine Families with Near Infrared Spectroscopy. *Forest Science*, *64*(2), 149–158. https://doi.org/10.1093/forsci/fxx009

Acquah, G. E., Via, B. K., Billor, N., Fasina, O. O., & Eckhardt, L. G. (2016). Identifying Plant Part Composition of Forest Logging Residue Using Infrared Spectral Data and Linear Discriminant Analysis. *Sensors*, *16*(9), Article 9. https://doi.org/10.3390/s16091375

Acquah, G. E., Via, B. K., Gallagher, T., Billor, N., Fasina, O. O., & Eckhardt, L. G. (2018). High Throughput Screening of Elite Loblolly Pine Families for Chemical and Bioenergy Traits with Near Infrared Spectroscopy. *Forests*, *9*(7), Article 7. https://doi.org/10.3390/f9070418

Aguiar-Conraria, L., & Soares, M. J. (2014). The continuous wavelet transform: Moving beyond uni-and bivariate analysis. *Journal of Economic Surveys*, *28*(2), 344–375.

Aldrich, E. (2013). *A Package of Functions for Computing Wavelet Filters, Wavelet Transforms and Multiresolution Analyses. 2013*.

Angadi, M. C., & Kulkarni, A. P. (2015). Time Series Data Analysis for Stock Market Prediction using Data Mining Techniques with R. *International Journal of Advanced Research in Computer Science*, *6*(6).

Aryana, N., Krismastuti, F. S. H., Arutanti, O., & Restu, W. K. (2023). *The preparation of lignin nanoparticles: Comparison between homogenization and ultrasonication treatments following anti-solvent precipitation method*. 080004. https://doi.org/10.1063/5.0172942

Atiwesh, G., Parrish, C. C., Banoub, J., & Le, T.-A. T. (2022). Lignin degradation by microorganisms: A review. *Biotechnology Progress*, *38*(2), e3226. https://doi.org/10.1002/btpr.3226

Avila, L. A. (2019a). The 2018 Atlantic Hurricane Season: Another Catastrophic Year for the United States. *Weatherwise*, *72*(4), 14–21. https://doi.org/10.1080/00431672.2019.1612201

Avila, L. A. (2019b). The 2018 Atlantic Hurricane Season: Another Catastrophic Year for the United States. *Weatherwise*, *72*(4), 14–21. https://doi.org/10.1080/00431672.2019.1612201

Beckham, G. T. (2018). *Lignin Valorization: Emerging Approaches*. Royal Society of Chemistry.

Beven, J. L., Avila, L. A., Blake, E. S., Brown, D. P., Franklin, J. L., Knabb, R. D., Pasch, R. J., Rhome, J. R., & Stewart, S. R. (2008). Atlantic hurricane season of 2005. *Monthly Weather Review*, *136*(3), 1109–1173.

Binkley, C. S., & Zhang, D. (2021). *From Backwoods to Boardrooms: The Rise of Institutional Investment in Timberland*. Oregon State University Press. http://muse.jhu.edu/book/94486

Bishop, C. (2006). Pattern recognition and machine learning. *Springer Google Schola*, *2*, 531–537.

Blake, E. S. (2018). The 2017 Atlantic Hurricane Season: Catastrophic Losses and Costs. *Weatherwise*, *71*(3), 28–37. https://doi.org/10.1080/00431672.2018.1448147

Blake, E. S., Rappaport, E. N., & Landsea, C. W. (2011). *The deadliest, costliest, and most intense United States tropical cyclones from 1851 to 2010 (and other frequently requested hurricane facts)*.

Brandeis, T., Turner, J., Baeza Castro, A., Brown, M., & Lambert, S. (2022). *Assessing forest resource damage following natural disasters using national forest inventory plots: A case study of Hurricane Michael* (SRS-RP-65; p. SRS-RP-65). U.S. Department of Agriculture, Forest Service, Southern Research Station. https://doi.org/10.2737/SRS-RP-65

Bryan, M. F., & Cecchetti, S. G. (1993). *The consumer price index as a measure of inflation*.

Calonego, F. W., Severo, E. T. D., & Furtado, E. L. (2010). Decay resistance of thermally-modified *Eucalyptus grandis* wood at 140 °C, 160 °C, 180 °C, 200 °C and 220 °C. *Bioresource Technology*, *101*(23), 9391–9394. https://doi.org/10.1016/j.biortech.2010.06.119

Cazelles, B., Chavez, M., Berteaux, D., Ménard, F., Vik, J. O., Jenouvrier, S., & Stenseth, N. C. (2008). Wavelet analysis of ecological time series. *Oecologia*, *156*(2), 287–304. https://doi.org/10.1007/s00442-008-0993-2

Chen, H., Song, Q., Tang, G., Feng, Q., & Lin, L. (2013). The Combined Optimization of Savitzky-Golay Smoothing and Multiplicative Scatter Correction for FT-NIR PLS Models. *International Scholarly Research Notices*, *2013*, e642190. https://doi.org/10.1155/2013/642190

Cherubini, F. (2010). The biorefinery concept: Using biomass instead of oil for producing energy and chemicals. *Energy Conversion and Management*, *51*(7), 1412–1421. https://doi.org/10.1016/j.enconman.2010.01.015

Chudy, R., & Cubbage, F. (2020). Research trends: Forest investments as a financial asset class. *Forest Policy and Economics*, *119*, 102273.

Clarke, M., Sharma, A., Stein, T., Vogel, J., & Nowak, J. (2023). Forest Disturbances and Nonindustrial Forest Landowners: Management of Invasive Plants, Fire Hazards and Wildlife Habitats After a Hurricane. *Journal of Forestry*, fvad022. https://doi.org/10.1093/jofore/fvad022

Cline, L. C., Schilling, J. S., Menke, J., Groenhof, E., & Kennedy, P. G. (2018). Ecological and functional effects of fungal endophytes on wood decomposition. *Functional Ecology*, *32*(1), 181–191.

CME Group Inc. (2009). *An introductory guide to random length lumber futures and options*. CMEGroup. https://www.cmegroup.com/trading/agricultural/files/AC-243_RanLenLumberBrochure.pdf

Consumer Price Index, South Region — February 2023: Southeast Information Office : U.S. Bureau of Labor Statistics. (2023, March 14). https://www.bls.gov/regions/southeast/news-release/consumerpriceindex_south.htm

Consumer Price Index Summary—2023 M06 Results. (2023). https://www.bls.gov/news.release/cpi.nr0.htm

Cristianini, N., & Shawe-Taylor, J. (2007). Support vector and kernel methods. In *Intelligent Data Analysis: An Introduction* (pp. 169–197). Springer.

Dashtban, M., Schraft, H., Syed, T. A., & Qin, W. (2010). Fungal biodegradation and enzymatic modification of lignin. *International Journal of Biochemistry and Molecular Biology*, *1*(1), 36–50.

Dean, A., Voss, D., & Draguljić, D. (2017). *Design and Analysis of Experiments*. https://doi.org/10.1007/978-3-319-52250-0

Derkacheva, O., & Sukhov, D. (2008). Investigation of Lignins by FTIR Spectroscopy. *Macromolecular Symposia*, *265*(1), 61–68. https://doi.org/10.1002/masy.200850507

Developers, S. (2013). Signal: Signal processing. *URL: Http://R-Forge. r-Project. Org/Projects/Signal*.

Dickson, R. L., Raymond, C. A., Joe, W., & Wilkinson, C. A. (2003). Segregation of Eucalyptus dunnii logs using acoustics. *Forest Ecology and Management*, *179*(1–3), 243–251.

Dima, B., Dima, Ş., & Barna, F. (2015). A wavelet analysis of capital markets' integration in Latin America. *Applied Economics*, *47*(10), 1019–1036.

Dutta, N., & Saha, M. K. (2019). Nanoparticle-induced enzyme pretreatment method for increased glucose production from lignocellulosic biomass under cold conditions. *Journal of the Science of Food and Agriculture*, *99*(2), 767–780. cmedm. https://doi.org/10.1002/jsfa.9245

Eberhardt, T. L., & Samuelson, L. J. (2022). Comparison of lignin and polysaccharide sugar contents for slash, longleaf, and loblolly pine growth rings formed during periods of soil moisture extremes. *Wood Science and Technology*, *56*(2), 389–408. https://doi.org/10.1007/s00226-022-01359-0

Emandi, A., Ileana Vasiliu, C., Budrugeac, P., & Stamatin, I. (2011). Quantitative investigation of wood composition by integrated FT-IR and thermogravimetric methods. *Cellulose Chemistry and Technology*, *45*(9), 579.

Essien, C., Via, B., Cheng, Q., Gallagher, T., McDonald, T., & Eckhardt, L. G. (2017). Multivariate modeling of acousto-mechanical response of 14-year-old loblolly pine (Pinus taeda) to variation in wood chemistry, microfibril angle and density. *General Technical Report-Forest Products Laboratory, USDA Forest Service*, *FPL-GTR-249*, 50–57.

Fang, Y., Park, J. I., Jeong, Y.-S., Jeong, M. K., Baek, S. H., & Cho, H. W. (2011). Enhanced predictions of wood properties using hybrid models of PCR and PLS with high-dimensional NIR spectral data. *Annals of Operations Research*, *190*(1), 3–15. https://doi.org/10.1007/s10479-009-0554-z

Fernholz, K., Bowyer, J. L., & Howe, J. (2007). *TIMOs & REITs: What, why & how they might impact sustainable forestry*. Dovetail Partners, Incorporated.

Figueiredo, P., Lahtinen, M. H., Agustin, M. B., de Carvalho, D. M., Hirvonen, S.-P., Penttilä, P. A., & Mikkonen, K. S. (2021). Green Fabrication Approaches of Lignin Nanoparticles from Different Technical Lignins: A Comparison Study. *ChemSusChem*, *14*(21), 4718–4730. https://doi.org/10.1002/cssc.202101356

Florida Forest Service. (2018, October 19). *Hurricane Michael: Initial Value Estimate of Altered, Damaged or Destroyed Timber in Florida*. https://www.google.com/search?q=Hurricane+Michael+Florida+Forest+Service+Initial+Value+Estimate+of+Altered%2C+Damaged+or+Destroyed+Timber+in+Florida&rlz=1C1ONGR_enUS942US942&oq=Hurricane+Michael+Florida+Forest+Service+Initial+Value+Estimate+of+Altered%2C+Damaged+or+Destroyed+Timber+in+Florida&aqs=chrome..69i57j69i60.751j0j7&sourceid=chrome&ie=UTF-8

Franklin, J. L., Pasch, R. J., Avila, L. A., Beven, J. L., Lawrence, M. B., Stewart, S. R., & Blake, E. S. (2006). Atlantic hurricane season of 2004. *Monthly Weather Review*, *134*(3), 981–1025.

Fukasawa, Y., & Matsukura, K. (2021). Decay stages of wood and associated fungal communities characterise diversity–decomposition relationships. *Scientific Reports*, *11*(1), 8972.

Fundová, I. (2012). *In situ wood quality assessment in interior spruce* [University of British Columbia]. https://doi.org/10.14288/1.0073230

Gan, J., Tian, N., Choi, J., & Pelkki, M. H. (2022). Synchronized movement between US lumber futures and southern pine sawtimber prices and COVID-19 impacts. *Canadian Journal of Forest Research*, *52*(4), 614–621. https://doi.org/10.1139/cjfr-2021-0326

Ganesan, R., Das, T. K., & Venkataraman, V. (2004). Wavelet-based multiscale statistical process monitoring: A literature review. *IIE Transactions*, *36*(9), 787–806.

Gatius, F., Ferran, J., & Puy, J. (2004). Experimental design procedures in the calibration of quality parameters of alfalfa pellets from near infrared spectra. *Journal of near Infrared Spectroscopy*, *12*(3), 167–176.

Goodell, B., Winandy, J. E., & Morrell, J. J. (2020). Fungal degradation of wood: Emerging data, new insights and changing perceptions. *Coatings*, *10*(12), 1210.

Goodell, J. W., & Goutte, S. (2021). Co-movement of COVID-19 and Bitcoin: Evidence from wavelet coherence analysis. *Finance Research Letters*, *38*, 101625.

Grgas, D., Rukavina, M., Bešlo, D., Štefanac, T., Crnek, V., Šikić, T., Habuda-Stanić, M., & Landeka Dragičević, T. (2023). The Bacterial Degradation of Lignin—A Review. *Water*, *15*(7), Article 7. https://doi.org/10.3390/w15071272

Hao, Y., Wang, Q., & Zhang, S. (2021). *Rapid Identification of Wood Species Based on Portable Near-Infrared Spectrometry and Chemometrics Methods*. *36*, 7–13.

He, W., & Hu, H. (2013). Rapid Prediction of Different Wood Species Extractives and Lignin Content Using Near Infrared Spectroscopy. *Journal of Wood Chemistry and Technology*, *33*(1), 52–64. https://doi.org/10.1080/02773813.2012.731463

Henderson, J. D., Abt, R. C., Abt, K. L., Baker, J., & Sheffield, R. (2022). Impacts of hurricanes on forest markets and economic welfare: The case of hurricane Michael. *Forest Policy and Economics*, *140*(7–8), Article 7–8. https://doi.org/10.1016/j.forpol.2022.102735

Hook, D. D., Buford, M. A., & Williams, T. M. (1991). Impact of Hurricane Hugo on the South Carolina coastal plain forest. *Journal of Coastal Research*, 291–300.

Janusz, G., Pawlik, A., Sulej, J., Świderska-Burek, U., Jarosz-Wilkołazka, A., & Paszczyński, A. (2017). Lignin degradation: Microorganisms, enzymes involved, genomes analysis and evolution. *FEMS Microbiology Reviews*, *41*(6), 941–962. https://doi.org/10.1093/femsre/fux049

Johnson, M. C., Kennedy, M. C., Harrison, S. C., Alvarado, E., Desautel, C., Holford, J., & Logue, S. (2023). Post-wildfire salvage logging effects on snag structure and dead woody fuel loadings. *Canadian Journal of Forest Research*, *53*(2), 103–118. https://doi.org/10.1139/cjfr-2021-0089

Jolliffe, I. T., & Cadima, J. (2016). Principal component analysis: A review and recent developments. *Philosophical Transactions of the Royal Society A: Mathematical, Physical and Engineering Sciences*, *374*(2065), 20150202. https://doi.org/10.1098/rsta.2015.0202

Jones, P. D., Schimleck, L. R., Peter, G. F., Daniels, R. F., & Clark, A. (2006). Nondestructive estimation of wood chemical composition of sections of radial wood strips by diffuse reflectance near infrared spectroscopy. *Wood Science and Technology*, *40*(8), 709–720. https://doi.org/10.1007/s00226-006-0085-6

Karatzoglou, A., Smola, A., Hornik, K., & Zeileis, A. (2004). Kernlab-an S4 package for kernel methods in R. *Journal of Statistical Software*, *11*, 1–20.

Kärhä, K., Anttonen, T., Poikela, A., Palander, T., Laurén, A., Peltola, H., & Nuutinen, Y. (2018). Evaluation of Salvage Logging Productivity and Costs in Windthrown Norway Spruce-Dominated Forests. *Forests*, *9*(5), Article 5. https://doi.org/10.3390/f9050280

Kelley, S. S., Rials, T. G., Groom, L. R., & So, C. L. (2004). *Use of near infrared spectroscopy to predict the mechanical properties of six softwoods*.

Kelley, S. S., Rials, T. G., Snell, R., Groom, LeslieH., & Sluiter, A. (2004). Use of near infrared spectroscopy to measure the chemical and mechanical properties of solid wood. *Wood Science and Technology*, *38*(4). https://doi.org/10.1007/s00226-003-0213-5

Kim, H., & Ralph, J. (2010). Solution-state 2D NMR of ball-milled plant cell wall gels in DMSO-d6/pyridine-d5. *Organic & Biomolecular Chemistry*, *8*(3), 576–591.

Kim, H., Ralph, J., & Akiyama, T. (2008). Solution-state 2D NMR of ball-milled plant cell wall gels in DMSO-d 6. *BioEnergy Research*, *1*, 56–66.

Kim, H., Sriram, S., Fang, T., Kelley, S., & Park, S. (2021). An eco-friendly approach for blending of fast-pyrolysis bio-oil in petroleum-derived fuel by controlling ash content of loblolly pine. *Renewable Energy*, *179*, 2063–2070. https://doi.org/10.1016/j.renene.2021.08.033

Kriechbaumer, T., Angus, A., Parsons, D., & Casado, M. R. (2014). An improved wavelet–ARIMA approach for forecasting metal prices. *Resources Policy*, *39*, 32–41.

Kumar, P., & Foufoula-Georgiou, E. (1997). Wavelet analysis for geophysical applications. *Reviews of Geophysics*, *35*(4), 385–412.

Lappalainen, N. (2023). *The Effectiveness of Forest Assets as Inflation Hedges*.

Leskinen, T., Kelley, S. S., & Argyropoulos, D. S. (2015). Refining of Ethanol Biorefinery Residues to Isolate Value Added Lignins. *ACS Sustainable Chemistry & Engineering*, *3*(7), 1632–1641. https://doi.org/10.1021/acssuschemeng.5b00337

Lievonen, M. (2015). *Preparation and characterization of lignin nanoparticles*. https://aaltodoc.aalto.fi:443/handle/123456789/15064

Lievonen, M., José Valle-Delgado, J., Mattinen, M.-L., Hult, E.-L., Lintinen, K., A. Kostiainen, M., Paananen, A., R. Szilvay, G., Setälä, H., & Österberg, M. (2016). A simple process for lignin nanoparticle preparation. *Green Chemistry*, *18*(5), 1416–1422. https://doi.org/10.1039/C5GC01436K

Liu, W., & Chen, W. (2019). Recent advancements in empirical wavelet transform and its applications. *IEEE Access*, *7*, 103770–103780.

Liu, Z., Peng, C., Work, T., Candau, J.-N., DesRochers, A., & Kneeshaw, D. (2018). Application of machine-learning methods in forest ecology: Recent progress and future challenges. *Environmental Reviews*, *26*(4), 339–350. https://doi.org/10.1139/er-2018-0034

Luceño, A., & Peña, D. (2008). Autoregressive integrated moving average (arima) modeling. *Encyclopedia of Statistics in Quality and Reliability*.

Lupoi, J. S., Singh, S., Simmons, B. A., & Henry, R. J. (2014). Assessment of Lignocellulosic Biomass Using Analytical Spectroscopy: An Evolution to High-Throughput Techniques. *BioEnergy Research*, *7*(1), 1–23. https://doi.org/10.1007/s12155-013-9352-1

Lustenhouwer, N., Maynard, D. S., Bradford, M. A., Lindner, D. L., Oberle, B., Zanne, A. E., & Crowther, T. W. (2020). A trait-based understanding of wood decomposition by fungi. *Proceedings of the National Academy of Sciences*, *117*(21), 11551–11558.

Luts, J., Ojeda, F., Van de Plas, R., De Moor, B., Van Huffel, S., & Suykens, J. A. K. (2010). A tutorial on support vector machine-based methods for classification problems in chemometrics. *Analytica Chimica Acta*, *665*(2), 129–145. https://doi.org/10.1016/j.aca.2010.03.030

Mancini, M., Mircoli, A., Potena, D., Diamantini, C., Duca, D., & Toscano, G. (2020). Prediction of pellet quality through machine learning techniques and near-infrared spectroscopy. *Computers & Industrial Engineering*, *147*, 106566.

Mandalika, A., Bragg, D., Schuler, J., Baker, D., Elder, T., & Groom, L. (2019). Potential of natural-origin loblolly pine tree fractions as a bioenergy feedstock. *Wood Fiber Sci.*, *51*(1), 26–40.

Manley, M. (2014). Near-Infrared Spectroscopy and Hyperspectral Imaging: Non-Destructive Analysis of Biological Materials. *Chemical Society Reviews*, *43*. https://doi.org/10.1039/c4cs00062e

Martelli-Tosi, M., Masson, M. M., Silva, N. C., Esposto, B. S., Barros, T. T., Assis, O. B. G., & Tapia-Blácido, D. R. (2018). Soybean straw nanocellulose produced by enzymatic or acid treatment as a reinforcing filler in soy protein isolate films. *Carbohydrate Polymers*, *198*, 61–68. https://doi.org/10.1016/j.carbpol.2018.06.053

Marten, G. C., Shenk, J., & Barton, F. (1985). *Near infrared reflectance spectroscopy (NIRS): Analysis of forage quality* (Issue 643). US Department of Agriculture, Agricultural Research Service.

Martin, B., Kline, E., Prisley, S., & Visser, R. J. (2007). *Online information systems for today's forest industry*.

Martínez, B., & Gilabert, M. A. (2009). Vegetation dynamics from NDVI time series analysis using the wavelet transform. *Remote Sensing of Environment*, *113*(9), 1823–1842.

McCarthy, J. K., Hood, I. A., Brockerhoff, E. G., Carlson, C. A., Pawson, S. M., Forward, M., Walbert, K., & Gardner, J. F. (2010). Predicting sapstain and degrade in fallen trees following storm damage in a Pinus radiata forest. *Forest Ecology and Management*, *260*(9), 1456–1466. https://doi.org/10.1016/j.foreco.2010.07.044

Medeghini, L., Mignardi, S., De Vito, C., & Conte, A. M. (2016). Evaluation of a FTIR data pretreatment method for Principal Component Analysis applied to archaeological ceramics. *Microchemical Journal*, *125*, 224–229. https://doi.org/10.1016/j.microc.2015.11.033

Meier, E.W. (2015). *Identifying and using hundreds of woods worldwide. Wood Database*.

Mendell, B. C., Sydor, T., & Freeman, S. (2007). Introduction to timber real estate investment trusts (timber REITs). *Timber Mart South, Market News Q.*, *1*, 8–10.

Merry, R. (2005). *Wavelet theory and applications: A literature study*.

Misztal, M. D. (2018). *Statistical Analysis of Southeastern United States Timber Prices by Regional Markets, Three-tier Product Differentiation, and Logging Margins*.

Modugno, M. (2013). Now-casting inflation using high frequency data. *International Journal of Forecasting*, *29*(4), 664–675. https://doi.org/10.1016/j.ijforecast.2012.12.003

Müller, K.-R., Mika, S., Tsuda, K., & Schölkopf, K. (2018). An introduction to kernel-based learning algorithms. In *Handbook of neural network signal processing* (pp. 4–1). CRC Press.

Musah, M., Diaz, J. H., Alawode, A. O., Gallagher, T., Peresin, M. S., Mitchell, D., Smidt, M., & Via, B. (2022). Field Assessment of Downed Timber Strength Deterioration Rate and Wood Quality Using Acoustic Technologies. *Forests*, *13*(5), Article 5. https://doi.org/10.3390/f13050752

NASDAQ stock market. https://search.library.wisc.edu/catalog/999790456002121

Nasiri, V., Darvishsefat, A. A., Arefi, H., Griess, V. C., Sadeghi, S. M. M., & Borz, S. A. (2022). Modeling forest canopy cover: A synergistic use of Sentinel-2, aerial photogrammetry data, and machine learning. *Remote Sensing*, *14*(6), 1453.

National Hurricane Center. (2021, May). *Saffir-Simpson Hurricane Wind Scale*. https://www.nhc.noaa.gov/aboutsshws.php

Newman, S. D., Soulia, M. E., Aber, J. D., Dewey, B., & Ricca, A. (1994). Analyses of forest foliage I: laboratory procedures for proximate carbon fractionation and nitrogen determination. *Journal of Near Infrared Spectroscopy*, *2*(1), 5–14.

Nison, S. (2001). *Japanese candlestick charting techniques: A contemporary guide to the ancient investment techniques of the Far East*. Penguin.

Nkansah, K., Dawson-Andoh, B., & Slahor, J. (2010). Rapid characterization of biomass using near infrared spectroscopy coupled with multivariate data analysis: Part 1 yellow-poplar (Liriodendron tulipifera L.). *Bioresource Technology*, *101*(12), 4570–4576.

NOAA. (2021a). *Hurricane Costs*. https://coast.noaa.gov/states/fast-facts/hurricane-costs.html

NOAA. (2021b). *Hurricanes in History*. https://www.nhc.noaa.gov/outreach/history/

NOAA. (2022). *Historical Hurricane Tracks*. https://coast.noaa.gov/hurricanes/#map=4/32/-80

Nørgaard, L., Bro, R., & Engelsen, S. B. (2012). Principal component analysis and near infrared spectroscopy. *A FOSS White Paper, Http://Www. Foss. de/Industry-Solution/Chemical-Analysis/Papers*.

Owen, K., Fasina, O., Taylor, S., & Adhikari, S. (2015). Thermal decomposition behavior of loblolly pine stemwood, bark, and limbs/foliage using TGA and DSC techniques. *Transactions of the ASABE*, *58*(2), 509–518.

Parfitt, D., Hunt, J., Dockrell, D., Rogers, H. J., & Boddy, L. (2010). Do all trees carry the seeds of their own destruction? PCR reveals numerous wood decay fungi latently present in sapwood of a wide range of angiosperm trees. *Fungal Ecology*, *3*(4), 338–346.

Paul, R., & Garai, S. (2021). Performance comparison of wavelets-based machine learning technique for forecasting agricultural commodity prices. *Soft Computing*, *25*. https://doi.org/10.1007/s00500-021-06087-4

Paul, R. K., Samanta, S., Paul, M. R. K., & LazyData, T. (2017). Package 'waveletarima.' *Seed*, *500*, 1–5.

Payne, C. M., Knott, B. C., Mayes, H. B., Hansson, H., Himmel, M. E., Sandgren, M., Ståhlberg, J., & Beckham, G. T. (2015). Fungal Cellulases. *Chemical Reviews*, *115*(3), 1308–1448. https://doi.org/10.1021/cr500351c

Peralta, P. N., Syme, J. H., & McAlister, R. H. (1993). Water storage and plywood processing of hurricane-downed southern pine timber. *Forest Products Journal*, *43*(4), 53.

Percival, D. B., & Walden, A. T. (2000). *Wavelet Methods for Time SeriesAnalysis*. Cambridge University Press. https://doi.org/10.1017/CBO9780511841040

Perrins, G., & Nilsen, D. (2010). Math calculations to better utilize CPI data. *Rep. Bureau of Labor Statistics, Nd Web*.

Pham, B. T., Jaafari, A., Avand, M., Al-Ansari, N., Dinh Du, T., Yen, H. P. H., Phong, T. V., Nguyen, D. H., Le, H. V., & Mafi-Gholami, D. (2020). Performance evaluation of machine learning methods for forest fire modeling and prediction. *Symmetry*, *12*(6), 1022.

Prado Osco, L., Marques Ramos, A. P., Roberto Pereira, D., Akemi Saito Moriya, É., Nobuhiro Imai, N., Takashi Matsubara, E., Estrabis, N., de Souza, M., Marcato Junior, J., & Gonçalves, W. N. (2019). Predicting canopy nitrogen content in citrus-trees using random forest algorithm associated to spectral vegetation indices from UAV-imagery. *Remote Sensing*, *11*(24), 2925.

Prestemon, J. P., & Abt, R. C. (2002). Southern Forest Resource Assessment highlights: The Southern Timber Market to 2040. *Journal of Forestry*, *100*(7), 16–22. https://doi.org/10.1093/jof/100.7.16

Prestemon, J. P., & Holmes, T. P. (1997). Effects of Hurricane Hugo on South Carolina timber prices. *Valuing Non-Timber Forest Resources: Timber Primacy Is Passé. Arkansas Forest Resources Center, Monticello, AR*, 93–100.

Prestemon, J. P., & Holmes, T. P. (2000). Timber Price Dynamics Following a Natural Catastrophe. *American Journal of Agricultural Economics*, *82*(1), 145–160. https://doi.org/10.1111/0002-9092.00012

Prestemon, J. P., & Holmes, T. P. (2004). Market Dynamics and Optimal Timber Salvage After a Natural Catastrophe. *Forest Science*, *50*(4), 495–511. https://doi.org/10.1093/forestscience/50.4.495

Prestemon, J. P., & Holmes, T. P. (2010). Economic impacts of hurricanes on forest owners. *Pye, John M; Rauscher, H Michael; Sands, Yasmeen; Lee, Danny C*, 207–221.

Prestemon, J. P., & Pye, J. M. (2000). A Technique for Merging Areas in Timber Mart-South Data. *Southern Journal of Applied Forestry*, *24*(4), 219–229. https://doi.org/10.1093/sjaf/24.4.219

Prestemon, J. P., Pye, J. M., & Holmes, T. P. (2004). Temporal Aggregation and Testing for Timber Price Behavior. *Natural Resource Modeling*, *17*(2), 123–162. https://doi.org/10.1111/j.1939-7445.2004.tb00131.x

Puth, M.-T., Neuhäuser, M., & Ruxton, G. D. (2015). Effective use of Spearman's and Kendall's correlation coefficients for association between two measured traits. *Animal Behaviour*, *102*, 77–84. https://doi.org/10.1016/j.anbehav.2015.01.010

Radu, S. (2006). The Ecological Role of Deadwood in Natural Forests. In D. Gafta & J. Akeroyd (Eds.), *Nature Conservation: Concepts and Practice* (pp. 137–141). Springer. https://doi.org/10.1007/978-3-540-47229-2_16

Rana, D., Rana, V., & Ahring, B. K. (2012). Producing high sugar concentrations from loblolly pine using wet explosion pretreatment. *Bioresource Technology*, *121*, 61–67. https://doi.org/10.1016/j.biortech.2012.06.062

Rane, S. S., & Choi, P. (2005). Polydispersity Index: How Accurately Does It Measure the Breadth of the Molecular Weight Distribution? *Chemistry of Materials*, *17*(4), 926–926. https://doi.org/10.1021/cm048594i

Rhif, M., Ben Abbes, A., Farah, I. R., Martínez, B., & Sang, Y. (2019). Wavelet transform application for/in non-stationary time-series analysis: A review. *Applied Sciences*, *9*(7), 1345.

Rösch, A., & Schmidbauer, H. (2016). WaveletComp 1.1: A guided tour through the R package. *URL: Http://Www. Hsstat. Com/Projects/WaveletComp/WaveletComp_guided_tour. Pdf*.

Russell, M. B., Fraver, S., Aakala, T., Gove, J. H., Woodall, C. W., D'Amato, A. W., & Ducey, M. J. (2015). Quantifying carbon stores and decomposition in dead wood: A review. *Forest Ecology and Management*, *350*, 107–128. https://doi.org/10.1016/j.foreco.2015.04.033

Saffir, H. S. (1973). Hurricane wind and storm surge. *The Military Engineer*, *65*(423), 4–5.

Saha, U. K., Sonon, L., & Kane, M. (2017). Prediction of calorific values, moisture, ash, carbon, nitrogen, and sulfur content of pine tree biomass using near infrared spectroscopy. *Journal of Near Infrared Spectroscopy*, *25*(4), 242–255. https://doi.org/10.1177/0967033517689981

Salazar, L., Nicolis, O., Ruggeri, F., Kiseľák, J., & Stehlík, M. (2019). Predicting hourly ozone concentrations using wavelets and ARIMA models. *Neural Computing and Applications*, *31*(8), 4331–4340. https://doi.org/10.1007/s00521-018-3345-0

Sanchez, G. (2013). PLS path modeling with R. *Berkeley: Trowchez Editions*, *383*(2013), 551.

Sandak, J., Sandak, A., Zitek, A., Hintestoisser, B., & Picchi, G. (2020). Development of Low-Cost Portable Spectrometers for Detection of Wood Defects. *Sensors*, *20*(2), Article 2. https://doi.org/10.3390/s20020545

Sannigrahi, P., Ragauskas, A. J., & Miller, S. J. (2009, October 9). *Lignin Structural Modifications Resulting from Ethanol Organosolv Treatment of Loblolly Pine* (world) [Research-article]. ACS Publications; American Chemical Society. https://doi.org/10.1021/ef900845t

Schimleck, L., Ayanleye, S., Avramidis, S., & Nasir, V. (2023). A chemistry-based explainable machine learning model based on NIR spectra for predicting wood properties and understanding wavelength selection. *Wood Material Science & Engineering*, *18*(6), 2116–2127. https://doi.org/10.1080/17480272.2023.2265349

Schimleck, L. R., Antony, F., Mora, C., & Dahlen, J. (2021). Mapping and modeling within-tree variation for loblolly pine pulp yield and lignin content. *SN Applied Sciences*, *3*(4), 468. https://doi.org/10.1007/s42452-021-04443-5

Schimleck, L. R., Evans, R., & Matheson, A. C. (2002). Estimation of Pinus radiata D. Don clear wood properties by near-infrared spectroscopy. *Journal of Wood Science*, *48*(2), Article 2. https://doi.org/10.1007/BF00767290

Schimleck, L. R., Matos, J. L. M., Trianoski, R., & Prata, J. G. (2018). Comparison of methods for estimating mechanical properties of wood by NIR spectroscopy. *Journal of Spectroscopy*.

Schneider, C. A., Rasband, W. S., & Eliceiri, K. W. (2012). NIH Image to ImageJ: 25 years of image analysis. *Nature Methods*, *9*(7), 671–675. https://doi.org/10.1038/nmeth.2089

Schölkopf, B., & Smola, A. J. (2002). *Learning with kernels: Support vector machines, regularization, optimization, and beyond*. MIT press.

Scholkopf, B., & Smola, A. J. (2018). *Learning with kernels: Support vector machines, regularization, optimization, and beyond*. MIT press.

Shah, S., Kelly, R. C., & Rathburn, D. (2021, September 29). *Consumer Price Index vs. Producer Price Index: What's the Difference?* Investopedia. https://www.investopedia.com/ask/answers/011915/what-difference-between-consumer-price-index-cpi-and-producer-price-index-ppi.asp

Shapiro, A. J., O'Dea, R. M., Li, S. C., Ajah, J. C., Bass, G. F., & Epps III, T. H. (2023). Engineering Innovations, Challenges, and Opportunities for Lignocellulosic Biorefineries: Leveraging Biobased Polymer Production. *Annual Review of Chemical and Biomolecular Engineering*, *14*, 109–140.

Sheets, R. C. (1990). The National Hurricane Center—Past, present, and future. *Weather and Forecasting*, *5*(2), 185–232.

Shi, X., Yao, L., & Pan, T. (2021). Visible and Near-Infrared Spectroscopy with Multi-Parameters Optimization of Savitzky-Golay Smoothing Applied to Rapid Analysis of Soil Cr Content of Pearl River Delta. *Journal of Geoscience and Environment Protection*, *9*(3), Article 3. https://doi.org/10.4236/gep.2021.93006

Shupe, T. F., Choong, E. T., & Yang, C. H. (1996). The effects of silvicultural treatments on the chemical composition of plantation-grown loblolly pine wood. *Wood and Fiber Science*, 295–300.

Silva, T. P., Ferreira, A. N., de Albuquerque, F. S., de Almeida Barros, A. C., da Luz, J. M. R., Gomes, F. S., & Pereira, H. J. V. (2022). Box–Behnken experimental design for the optimization of enzymatic

saccharification of wheat bran. *Biomass Conversion and Biorefinery*, *12*(12), 5597–5604. https://doi.org/10.1007/s13399-021-01378-0

Sluiter, A., Hames, B., Ruiz, R., Scarlata, C., Sluiter, J., Templeton, D., & Crocker, D. (2008). Determination of Structural Carbohydrates and Lignin in Biomass. Laboratory Analytical Procedure (LAP), Technical Report NREL/TP-510-42618. *Natl. Renew. Energy Lab.*

Sluiter, A., Ruiz, R., Scarlata, C., Sluiter, J., & Templeton, D. (2008). Determination of extractives in biomass: Laboratory analytical procedure (LAP). *National Renewable Energy Laboratory*, 1–9.

Soares, M. J. (2011). Business cycle synchronization and the Euro: A wavelet analysis. *Journal of Macroeconomics*, *33*(3), 477–489.

Song, Z., Kennedy, P. G., Liew, F. J., & Schilling, J. S. (2017). Fungal endophytes as priority colonizers initiating wood decomposition. *Functional Ecology*, *31*(2), 407–418.

Stanturf, J. A., Goodrick, S. L., & Outcalt, K. W. (2007). Disturbance and coastal forests: A strategic approach to forest management in hurricane impact zones. *Forest Ecology and Management*, *250*(1), 119–135. https://doi.org/10.1016/j.foreco.2007.03.015

Sun, C. (2016). Timber Market Recovery after a Hurricane. *Forest Science*, *62*(6), 600–612. https://doi.org/10.5849/forsci.15-123

Syme, J. H. (1992). *Impacts of Hugo timber damage on primary wood manufacturers in South Carolina* (Vol. 80). US Department of Agriculture, Forest Service, Southeastern Forest Experiment ….

Tao, J., Liang, R., Li, J., Yan, B., Chen, G., Cheng, Z., Li, W., Lin, F., & Hou, L. (2020). Fast characterization of biomass and waste by infrared spectra and machine learning models. *Journal of Hazardous Materials*, *387*, 121723.

Taylor, E. L., & Foster, C. D. (2005). *Salvaging Timber: Landowner Do's and Don'ts*. 2.

Tharwat, A. (2019). Parameter investigation of support vector machine classifier with kernel functions. *Knowledge and Information Systems*, *61*, 1269–1302.

Thevenot, M., Dignac, M.-F., & Rumpel, C. (2010). Fate of lignins in soils: A review. *Soil Biology and Biochemistry*, *42*(8), 1200–1211. https://doi.org/10.1016/j.soilbio.2010.03.017

TimberMart-South | Home. (2022). http://www.timbermart-south.com/news.html

TimberMart-South | Resources. (2023, April 11). http://www.timbermart-south.com/resources.html

Tolbert, A., Akinosho, H., Khunsupat, R., Naskar, A. K., & Ragauskas, A. J. (2014). Characterization and analysis of the molecular weight of lignin for biorefining studies. *Biofuels, Bioproducts and Biorefining*, *8*(6), 836–856. https://doi.org/10.1002/bbb.1500

Tolvaj, L. (2023). Measurement Methods and Characterisation of the Optical Parameters of Wood. In *Optical Properties of Wood: Measurement Methods and Result Evaluations* (pp. 1–49). Springer.

TradingView. (2021). *TradingView*. TradingView. https://www.tradingview.com/

Tuncer, F. D., Dogu, D., & Akdeniz, E. (2023). Efficiency of preprocessing methods for discrimination of anatomically similar pine species by NIR spectroscopy. *Wood Material Science & Engineering*, *18*(1), 212–221. https://doi.org/10.1080/17480272.2021.2012821

Türker-Kaya, S., & Huck, C. W. (2017). A review of mid-infrared and near-infrared imaging: Principles, concepts and applications in plant tissue analysis. *Molecules*, *22*(1), 168.

Tzabazis, A., Eisenried, A., Yeomans, D. C., & Hyatt, M. I. (2018). Wavelet analysis of heart rate variability: Impact of wavelet selection. *Biomedical Signal Processing and Control*, *40*, 220–225.

Udovičić, M., Baždarić, K., Bilić-Zulle, L., & Petrovečki, M. (2007). What we need to know when calculating the coefficient of correlation? *Biochemia Medica*, *17*(1), 10–15.

U.S. Bureau of Labor Statistics. (2022). *Consumer Price index: US Department of Labor*. https://www.bls.gov/cpi/tables/supplemental-files/home.htm

U.S. Bureau of Labor Statistics. (2023, July 19). *Calculation: Handbook of Methods*. https://www.bls.gov/opub/hom/cpi/calculation.htm

US Department of Commerce, N. (2018, September 14). *Hurricane Florence:* NOAA's National Weather Service. https://www.weather.gov/ilm/HurricaneFlorence

Vacha, L., & Barunik, J. (2012). Co-movement of energy commodities revisited: Evidence from wavelet coherence analysis. *Energy Economics*, *34*(1), 241–247.

Van Hensbergen, H., & Cedergren, J. (2021). *Forest-related disasters–Three case studies and lessons for management of extreme events* (Vol. 17). Food & Agriculture Org.

Vermaas, J. V., Petridis, L., Qi, X., Schulz, R., Lindner, B., & Smith, Jeremy. C. (2015). Mechanism of lignin inhibition of enzymatic biomass deconstruction. *Biotechnology for Biofuels*, *8*(1), 217. https://doi.org/10.1186/s13068-015-0379-8

Via, B. K., & Jiang, W. (2013). Nonlinear multivariate modeling of strand mechanical properties with near-infrared spectroscopy. *The Forestry Chronicle*, *89*(5), 621–630.

Via, B. K., So, C. L., Groom, L. H., Shupe, T. F., Stine, M., & Wikaira, J. (2007). Within tree variation of lignin, extractives, and microfibril angle coupled with the theoretical and near infrared modeling of microfibril angle. *Iawa Journal*, *28*(2), 189–210.

Via, B. K., Zhou, C., Acquah, G., Jiang, W., & Eckhardt, L. (2014). Near Infrared Spectroscopy Calibration for Wood Chemistry: Which Chemometric Technique Is Best for Prediction and Interpretation? *Sensors*, *14*(8), Article 8. https://doi.org/10.3390/s140813532

Via, B., McDonald, T., & Fulton, J. (2012). Nonlinear multivariate modeling of strand density from near-infrared spectra. *Wood Science and Technology*, *46*(6), 1073–1084. https://doi.org/10.1007/s00226-012-0467-x

Vonesch, Cé., Blu, T., & Unser, M. (2007). Generalized Daubechies Wavelet Families. *IEEE Transactions on Signal Processing*, *55*(9), 4415–4429. https://doi.org/10.1109/TSP.2007.896255

Walker, G. M., & White, N. A. (2017). Introduction to Fungal Physiology. In *Fungi* (pp. 1–35). John Wiley & Sons, Ltd. https://doi.org/10.1002/9781119374312.ch1

Wang, C., & Ross, B. (2007). Acoustic Assessment of Wood Quality of Raw Forest Materials—A path to increased profitability. *FOREST PRODUCTS JOURNAL*, *57*(5), 9.

Wang, L., Zou, H., Su, J., Li, L., & Chaudhry, S. (2013). An ARIMA-ANN hybrid model for time series forecasting. *Systems Research and Behavioral Science*, *30*(3), 244–259.

Wang, Y.-Y., Sengupta, P., Scheidemantle, B., Pu, Y., Wyman, C. E., Cai, C. M., & Ragauskas, A. J. (2020). Effects of CELF Pretreatment Severity on Lignin Structure and the Lignin-Based Polyurethane Properties. *Frontiers in Energy Research*, *8*. https://www.frontiersin.org/articles/10.3389/fenrg.2020.00149

Wang, Y.-Y., Wyman, C. E., Cai, C. M., & Ragauskas, A. J. (2019). Lignin-Based Polyurethanes from Unmodified Kraft Lignin Fractionated by Sequential Precipitation. *ACS Applied Polymer Materials*, *1*(7), 1672–1679. https://doi.org/10.1021/acsapm.9b00228

Weisbrod, K. (2022, March 22). Hurricane Michael Hit the Florida Panhandle in 2018 With 155 MPH Winds. Some Black and Low-Income Neighborhoods Still Haven't Recovered. *Inside Climate News*. https://insideclimatenews.org/news/22032022/hurricane-michael-black-low-income-neighborhoods/

Wu, K.-P., & Wang, S.-D. (2009). Choosing the kernel parameters for support vector machines by the inter-cluster distance in the feature space. *Pattern Recognition*, *42*, 710–717. https://doi.org/10.1016/j.patcog.2008.08.030

Wu, S., Chang, H., Jameel, H., & Philips, R. (2010). Novel Green Liquor Pretreatment of Loblolly Pine Chips to Facilitate Enzymatic Hydrolysis into Fermentable Sugars for Ethanol Production. *Journal of Wood Chemistry and Technology*, *30*(3), 205–218. https://doi.org/10.1080/02773811003746717

Xu, X., Pan, R., & Chen, R. (2021). Combustion Characteristics, Kinetics, and Thermodynamics of Pine Wood Through Thermogravimetric Analysis. *Applied Biochemistry and Biotechnology*, *193*(5), 1427–1446. https://doi.org/10.1007/s12010-020-03480-x

Yamakawa, C. K., Qin, F., & Mussatto, S. I. (2018). Advances and opportunities in biomass conversion technologies and biorefineries for the development of a bio-based economy. *Biomass and Bioenergy*, *119*, 54–60. https://doi.org/10.1016/j.biombioe.2018.09.007

Yang, H., Liu, Y., Xiong, Z., & Liang, L. (2020). Rapid Determination of Holocellulose and Lignin in Wood by Near Infrared Spectroscopy and Kernel Extreme Learning Machine. *Analytical Letters*, *53*(7), 1140–1154. https://doi.org/10.1080/00032719.2019.1700267

Yin, R., & Newman, D. H. (1999). *An intervention analysis of Hurricane Hugo's effect on South Carolina's stumpage prices*. *29*, 9.

Zhang, D., Butler, B. J., & Nagubadi, R. V. (2012). Institutional timberland ownership in the US South: Magnitude, location, dynamics, and management. *Journal of Forestry*, *110*(7), 355–361.

Zhang, M., Mei, B., Harris, T. G., Siry, J. P., Clutter, M. L., & Baldwin, S. S. (2011). Can Timber Hedge against Inflation? An Analysis of Timber Prices in the US South. *Forest Products Journal*, *61*(4), 276–282. https://doi.org/10.13073/0015-7473-61.4.276

Zhang, W., Kasun, L. C., Wang, Q. J., Zheng, Y., & Lin, Z. (2022). A Review of Machine Learning for Near-Infrared Spectroscopy. *Sensors*, *22*(24), Article 24. https://doi.org/10.3390/s22249764

Zhu, C., & Liu, X. (2013). Optimization of extraction process of crude polysaccharides from Pomegranate peel by response surface methodology. *Carbohydrate Polymers*, *92*(2), 1197–1202. https://doi.org/10.1016/j.carbpol.2012.10.073

List of publications and contributions

Published peer-reviewed articles (N = 1) derived from this dissertation:

PAPER I: **Hernandez-Diaz, J. A.,** Musah, M., Morgan, T. R., Richey, R. G., Maggard, A. O., Via, B., & Peresin, M. S. (2024). Wavelet Analysis and Forecasting using Open-Access Lumber Market Indices for Assessing the Impact of Hurricanes on Southern US Stumpage Prices. Forest Products Journal, 74(1), 10-27.

Articles submitted to peer reviewed journals (N =1) derived from this dissertation:

PAPER II: **Hernandez, J. A.**, Musa, M., Bello, F., Via, B., & Peresin, M. S. Loblolly Pine Downed Timber: Box-Behnken Design and First Derivative Pretreatment Boost Predictive Modeling with Near-Infrared Spectroscopy and Machine Learning (NIRS-ML). *(Submitted to Holzforschung, March 1st, 2024).*

Peer reviewed articles under preparation (N =2) derived from this dissertation:

PAPER III: **Hernandez, J. A.,** Musa, M., Bello, F., Via, B., & Peresin, M. S. Field Assessment of Downed Timber Deterioration Rate using rapid Near Infra-red Spectroscopy and Acoustic Technologies; Correlation with Chemical Changes over time. *(Under preparation).*

PAPER IV: **Hernandez, J. A.,** Godwin, J. A., Chmely, S. & Peresin, M. S. Downed Timber Deterioration Rate: Influence in Properties and Recovery of Lignin by Co-Solvent Enhanced Lignocellulosic Fractionation (CELF). *(Under preparation).*

Peer-reviewed manuscripts in archival literature not included in this document (N = 4):

1. Musah, M., Alawode, A. O., **Diaz, J. H.**, Asafu-Adjaye, O., Gallagher, T., Peresin, M. S., ... & Via, B. (2023). Prediction of Acoustic Velocity Properties of Downed Pine Trees Using Near-Infrared Spectroscopy. Forest Products Journal, 73(2), 133-141.
2. Musah, M.; **Diaz, J.H.**; Alawode, A.O.; Gallagher, T.; Peresin, M.S.; Mitchell, D.; Smidt, M.; Via, B. (2022). Field Assessment of Downed Timber Strength Deterioration Rate and Wood Quality Using Acoustic Technologies. Forests, 13, 752.
3. **Hernandez, J. A.**, Soni, B., Iglesias, M. C., Vega Erramuspe, I. B., Frazier, C. E., & Peresin, M. S. (2022). Soybean hull pectin and nanocellulose: tack properties in aqueous pMDI dispersions. Journal of Materials Science, 57(8), 5022-5035.
4. Gomez-Maldonado, D., Filpponen, I., **Hernandez-Diaz, J. A.**, Waters, M. N., Auad, M. L., Johansson, L. S., ... & Peresin, M. S. (2021). Simple functionalization of cellulose beads with pre-propargylated chitosan for clickable scaffold substrates. Cellulose, 28(10), 6073-6087.

Appendix

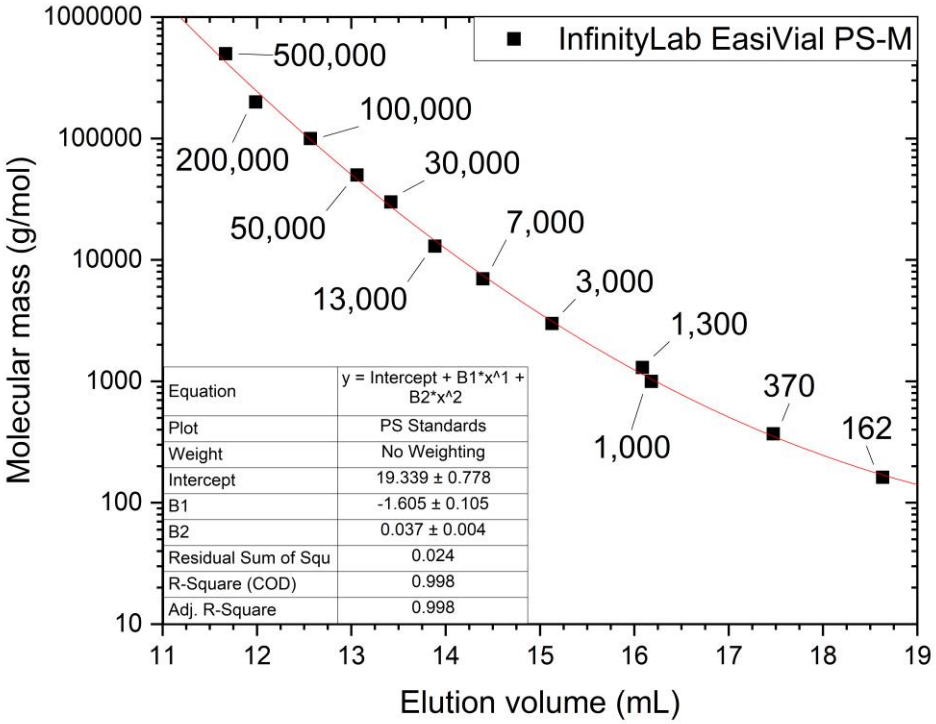

Figure 0.1. GPC/SEC calibration with PS standards for CELF Lignin molecular weight.

Figure 0.2. CELF Lignin particle production, evidence of complete solubilization of lignin (left). THF-salt solution ratio dissolution test (right).

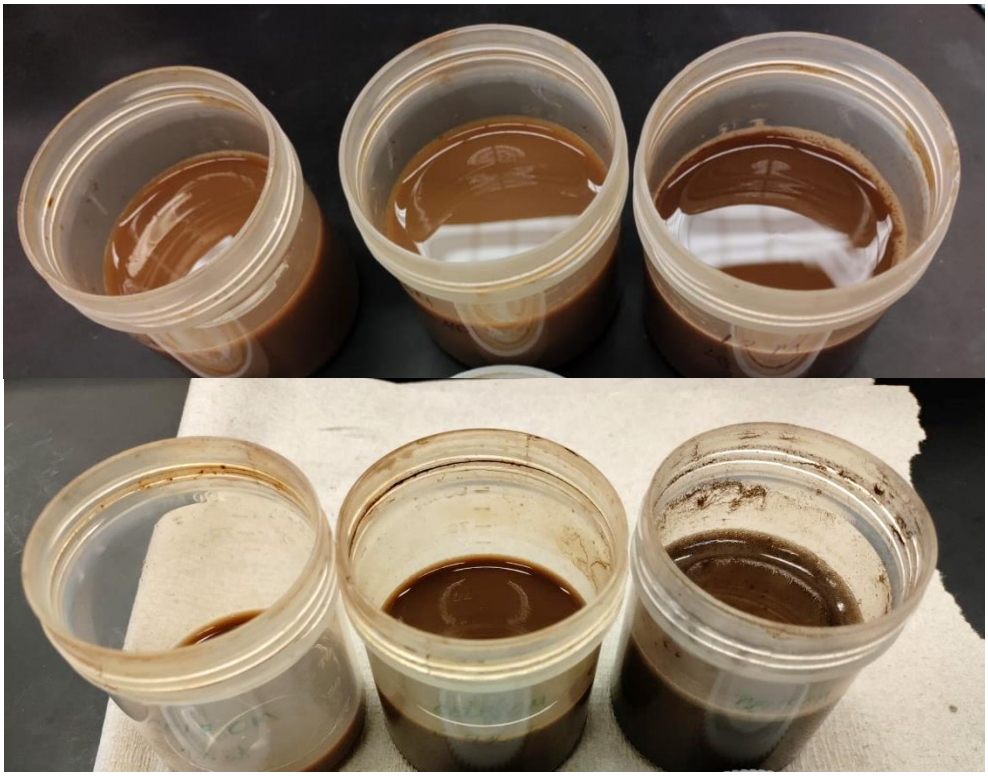

Figure 0.3. CELF Lignin particle production, stability over time. Initial production (top) and the same samples after 5 months of storage in room temperature conditions (bottom).